Interplay of Structural, Dynamical, and Electronic Properties in Doped Semiconducting Polymer Systems

Sophia Ackling
B.Sc. (Advanced)

A thesis submitted in partial fulfilment of the
requirements for the degree of
Master of Philosophy in Chemical Science

February 2017

THE UNIVERSITY of ADELAIDE

Department of Chemistry
The University of Adelaide
North Terrace Campus
Adelaide, South Australia 5005

Supervisors:
Dr David M. Huang
A/Prof. Tak W. Kee

Contents

Abstract

High-performing cost-efficient organic electronics will play an important role in shaping the future of flexible electronic devices. Applications for such technology range from smart device screens to sensors and photovoltaics. Precise optical control over polymer structure has recently been reported, with applications in optical film patterning for cost-efficient organic device fabrication. This process was demonstrated within the archetypal poly(3-hexylthiophene) (P3HT) and 2,3,5,6-tetrafluoro-7,7,8,8-tetracyanoquinodimethane (F4TCNQ) polymer/dopant system, wherein optical control over solubility was performed using light at a specific wavelength. However, the underlying mechanism responsible for the solubility change is yet to be fully elucidated. The work presented in this dissertation aims to provide insight into a number of related physical and electronic properties within this polymer/dopant system by means of computational investigation.

Density functional theory is used to investigate how structural and environmental properties of the P3HT/F4TCNQ system affect charge transfer. A simplified oligomer/dopant complex is constructed, and the impacts of oligothiophene chain length and substitution are investigated. An oligomer close to the P3HT conjugation length, with methyl side chains, is found to best replicate experimental results. A dielectric medium is introduced to simulate the effects of the surrounding P3HT chains that are present in the experimental system. The surrounding environment is shown to be intrinsic to realistic charge transfer, as quantitative charge transfer is achieved.

The initial hypothesis for the optical solubility control process suggested a photo-induced charge back-transfer reaction from dopant to polymer, resulting in the latter returning to its neutral, and hence soluble, state. Excited-state density functional theory calculations on the aforementioned optimal model system reveal that the complex does display excitations with charge transfer character near the optical de-doping wavelength. However, constrained density functional theory calculations reveal that the optimised charge-neutral state is unstable, and the charge-separated state is thermodynamically favoured. These calculations illuminate important electronic characteristics of the system, and suggest that a photo-induced charge transfer mechanism is not responsible for the solubility change.

Diffusion processes can dictate physical and electronic properties in doped polymer systems. Density functional theory calculations are used in this work to explain

experimental measurements of atomic motions in P3HT doped with methyl-ester-substituted F4TCNQ. Calculations quantitatively confirm the assignment of experimental measurements of a diffusive process in the system to the methyl rotation on the F4TCNQ analogue. A set of calculations replicating the hopping of the F4TCNQ analogue along the P3HT backbone, a hypothesis for the second experimentally measured process, demonstrates that neither the energy barrier nor the diffusion coefficient for this calculated process are on the order of the experimental results, and hence an alternative process may be responsible for the experimental observations.

Finally, the thermodynamics of the photo-induced solubility change are investigated using classical and quantum techniques. Steered molecular dynamics simulations demonstrate that charge distribution influences the free energy of separation of polymer and dopant. However, these simulations do not account for quantum relaxation or dynamic charge distributions. Density functional theory calculations, which do account for these properties, yield the free energy change for separation using a continuum solvent model. The explicit solvent contribution to the free energy of species separation is extracted from alchemical free energy perturbation simulations. Applying this contribution to the quantum calculations in place of the continuum model contribution yields a free energy change for separation that is in excellent agreement with experimental measurements.

Declaration

I certify that this work contains no material which has been accepted for the award of any other degree or diploma in my name, in any university or other tertiary institution and, to the best of my knowledge and belief, contains no material previously published or written by another person, except where due reference has been made in the text. In addition, I certify that no part of this work will, in the future, be used in a submission in my name, for any other degree or diploma in any university or other tertiary institution without the prior approval of the University of Adelaide and, where applicable, any partner institution responsible for the joint-award of this degree.

I give consent to this copy of my thesis, when deposited in the University Library, being made available for loan and photocopying, subject to the provisions of the Copyright Act 1968.

I acknowledge that copyright of published works contained within this thesis resides with the copyright holder(s) of those works.

I also give permission for the digital version of my thesis to be made available on the web, via the University's digital research repository, the Library Search and also through web search engines, unless permission has been granted by the University to restrict access for a period of time.

Sophia Ackling
February 2017

Acknowledgements

There are a number of important people who have contributed to this thesis, to varying degrees and both directly and indirectly. I wish to first acknowledge my supervisor, Dr David Huang, for his considerable contribution. Without your ongoing assistance when the results did not match our expectations, and your continued optimism that just one more calculation would give us the insight we needed, it would have been a far greater challenge to complete this project. Your extensive knowledge, patience and encouragement have made this thesis possible.

I must also thank our American collaborators for including us in their journey towards understanding the interesting chemistry of the doped polymer system. The underlying mechanism turned out to be a little more complicated, but no less exciting, than we originally postulated. I am pleased to have been able to contribute in a small way to the discovery process, and I am grateful for being included in the discussion along the way.

During my time as a Masters student I encountered a number of people who showed interest in my research and helped with the stumbling blocks that I met along the way. Thank you to Leaf Lin for all of your help with the NCI supercomputer and the Q-Chem software that made my project possible, and to Dr Lars Goerigk and Rika Kobayashi for your willingness to share your knowledge of density functional theory. To everyone in the Huang research group: your incredible work ethic does you great credit, and it has helped me to continue to strive towards personal improvement. I have really enjoyed working with you, and appreciate your help along the way. Thanks to Mr Patrick Tapping and Mr Andrew Tarzia, in particular, for your assistance with software.

Successful completion of this research project is also the result of the support of a number of people outside the field of chemistry. Thank you to those at the City Cross General Trader/Minimax store for allowing me to remain a part of the team and covering for me when my studies limited my availability, and in particular thank you to my manager Vicki Gorton for your belief in my ability to complete my studies and your understanding when I had to put my research first. Thank you also to my wonderful friends for the great times we shared over the last two years. These were a welcome break from my studies.

My success as a scientist is owed in large part to my dad, who introduced me to that which underpins science: the wonder of the unknown. Equally importantly,

mum has helped me to stay grounded and focused during the harder times. I am grateful for the continued support from both of my parents and my sister, Chloe, throughout this project. And finally, I wish to express my immense gratitude to my husband, Thomas. Your boundless enthusiasm for everything, including my research, has made the last two years considerably easier. Thank you for believing in me.

Abbreviations

B3LYP	Becke three-parameter Lee-Yang-Parr
CDFT	constrained density functional theory
CHELPG	charges from the electrostatic potential on a grid
COM	centre of mass
CPCM	conductor-like polarisable continuum model
DFT	density functional theory
EA	electron affinity
F4TCNQ	2,3,5,6-tetrafluoro-7,7,8,8-tetracyano-quinodimethane
FEP	free energy perturbation
GGA	generalised gradient approximation
HF	Hartree-Fock
HOMO	highest occupied molecular orbital
IEFPCM	integral equation formalised polarisable continuum model
IP	ionization potential
LDA	local density approximation
LJ	Lennard Jones
LRC-ωPBEh	optimally tuned long-range corrected Perdew-Burke-Ernzerhof
LUMO	lowest unoccupied molecular orbital
M8	eight-unit methyl-substituted oligothiophene
MD	molecular dynamics
mF4TCNQ	methyl-ester substituted 2,3,5,6-tetrafluoro-7,7,8,8-tetracyano-quinodimethane
MO	molecular orbital
NMR	nuclear magnetic resonance
NTO	natural transition orbital
OFET	organic field-effect transistor
OLED	organic light emitting diode
OPV	organic photovoltaic
P3HT	poly(3-hexylthiophene)
PCM	polarisable continuum model
PMF	potential of mean force
PPPM	particle-particle particle-mesh
QENS	quasi-elastic neutron scattering
SMD	steered molecular dynamics
TDDFT	time-dependent density functional theory
THF	tetrahydrofuran

List of Figures

List of Tables

Dedication

For my family

1 Introduction

Intense interest in the properties of organic electronic devices has motivated a large body of research to be conducted in recent years. In contrast to their silicon counterparts, organic electronic devices have the potential for cheaper large-scale production. Organic transistors, light-emitting diodes (OLEDs) and photovoltaics (OPVs) are all examples of organic electronic devices with considerable commercial potential. While organic field-effect transistors (OFETs) have exceeded silicon performance,[1] in general silicon-based devices remain superior in terms of electron transport efficiency.[2] However, their production remains costly due to the high precision required for effective device performance. Moreover, a great deal of waste is generated during the production process. Organic electronic devices, on the other hand, have the possibility to be produced using cheaper techniques such as solution processing.

Enhanced flexibility is an intrinsic feature that, although lacking particularly in crystalline silicon-based devices, organic electronic devices can deliver. OLED technologies are already being incorporated into smart device screens,[3] and OPVs continue to show promise as alternative energy sources in places that their silicon counterparts cannot be used. Beyond display and power generation applications, flexible organic electronics also have applications in biology as chemical sensors and electrodes to stimulate cells.[4] Furthermore, recent studies indicate the vast potential for stretchable organic electronic devices, in which elasticity could yield longer product lifetimes as well as improved diversity of applications.[5,6]

While the field of organic electronic device development shows enormous promise, key challenges remain in the conceptualisation and subsequent development of these devices. In particular, the electronic properties of these organic systems are often poorly understood, and device improvement is often made on a trial-and-error basis. With a greater understanding of the electronic mechanisms involved in charge transport and morphology, better design principles will allow for optimising of device properties and perhaps increase production efficiencies. This work investigates charge transfer in an archetypal polymer-based system using computational techniques, and seeks to clarify the experimentally observed physical manipulation of the system using light.

1.1 Organic electronics

1.1.1 Semiconducting polymers

The organic component of organic electronic devices comprises either organic polymers or small organic molecules. In either case, the material must possess semiconducting properties. For OPVs and transistors, polymers are often chosen because of their ability to form a smoother film. This work focuses on organic polymers.

Semiconducting properties arise within organic polymers as a result of their conjugated backbone. Alternating single and double carbon-carbon bonds in an extended π-system allows for electron migration along conjugated sections of this backbone. It is this conjugated π-system that gives rise to the characteristic optoelectronic properties of these polymers and allows them to absorb and emit light in the visible region. The conjugated backbone also allows for transport of charge throughout the system, provided sufficient structural order is present. π-π stacking within polymer films can provide a high level of structural order, which is often desirable for an efficient and defect-free device. However, such stacking can be challenging to achieve as a result of torsional flexibility within the polymer, and can result in charge traps.[7]

For the purpose of solution processing of polymer films, solubility of the polymer in common solvents is desirable. Solubility within a chosen solvent can be improved by modifying the side chains connected to the conjugated backbone.[8] However, in the case of linear alkyl side chains, while increasing their length improves solubility in some solvents, it also decreases charge transport in mixtures pertinent for OPVs.[9] Other properties of the semiconducting polymer are also affected by side chains. Mei and Bao provide a comprehensive review in ref 8. As well as modifications to side chain properties, the backbone of the polymer may also be constructed as a homo- or copolymer. In the latter, different chain units are alternated as a means to improve charge transport or solubility.[10,11]

1.1.2 Molecular doping

An important consideration for the conductive properties of organic semiconductors is the Fermi level. The Fermi level lies between the valence and conduction band in inorganic semiconductors, and between the occupied and virtual orbitals in organic semiconductors, and provides a virtual energy level that would be 50 % occupied at thermal equilibrium. This energy depends on the proportion of electrons (negative charges) and holes (positive charges) in the system. A common technique employed to improve charge transport is to introduce dopants, which change the Fermi energy level and make the system more conducive to charge transport. Doping of semiconducting polymers was first performed by Shirakawa *et al.* Halogen atoms such as chlorine and iodine were introduced into a polyacetylene film and charge transport efficiencies were observed to increase seven orders of magnitude.[12] Using ultraviolet photoelectron spectroscopy, lithium atoms have been observed to raise

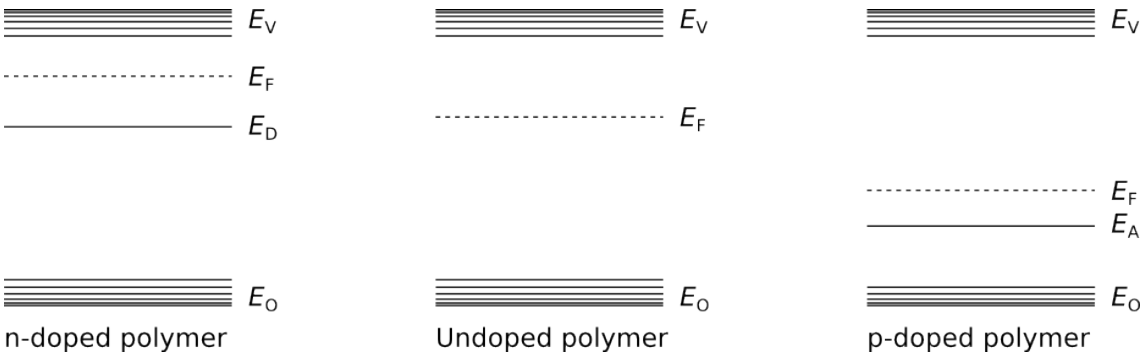

Figure 1.1: Typical energy level diagram for doped and undoped organic semiconductors. Molecular doping improves electron transport efficiency by modifying the proportion of electrons to holes in the polymer system and hence changing the Fermi energy level, E_F. Occupied and virtual orbitals are denoted E_O and E_V, respectively, and E_A and E_D are the states introduced by acceptor or donor dopant.

the Fermi level in an organic semiconductor system, resulting in improved charge transport.[13] A more common approach in recent times has been to include small organic molecules instead of halogen or metal atoms, as the latter tend to diffuse out of the polymer film due to their small size.[13]

Small organic dopant molecules tend to be strongly electron donating or accepting. The latter introduce holes in the occupied energy levels of the polymer system, which lowers the energy of the Fermi level (Figure 1.1). Electron donating dopants introduce electrons above the occupied energy levels of the polymer, which increases the Fermi level. In both cases, the generation of free charges increases charge transport efficiency within the polymer system by changing the proportion of electrons to holes. Optimal dopants are chosen such that their molecular orbitals align favourably with those of the polymer, or equivalently such that their electron affinity (EA) is greater than the ionization potential of the polymer (IP) for p-type dopants (vice versa for n-type dopants).[14] In the case of electron accepting molecules (p-type dopants), this requires the lowest unoccupied molecular orbital (LUMO) of the dopant to lie below the highest occupied molecular orbital (HOMO) of the polymer. The system is thus susceptible to charge transfer from polymer to dopant under a p-type doping regime. Such a process generates a hole on the polymer and the dopant possesses the extra electron. If the charge pair can overcome Coulombic attraction, these charges can separate and move throughout the system, generating a current.

1.1.3 Device fabrication

One of the most attractive aspects of organic electronic devices is the ease of production. Solution processing of organic electronics has the potential to vastly improve production efficiency and hence appreciably reduce the cost of production when compared to silicon-based devices. Although wasteful in terms of material, spin coating is commonly used in research as a time-efficient means to produce polymer

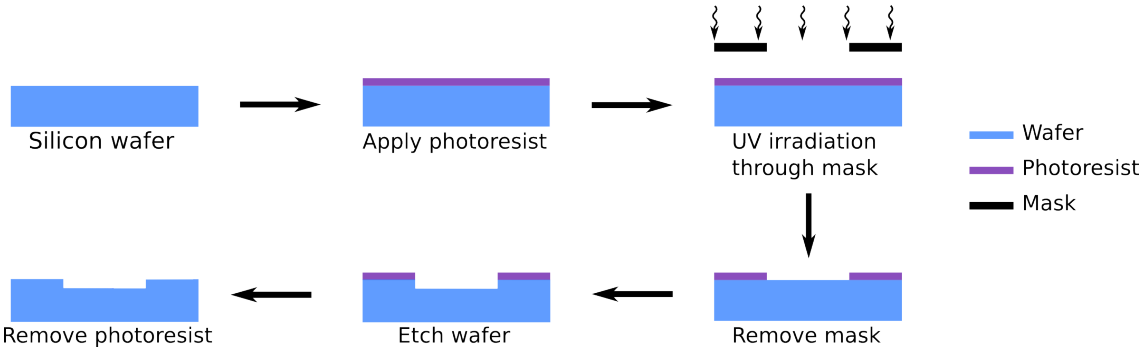

Figure 1.2: Photolithographic process for patterning a silicon wafer. A similar process can be applied in which an organic polymer layer is placed on a substrate and patterned instead of the wafer.

films. As a more commercially geared option, inkjet printing uses the solvated polymer as "ink" and prints droplets of this ink onto a substrate. The solvent is then evaporated to yield a smooth polymer film.[15] This process generates minimal waste while achieving the desired film properties in an efficient manner.

In the case of doped polymer films, variation in how the dopant is introduced can result in vastly different properties of the resulting thin film. The organic semiconductor and dopant can be layered sequentially onto a substrate, or mixed together and deposited as a bulk heterojunction wherein polymer/dopant contact is present throughout the film, and not just at an interface.[16] The latter allows for improved polymer/dopant interactions as a result of increased surface area of the dopant, and hence is used preferentially. However, where the polymer itself may assemble into a highly ordered system, forming a film from a polymer/dopant mixture can result in disruption of crystallinity of the polymer by the dopant. Recent work by Kang *et al.* demonstrated improved order in their system by introducing the dopant via diffusion after first forming the polymer film.[17]

Inkjet printing is a promising technique for producing thin polymer films, but limitations are still present. In particular, patterning polymer films on a sufficiently small scale for organic devices remains a challenge. Some silicon-based devices are produced from wafers of pure crystalline silicon cut down to a specific size using photolithography (Figure 1.2). This process generates waste, and requires considerable precision in order to produce consistent chips.

Organic electronic devices can also be produced using photolithography, albeit with modified solvents and photoresists. This process involves creating a film of the required polymer, applying a resist layer as in Figure 1.2, irradiation through a mask in order to generate a pattern, and using an appropriate solvent to remove the resist and etch the polymer film beneath. The resist is then removed to yield a patterned polymer film. Although techniques based on this approach have been used with some success,[18–20] the same problems remain as with silicon device production: high cost, potentially harsh solvents and wasted materials. Furthermore, the organic layer is sensitive to production conditions and can be damaged by the process.

1.1.4 Structural control and stability in organic devices

As already discussed, the structure of the polymer film in an organic electronic device, and hence its charge transport performance, can depend on a great number of factors. Polymer crystallinity is often synonymous with efficient charge transport, as increased order within the system provides uninterrupted paths for charge migration. Processing conditions such as temperature and solvent have been modified in order to control crystallinity within a fullerene-based organic system used in photovoltaic devices,[21–23] and charge transport efficiency has been shown to increase in some polymer/dopant systems for a given dopant concentration with decreasing temperature.[24] Alternatively, properties of the polymer and dopant may be modified in order to improve structural or electronic properties.[25] Optimal dopant concentrations are also a consideration for structural control, as doping beyond a certain concentration can begin to disaggregate the polymer as a result of disrupted π-π stacking.[26]

One aspect of organic electronic devices that is largely overlooked in publications is the long-term stability of these devices. In general, polymer/dopant mixtures are sensitive to oxygen degradation either by exposure to air or water,[27,28] and so long-term stability tests are pertinent. There is some evidence to suggest that degradation in OLEDs is the result of unavoidable impurities introduced during the production process.[29] Perhaps more easy to control is the issue of dopant diffusion. The previously discussed halogen and metal atom dopants have been largely abandoned due to their propensity to diffuse out of the polymer within moderate timescales. Small organic molecules are bulkier, and hence diffuse less readily. However, diffusion is still possible on moderate timescales. For example, in spite of its aromaticity, which results in π-interactions with organic semiconducting polymers, popular electron acceptor 2,3,5,6-tetrafluoro-7,7,8,8-tetracyano-quinodimethane (F4TCNQ) diffuses out of some organic molecular films.[30,31] However, modifying the functional groups of popular dopants may allow for control over long-term device stability to dopant diffusion.

1.2 Structure dynamics and optoelectronics of donor-acceptor systems

1.2.1 Aggregation in the P3HT/F4TCNQ system

The work discussed thus far pertains to broad aspects of doped organic polymers for the purposes of organic electronic devices. In particular, fabrication methods and structural control have been discussed. In the following sections a particular polymer/dopant system will be considered. This system comprises poly(3-hexylthiophene) (P3HT) and the F4TCNQ dopant (Figure 1.3), both of which have been studied in detail over the last two decades. This system is of particular interest due to developments in the last year which highlight novel solubility properties.

There has been some discussion of the doping mechanism of F4TCNQ with

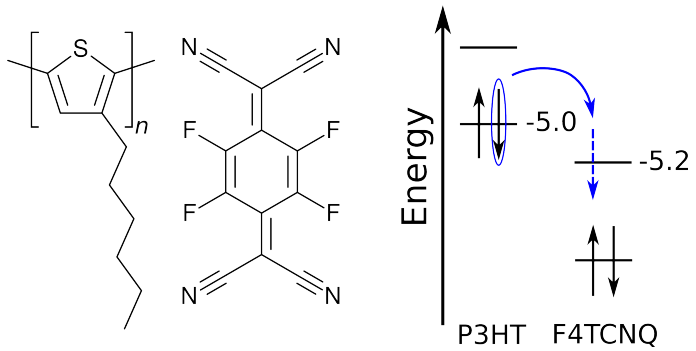

Figure 1.3: Structures of P3HT (left) and F4TCNQ (center), and a sketch of the molecular orbital energy levels (in eV) of polymer and dopant (right).

various polymers. A previous study by Salzmann *et al.* showed that interactions between pentacene and F4TCNQ result in a bound hybrid complex, wherein partial charge transfer occurs.[32] Such a doping scheme has also been noted elsewhere for similar systems.[33] Additionally, Méndez *et al.* observed partial charge transfer between quarterthiophene and F4TCNQ. However, they also found that integer charge transfer occurs when quarterthiophene is replaced with P3HT.[34] Numerous groups have reported integer charge transfer between P3HT and F4TCNQ by observing F4TCNQ anion peaks in ultraviolet-visible and near infrared spectra of the doped system.[35,36] This property is of interest as it has the potential to lead to improved charge mobility, if the charges can overcome Coulombic attraction. Indeed, the charge transport efficiency of P3HT has been observed to increase substantially upon introduction of F4TCNQ.[24,37]

In a novel study on P3HT/F4TCNQ mixtures, Jacobs *et al.* demonstrated photophysical control over aggregation in a doped polymer thin film.[38] The team observed that mixing F4TCNQ with P3HT in solution resulted in aggregation of the polymer as it precipitated out of solution. Irradiation of this aggregated system using 405 nm light saw the polymer dissolve back into solution. Based on the observation of this phenomenon at a very specific wavelength of light, the team proposed that a photo-induced charge transfer reaction was taking place. As already mentioned, P3HT and F4TCNQ undergo spontaneous integer charge transfer upon mixing, giving $F4TCNQ^{-}$, and a hole localized over four thiophene units in P3HT.[39] At sufficient dopant concentrations, these charged species are insoluble in solvents used for P3HT. It was then postulated that photo-excitation at 405 nm excites the F4TCNQ anion, causing it to transfer the excess electron back onto P3HT. The two species are then neutral and hence the polymer may dissolve back into solution. This technique, irrespective of mechanism, is an example of using electronic modifications (i.e. the charge transfer process through introduction of a dopant) to modify physical properties (i.e. solubility and morphology of the polymer).

This technique has broad applications in industrial production of organic electronic devices using lithography. The limitations highlighted regarding photolithography do not apply to this system, as the dopant may be removed from the polymer

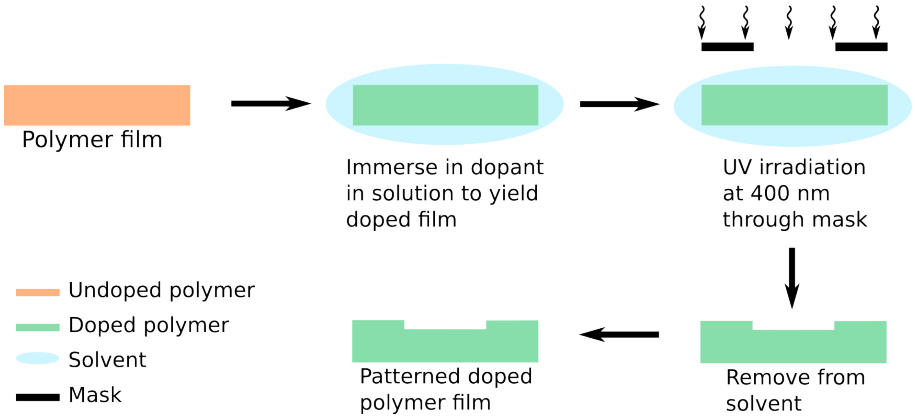

Figure 1.4: Lithographic patterning of an F4TCNQ-doped P3HT film using the photo-induced solubility change reported by Jacobs *et al.*[38]

using only a laser and a solvent to wash away the dissolved polymer. It has also recently been suggested that the removed dopant can be re-used, leading to less waste produced.[40] A schematic of the optical de-doping process is shown in Figure 1.4. Sub-diffraction-limit control over features has already been demonstrated using this technique.[41] It is also possible that analogous processes may occur in different polymer/dopant mixtures. A thorough understanding of the mechanism is hence of fundamental importance. The work presented in Chapter 4 seeks to provide insight into the mechanism of photo-induced solubility control using computational techniques.

1.2.2 Theoretical studies of the P3HT/F4TCNQ system

While experimental studies hint at interesting electronic processes, it is often not possible to elucidate electronic mechanisms or quantify the electronic properties of a given system without the aid of computer modelling. Density functional theory (DFT) calculations, for example, have been used to investigate a number of aspects of the P3HT/F4TCNQ system.

The recent experimental and computational paper by Méndez *et al.* studied the charge transfer mechanism between P3HT and F4TCNQ upon mixing of the two species.[34] Consistent with previous studies,[35,36] the team observed integer charge transfer for F4TCNQ-doped P3HT as a result of favourable alignment of the P3HT HOMO and F4TCNQ LUMO,[42,43] but a partial charge transfer complex for F4TCNQ-doped quarterthiophene. This work highlighted a key property for charge transport efficiency: chain structure. It also brought to light limitations in a great number of DFT studies on P3HT-based systems, as the polymer chain is generally represented by quarterthiophene.

Gao *et al.* used quarterthiophene to represent P3HT in their DFT studies on planarity in P3HT as a result of charge transfer with F4TCNQ.[44] Likewise, Zhu *et al.* investigated charge transfer in the P3HT/F4TCNQ system by modelling the quarterthiophene/F4TCNQ complex.[45] This latter work has been cited a number

of times, and yet in light of Méndez's work the results do not present a realistic description of charge transfer in the polymer system. In order to overcome size limitations when studying P3HT, DFT extrapolation schemes on short oligomers have been shown to reproduce a number of properties of P3HT in a semi-quantitative manner.[46] However, experimental properties of P3HT, particularly those related to doping with small molecules, tend to arise from short conjugated segments of the backbone and hence modelling the entire polymer is unnecessary and time-consuming. Furthermore, while explicit modelling of hexyl chains on P3HT yields a more physically realistic model, computational work by Chou *et al.* indicated that energy levels in the methyl-substituted polythiophene differ only slightly from P3HT itself.[47] This suggests that charge transfer in P3HT-doped F4TCNQ could be modelled using a methyl-substituted thiophene oligomer as an accurate simplified system.

While a number of DFT studies on P3HT-based systems simplify the P3HT polymer to a short oligothiophene,[44,45,48,49] little emphasis has been placed on the accuracy of this simplification. Furthermore, consistency between computational methods, i.e. basis set, functional and the inclusion of solvent effects, is not present among these studies. In this work, the process of interest is the charge transfer that occurs between polymer and dopant, and the subsequent photo-induced control over morphology. A systematic investigation into the necessary oligothiophene length for realistic modelling of the integer charge transfer doping mechanism is performed, and the importance of side chains is also considered. Because the surrounding P3HT chains are likely to affect charge transfer, implicit solvent is also considered. Finally, an investigation into density functional performance is included to highlight the importance of technical details. Details of this study may be found in Chapter 3.

1.2.3 Intermolecular interactions in the P3HT/F4TCNQ system

Charge transfer reactions are of fundamental importance in organic semiconductors, as charge transfer between polymer and dopant results in free charges that can migrate through the system, generating a current. As such, it is important to understand the charge transfer mechanism within these systems. The work by Jacobs *et al.* demonstrated that mixing F4TCNQ with P3HT results in aggregation of the P3HT and the polymer precipitates out of solution.[38] Previous studies have also observed this increase in polymer crystallinity upon doping.[24] It is likely that this aggregation, and resulting considerable decrease in polymer solubility, is a direct result of the integer charge transfer process, but the role of charge transfer in aggregation of this system has yet to be quantified and characterised.

In a recent study by Sweetnam *et al.* it was found that the strong attractive intermolecular interactions in polymer/fullerene systems are unrelated to ground state charge transfer, and instead arise from van der Waals interactions.[50] This observation is somewhat counter-intuitive, as one would expect even the partial charge

transfer that occurs in the system to result in Coulombic attraction between the charges. It is of interest to ascertain whether this behaviour is a property common to polymer/organic dopant systems, or characteristic of fullerene as a dopant. Given the integer charge transfer that occurs upon mixing in the F4TCNQ-doped P3HT system, it is anticipated that electrostatic interactions play an important role in aggregation.

DFT calculations have been used to probe quantum properties of the P3HT/F4-TCNQ system, but they cannot provide completely realistic insight into the solubility change upon photo-excitation due to the infeasibility of explicitly modelling the surrounding solvent. Classical molecular dynamics (MD) simulations, in which solvent molecules are classically and explicitly modelled, are a promising technique for quantifying the free energy of this process. A number of properties of the P3HT polymer have been investigated using classical MD simulations, including the impact of cyano-substitution on stacking distance,[51] hole mobility[52] and solvatochromic shift as a result of solvent-polymer interactions.[53] MD studies have also been used to investigate properties of P3HT mixed with fullerene and a related derivative.[54,55] However, a surprising absence of this technique is present in the literature for studying the thermodynamics of the P3HT/F4TCNQ system. As such, this work presents a novel approach to studying free energy changes purely as a result of changing the charge distribution in this system using classical MD simulations. A mixture of DFT calculations and free energy perturbation simulations is also used to quantify the free energy cost for separating the dopant from the polymer while accounting for dynamic charge distributions and quantum relaxation. Details of this work may be found in Chapter 6.

1.2.4 Stability in the P3HT/F4TCNQ system

Details of the P3HT/F4TCNQ system discussed so far present the exciting possibility of controlling polymer morphology using electronic properties. However, consideration must also be given to the stability of the resulting system. More specifically, the diffusion rate of the dopant through the polymer film and potentially into neighbouring layers may impede device longevity in any application of the photo-induced structure control technique. F4TCNQ as a dopant has been shown to diffuse readily in metal-organic systems,[42] and organic molecular systems,[56–58] particularly at high temperatures.[59] This is a concern given its widespread popularity in polymer/dopant systems.

Another property of F4TCNQ that can hinder production of F4TCNQ-doped polymers is its poor solubility in solvents commonly used for polymers. As a means to address this problem, Li *et al.* recently presented a number of F4TCNQ-based dopants with modified functional groups in place of the cyano groups,[60] some of which are shown in Figure 1.5. By substituting cyano groups with methyl-ester groups, the resulting dopants were more soluble in popular polymer solvents. These dopants are also potentially less prone to diffusion. A decrease in diffusion is hy-

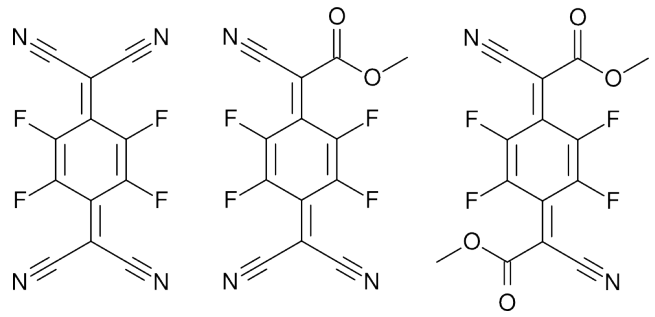

Figure 1.5: F4TCNQ (left) and the monoester-substituted (centre) and diester-substituted variants (right).

pothesised in particular for the diester substituted dopant, which has been shown to undergo a dimerisation reaction prior to doping the polymer, resulting in a much bulkier structure. However, it is possible that the added bulk of the methyl group on the monoester-substituted dopant can also improve its stability to diffusion due to unfavourable interactions between polymer side chains and the methyl group on the dopant.

DFT calculations are once again exploited in this work in order to quantify the energy barrier to translation of dopant molecules along the P3HT polymer backbone. Such a methodology is not found in the literature for doped organic semiconductor systems, and yet has the potential to provide at least a qualitative insight into stability of polymer/dopant systems with respect to dopant diffusion. The monoester-substituted analogue of F4TCNQ is compared with F4TCNQ itself and the energy barrier to translation, and hence translational diffusion, is quantified. Details of this work are presented in Chapter 5.

2 | Computational methods

2.1 Density functional theory

2.1.1 Technical details

Density functional theory is a powerful technique for accurately modelling static properties of a molecular system in an efficient manner. Electronic properties of a molecular system play an important role in determining both structural properties and reactivity of the system. While experimental observations can provide some insight into these characteristics, many questions cannot be answered experimentally. In order to understand the experimental observations, computational studies are often required.

Finding the true minimum energy of a specific geometry of a molecule requires the formidable task of solving the $3N$-dimensional electronic Schrödinger equation (Equation 2.1), where N is the number of electrons within the system. Within this equation, the electronic state of the system is described by the electronic wave function, ψ, and the Hamiltonian, H, comprises five energetic components: electron kinetic, nuclear kinetic, electronic-nuclear interaction, electron-electron interaction and nucleus-nucleus interaction energies, respectively, as shown in Equation 2.2.[61]

$$H\psi = E\psi \tag{2.1}$$

$$H = -\frac{\hbar^2}{2m_e}\sum_{i=1}^{N}\nabla_i^2 - \frac{\hbar^2}{2m_I}\sum_{I=1}^{M}\nabla_I^2 - \sum_{I=1}^{M}\sum_{i=1}^{N}\frac{Z_I e^2}{4\pi\epsilon_0 r_{Ii}} + \sum_{i=1}^{N-1}\sum_{j>i}^{N}\frac{e^2}{4\pi\epsilon_0 r_{ij}} + \sum_{I=1}^{M-1}\sum_{J>I}^{M}\frac{Z_I Z_J e^2}{4\pi\epsilon_0 r_{IJ}} \tag{2.2}$$

Lower case subscripts refer to electronic contributions, while upper case subscripts refer to nuclear contributions. Z_I and m_I refer to the valency and mass of a nucleus, respectively, m_e is the mass of an electron, r is the separation between electrons or nuclei and ϵ_0 is the vacuum permittivity.

The Born-Oppenheimer approximation notes that nuclei are more massive than electrons and hence move much slower, which in this instance means that the Schrödinger equation can now be solved in two parts: first the electronic motion is

considered, and then the electron-nuclear interactions. Furthermore, nucleus-nucleus interaction energy can be considered constant on the timescale of interest. A Hartree product is often used to simplify the problem, by splitting the total wave function into a product of one-electron wave functions, i.e. $\psi = \psi_1(\boldsymbol{r})\psi_2(\boldsymbol{r})...\psi_N(\boldsymbol{r})$. However, solving this many-body problem remains insurmountable for large molecules.

Seminal work by Hohenberg and Kohn proved two theorems which define the field of density functional theory, and make it possible to find a solution to the Schrödinger equation for large multi-atom systems. The first states that there is a unique functional of electron density that corresponds to the ground state energy obtained from the Schrödinger equation.[62] This reduces the problem to one of finding a three-dimensional electron density. The second theorem of Hohenberg and Kohn proves that the electron density that minimises the energy functional is the true solution to the Schrödinger equation. Unfortunately, although it certainly exists, the form of the density functional is unknown.

In the absence of the true density functional, Kohn-Sham theory instead replaces the potential of the real system with an effective potential for a system of non-interacting electrons with the same density. All electrons in the system are described using separate Kohn-Sham orbitals. The electron density in this system, subject to the effective potential, is then equivalent to the electron density of the real system upon solving the Kohn-Sham equations[61]

$$\Big[-\frac{\hbar^2}{2m}\nabla^2 + V[\rho] + V_{\mathrm{H}}[\rho] + V_{\mathrm{XC}}[\rho]\Big]\psi_i(\boldsymbol{r}) = \epsilon_i\psi_i(\boldsymbol{r}). \tag{2.3}$$

$V[\rho]$ describes the component of the energy functional that is known, while $V_{\mathrm{H}}[\rho]$ is the Hartree potential, and describes the interactions between a given electron and the electron density that arises from all other electrons in the system. The nature of this potential is such that it also includes an erroneous interaction energy of the electron with itself, which is accounted for in the $V_{\mathrm{XC}}[\rho]$ potential. As well as this correction, the potential also describes electron exchange, which reproduces the change in wave function sign upon interchange of two electrons, and electron correlation, which describes many-body electronic interactions within the system. This potential is an approximation as a result of not knowing the true energy density functional.

The Kohn-Sham equations are solved self-consistently, as V_{H} and V_{XC} depend on the electron density, $\rho(\boldsymbol{r})$, which depends on the Kohn-Sham orbitals.[61]

$$\rho(\boldsymbol{r}) = \sum_{i}^{occ} \psi_i^*(\boldsymbol{r})\psi_i(\boldsymbol{r}) \tag{2.4}$$

2.1.2 Density functionals

The accuracy of any results obtained from density functional theory calculations depend on how the exchange correlation term of the Kohn-Sham equations is de-

scribed. Practically, there are a number of ways in which this term is approximated. The simplest approximation is to use a continuous function to define the functional at each point in the system based upon the exact functional found in a uniform electron gas, which is known. This is called the local density approximation (LDA). Improvements on this approximation can be made by including the gradient and Laplacian of the electron density, denoted the generalized gradient approximation (GGA) and meta-GGA, respectively.

The Hartree-Fock exchange (HF) potential is an exact description of electron exchange and is given by

$$V^{HF}(\boldsymbol{r}) = -\frac{1}{2}\sum_{i,j}^{occ}\int d\boldsymbol{r}\int d\boldsymbol{r}'\frac{\phi_i^*(\boldsymbol{r})\phi_j^*(\boldsymbol{r}')\phi_j(\boldsymbol{r})\phi_i(\boldsymbol{r}')}{|\boldsymbol{r}-\boldsymbol{r}'|} \tag{2.5}$$

Hybrid functionals approximate the exchange correlation functional by mixing in a portion of exact exchange, E^{HF}, with LDA or GGA functionals.

By far the most commonly used functional in the literature, the Becke three-parameter Lee-Yang-Parr[63] (B3LYP) functional, is an example of a hybrid functional, and its exchange-correlation potential is

$$\begin{aligned} V_{\mathrm{XC}}^{\mathrm{B3LYP}} = V_{\mathrm{XC}}^{\mathrm{LDA}} &+ \alpha_1(V^{\mathrm{HF}} - V_{\mathrm{X}}^{\mathrm{LDA}}) \\ &+ \alpha_2(V_{\mathrm{X}}^{\mathrm{GGA}} - V_{\mathrm{X}}^{\mathrm{LDA}}) + \alpha_3(V_{\mathrm{C}}^{\mathrm{GGA}} - V_{\mathrm{C}}^{\mathrm{LDA}}) \end{aligned} \tag{2.6}$$

The subscripts X and C correspond to the exchange and correlation functionals, respectively, while the α values are scaling constants chosen to provide optimal parameters for a range of sample systems. The B3LYP functional is hence classified as empirical, and its performance for a given system will depend on how close the system is to the test suite for which these α parameters were optimised. Note also that here $V_{\mathrm{X}}^{\mathrm{GGA}}$ and $V_{\mathrm{C}}^{\mathrm{GGA}}$ are the Becke88 exchange functional[64] and Lee-Yang-Parr correlation functional,[65] respectively.

One aspect that a great number of LDA, GGA and hybrid functionals fail to capture is the van der Waals interactions in dispersion bound systems.[66] This is a result of their inability to accurately describe long-range electron correlation. As a means to combat this, a number of dispersion correction schemes have been implemented into computational quantum chemistry packages as the DFT-D method.[67,68] This method makes an adjustment to the total energy of the system by adding a dispersion energy term. In this work, Grimme's D2 dispersion correction is included,[67] as it has previously been used successfully for a small P3HT/F4TCNQ complex.[45] The dispersion energy term is of the form

$$E_{\mathrm{disp}} = -s_6\sum_{i=1}^{N_{\mathrm{a}}-1}\sum_{j=i+1}^{N_{\mathrm{a}}}\frac{C_6^{ij}}{R_6^{ij}f_{\mathrm{damp}}(R_{ij})}, \tag{2.7}$$

where s_6 is a scaling factor unique to the chosen functional, N_a is the number of atoms in the system, C_6^{ij} is the dispersion coefficient for the atom pair ij, R_6^{ij} is the interatomic distance and f_damp is the damping function. This function is of the form

$$f_\mathrm{damp}(R_{ij}) = \frac{1}{1+\mathrm{e}^{-d(R_{ij}/R_\mathrm{r}-1)}}, \tag{2.8}$$

where R_r is the sum of atomic radii and d is a coefficient that determines the steepness of the damping function. For the B3LYP functional, $s_6 = 1.05$ and $d = 20$. For the majority of the work presented in this dissertation, the B3LYP functional is used with this dispersion correction scheme, and denoted B3LYP-D.

As a result of their consistent performance, recent focus has shifted to range-corrected methods. Range-correction is applied as a way to reproduce the r^{-1} scaling of Coulombic interactions at large distances, and is accomplished by splitting the the description of these interactions into short-range and long-range components using the standard error function[69]

$$\frac{1}{r} = \frac{1-\mathrm{erf}(\omega r)}{r} + \frac{\mathrm{erf}(\omega r)}{r}. \tag{2.9}$$

The functional can then incorporate a small portion of HF exchange at short range, and 100 % HF at long range. The ω value determines the decay to zero of the short-range component, which scales with $1/\omega$. In certain software packages it is possible to tune ω for the chosen system, resulting in substantially improved performance, as the optimal value is highly system dependent.[70–72] The long-range-corrected exchange correlation functional, $V_\mathrm{XC}^\mathrm{LRC}$, can be written as

$$V_\mathrm{XC}^\mathrm{LRC} = V_\mathrm{C} + (1-C_\mathrm{HF})V_\mathrm{X,GGA}^\mathrm{SR} + C_\mathrm{HF}V_\mathrm{X,HF}^\mathrm{SR} + V_\mathrm{X,HF}^\mathrm{LR}, \tag{2.10}$$

where the superscripts SR and LR correspond to short and long range components of the functional, and C_HF corresponds to a coefficient that determines the % HF included at short range. Recent work by Rohrdanz *et al.* considered the long-range-corrected version of the hybrid Perdew-Burke-Ernzerhof functional (LRC-ωPBEh) and found $C_\mathrm{HF} = 0.2$ to be optimal.[70] This value of C_HF is used when performing calculations with the LRC-ωPBEh functional throughout this dissertation.

2.1.3 Basis sets

The Kohn-Sham orbitals used to solve for the minimised energy of the system are described using basis functions, ϕ. Gaussian type orbitals[73] (GTOs) are often used to describe these basis functions, and in normalised Cartesian coordinates these take the form[74]

$$\phi(x,y,z;\alpha,i,j,k) = \left(\frac{2\alpha}{\pi}\right)^{3/4}\left[\frac{(8\alpha)^{i+j+k}i!j!k!}{(2i)!(2j)!(2k)!}\right]^{1/2} x^i y^k z^k \mathrm{e}^{-\alpha(x^2+y^2+z^2)}, \tag{2.11}$$

where α controls the width of the GTO and i, j and k control the shape of the orbital.

Electrons on any atom type can be described by s, p, d, ... functions, formed when i, j and k all equal zero (s-function), one of them is equal to one (p-function), two of them are equal to one (d-function), and so on. The collection of all of these basis functions is called a basis set. Improvements to accuracy can be made by using a double, triple, quadruple, ... ζ basis set, where each level includes an additional set of equivalent orbitals on a given atom. Including these extra functions allows for accurate description of directionality within bonds. Further improvement can be made by including polarisation functions, in which higher angular momentum functions are added.

Diffuse functions are necessary when the property of interest involves the tail of the orbital, far from the nucleus. GTOs decay too rapidly away from the nucleus to accurately describe this tail, and hence diffuse functions are added. These functions are beneficial when electron density within the system is spatially extended, such as in the case of anions.

In order to avoid unnecessary calculations on core electrons, whose properties do not have a significant impact on the chemistry of the system, these orbitals are described using optimised but constant exponents. This results in a contracted basis set. There are numerous ways in which basis sets may be contracted, giving rise to Pople,[75] Dunning[76] and Ahlrichs basis sets,[77] among others.

In the majority of this work, the Pople-type basis set 6-31G(d) is used. This basis set is a split-valence double-zeta basis set, meaning higher angular momentum basis functions are added to all atoms and additional basis functions are added to valence orbitals only. It includes six GTO basis functions on core electrons, three on inner valence electrons and one on outer valence electrons. Polarisation functions (denoted "(d)" and here representing d-functions) are added to non-hydrogen atoms to improve directionality in bonds. p-functions are not included on hydrogen atoms due to the added computational cost, and the fact that the hydrogen atoms play a minimal role in the properties of interest in this work. Later calculations in this work also include diffuse functions (denoted "+") in order to improve the long-range description of electron density.

2.1.4 Constrained density functional theory

In a regular DFT calculation, the optimal electron density is found in a given external potential, $V[\rho]$, which was discussed above as the "known" potential (Equation 2.3). Alternative ground states of the system can be found in the presence of different external potentials. Constrained density functional theory[78] (CDFT) calculations allow for the optimal electron density to be found subject to constraints on location of electron density or spin. The electron density, $\rho(\boldsymbol{r})$, is weighted by a spatially

varying function, $w_{\mathrm{L}}^{\sigma}(\boldsymbol{r})$, to enforce the constraint

$$\sum_{\sigma} \int w_{\mathrm{L}}^{\sigma}(\boldsymbol{r}) \rho^{\sigma}(\boldsymbol{r}) d\boldsymbol{r} = N_{\mathrm{L}}, \tag{2.12}$$

where σ refers to the spin state (α or β) and N_{c} is the number of electrons in the system. A Lagrange multiplier can then be implemented in order to minimise the energy of the system, $W[\rho, V_{\mathrm{L}}]$, subject to this density constraint, i.e.

$$W[\rho, V_{\mathrm{L}}] = E[\rho] + V_{\mathrm{L}}\Big(\sum_{\sigma} \int w_{\mathrm{L}}^{\sigma}(\boldsymbol{r}) \rho^{\sigma}(\boldsymbol{r}) d\boldsymbol{r} - N_{\mathrm{L}} \Big). \tag{2.13}$$

Here $E[\rho]$ is the electronic energy of the unconstrained system, and V_{L} is the Lagrange multiplier. It is then possible to obtain a modified version of the Kohn-Sham equations, which can be solved to give the optimised electron density (and hence geometry) subject to the constraint:

$$\Big[-\frac{\hbar^2}{2m}\nabla^2 + V[\rho] + V_{\mathrm{H}}[\rho] + V_{\mathrm{XC}}[\rho] + V_{\mathrm{L}} w_{\mathrm{L}}^{\sigma}(\boldsymbol{r}) \Big] \psi_i(\boldsymbol{r}) = \epsilon_i \psi_i(\boldsymbol{r}) \tag{2.14}$$

In this work, CDFT is used to apply a charge constraint on F4TCNQ within the dimer complex. In order to elucidate the energy and geometry differences between ground state and the state in which each of the molecules in the dimer complex is neutral (which will be referred to as the "charge-neutral state" for brevity), a constraint of zero charge is applied to F4TCNQ, with an implicit constraint also applied to the oligomer. To evaluate the metastability of this charge-neutral state, various fractional charges between zero and one are applied to F4TCNQ.

2.1.5 Excited states: time-dependent density functional theory

Time-dependent density functional theory (TDDFT) is a technique capable of providing moderately accurate excitation energies in a highly efficient manner. Properties of a system interacting with a field that varies with time, for example representing light-matter interactions, can be investigated by solving the time-dependent version of the Kohn-Sham equations[79]

$$\Big[-\frac{\hbar^2}{2m}\nabla^2 + V_{\mathrm{ext}}[\rho; t] + V_{\mathrm{H}}[\rho; t] + V_{\mathrm{XC}}[\rho; t] \Big] \psi_i(\boldsymbol{r}, t) = i\hbar \frac{\partial \psi_i(t)}{\partial t}. \tag{2.15}$$

Here $V_{\mathrm{XC}}[\rho; t]$ also contains information about the history of the density, and ground-state exchange correlation functionals may be used for this term.

This methodology is made possible as a result of a theorem by Runge and Gross,[80] which states that there is a one-to-one mapping between the time-dependent potential $V_{\mathrm{ext}}[\rho; t]$ and the electron density, $\rho(\boldsymbol{r}, t)$. By solving the Kohn-Sham equations for the time-dependent system, excitation energies may be extracted. For a

more in-depth derivation and discussion of excited state methods, the reader is referred to a comprehensive review by Dreuw and Head-Gordon.[81]

It is important to note that TDDFT has some shortcomings, not least of which is its limited ability to accurately describe charge transfer interactions when standard density functionals are used.[82,83] This has been attributed to the poor asymptotic behaviour of the exchange-correlation potential, which does not decay with r^{-1} in standard functionals as required. Using a range-corrected functional is one possible solution to this problem.[84] Because the excited states of interest in Chapter 4 are indeed charge transfer excitations, both the common B3LYP functional and the optimally tuned, range corrected LRC-ωPBEh functionals are used for all calculations. In this way, the anticipated poor behaviour of the B3LYP functional can be accounted for.

Excited state geometry optimisation

Single-point TDDFT calculations use the electron density of the given geometry, and do not modify the nuclear positions of the system. However, the state of interest may display different structural or electronic properties upon relaxation. In this case an excited state geometry optimisation can be performed.

The electron density obtained from ground state DFT calculations is a linear combination of Kohn-Sham orbitals. In order to relax the system into an excited state, the system is progressively relaxed to each excited state, and then the vector contributions of each excited state are projected out to yield the optimised electron density of the excited state of interest.

In this work, an excited state geometry optimisation is performed on an excited state of the dimer complex. The property of interest in this state is the charge distribution, which is obtained using Mulliken charge analysis.

Natural transition orbitals

Natural transition orbitals[85] (NTOs) are used to visualise and quantify excitations. These provide a more accurate description of the change in electron density upon excitation than inspection of molecular orbitals.[86] A TDDFT calculation yields a transition density matrix, $\mathbf{T}$, with elements describing coupling between ground, ψ_0, and excited, ψ_{exc}, states. A unitary transform[87] is applied to to all occupied, N_0, and virtual, N_v, orbitals:

$$(\phi_1, \phi_2, ..., \phi_{N_0}) = (\psi_1, \psi_2, ..., \psi_{N_0})\mathbf{U}, \tag{2.16}$$

$$(\phi'_1, \phi'_2, ..., \phi'_{N_\text{v}}) = (\psi'_1, \psi'_2, ..., \psi'_{N_\text{v}})\mathbf{V}, \tag{2.17}$$

and the vectors $\mathbf{U}$ and $\mathbf{V}$ are solved for using

$$\mathbf{T}\mathbf{T}^\dagger u_i = \lambda_i u_i, i = 1, ..., N_0, \tag{2.18}$$

$$\mathbf{T}^{\dagger}\mathbf{T}v_i = \lambda_i' v_i, i = 1, ..., N_v. \tag{2.19}$$

The λ eigenvalues represent the importance of a given particle-hole contribution to the overall transition. In this context, the hole and particle refer to the "before" and "after" electron densities, such that considering a hole to particle transition provides insight into where the electron density has moved during the excitation. This methodology can hence provide a clearer picture as to the qualitative characteristics of a transition. The nature of possible charge transfer excitations is evaluated in Chapter 4 using this method.

2.1.6 Solvent models

All aspects of DFT discussed so far provide insight into gas-phase properties of the modelled system. However, the presence of solvent can dramatically affect bond lengths, charge distributions and structural conformations. An efficient way to include solvent effects is by introducing a dielectric medium, with dielectric constant, ϵ, equal to that of the required solvent, around the solute by means of an electric field.

In all continuum solvent models, a cavity in the dielectric medium is constructed around the solute, and the interaction of the solute charge distribution with the dielectric medium affects the charge distribution and dipole of the solute. Polarisable continuum models (PCMs) create this cavity by summing the space generated by scaled van der Waals radii on each atom. The surface of the cavity is divided into fragments, and the charge distribution on the solute is mapped onto this collection of fragments, with the charge on each section quantified by $\sigma(\boldsymbol{r}_s)$[88]

$$4\pi\epsilon\sigma(\boldsymbol{r}_s) = (\epsilon - 1)\boldsymbol{F}(\boldsymbol{r}_s), \tag{2.20}$$

where $\boldsymbol{F}$ represents the electric field.

PCMs differ in the linear equations used to map the charge distribution of the solute onto the surface of the cavity. In all cases these equations take the form

$$\mathbf{Kq} = \mathbf{Rv}, \tag{2.21}$$

where $\mathbf{q}$ represents the cavity surface charges and $\mathbf{v}$ represents the charges on the solute. $\mathbf{K}$ and $\mathbf{R}$ take different forms depending on the specific model, but generally one or both involve contributions from a matrix $\mathbf{S}$ of Coulomb interactions, a matrix $\mathbf{D}$ containing information about the electric field and a matrix $\mathbf{A}$ containing surface areas of the discrete fragments of the cavity. The form of the screening factor, f_ϵ, also differs between models.

In this work, two PCMs are used: the more simplistic conductor-like PCM (CPCM),[89] and the more computationally intensive integral equation formalism PCM (IEFPCM).[90,91] The matrices $\mathbf{K}$ and $\mathbf{R}$ and the screening factor, f_ϵ, for CPCM

and IEFPCM, respectively, are[92]

$$\mathbf{K} = \mathbf{S}, \mathbf{R} = -f_\epsilon \mathbf{1}, f_\epsilon = \frac{\epsilon - 1}{\epsilon} \tag{2.22}$$

$$\mathbf{K} = \mathbf{S} - \frac{f_\epsilon}{2\pi}\mathbf{DAS}, \mathbf{R} = -f_\epsilon(\mathbf{1} - \frac{1}{2\pi}\mathbf{DA}), f_\epsilon = \frac{\epsilon - 1}{\epsilon + 1}. \tag{2.23}$$

Excitation of an implicitly solvated system results in a change in charge distribution, as the electrons are affected by the excitation potential. However, the nuclei of the system remain unaffected. This results in the solute no longer being in equilibrium with the surrounding medium. Linear response TDDFT may be applied to a PCM system, within which solute-solvent interactions are described by Coulomb interactions only. This method is widely used due to its ability to efficiently reproduce excited state properties of solvated systems, wherein the solvent properties are modelled using a PCM, to within a fraction of an eV of results obtained with higher cost wave function methods.[93,94] This technique is applicable in systems where excited states do not exhibit specific interactions with solvent molecules. The dielectric constant is given by the optical, rather than static, dielectric constant in order to capture non-equilibrium effects, which provides a reasonable approximation to the behaviour of the solvent upon excitation. The linear equations from Equation 2.21 used to describe the cavity charges then become[95]

$$\mathbf{K}_{\epsilon_\infty}\mathbf{q}_i^{\text{fast,LR}} = \mathbf{R}_{\epsilon_\infty}\mathbf{v}(\rho_i^{\text{tr}}), \tag{2.24}$$

where ϵ_∞ is the optical dielectric constant of the solvent. The charge distribution $\mathbf{q}_i^{\text{fast,LR}}$ now corresponds to the distribution of state i subject to a fast response to excitation, and ρ_i^{tr} is the transition surface charge density for state i.

2.1.7 Thermodynamic correction

Typical quantum calculations on a small molecular system using DFT provide only the electronic energy of the system, and do not consider molecular contributions from translational, rotational and vibrational energies. These contributions can be quantified in order to provide a correction to the free energy due to the finite temperature. Statistical mechanics allows for the definition of a partition function, Q, which contains information about all energy levels within the ensemble. From this partition function, the potential energy, enthalpy, entropy and Gibbs free energy of a given system can be defined using the following equations[74]

$$U = k_\text{B}T^2\left(\frac{\partial \log Q}{\partial T}\right)_{N,V} \tag{2.25}$$

$$H = U + PV \tag{2.26}$$

$$S = k_{\mathrm{B}}T\log Q + k_{\mathrm{B}}T\left(\frac{\partial \log Q}{\partial T}\right)_{N,V} \tag{2.27}$$

$$G = H - TS. \tag{2.28}$$

The ensemble partition function can be simplified to the molecular partition function, q, and the aforementioned energy contributions are assumed to be independent of each other such that q is the product of partition functions for each component. Chapter 10 in ref 74 provides a detailed explanation of the derivation of partition functions. Quantum chemistry packages evaluate thermodynamic corrections using frequency calculations, and in this work the methodology used in Q-Chem is applied.[96] Frequency calculations are used in Chapter 6 to obtain the entropic, enthalpic and free energy contributions to the separation of a two-component system.

2.2 Molecular dynamics

2.2.1 Equilibrium simulations

The previous section of this chapter highlighted how the quantum properties of a molecular system can be investigated using Kohn-Sham density functional theory. Unfortunately, these methods are far too computationally expensive to be applied to a condensed-phase system containing thousands or tens of thousands of atoms. Many important and interesting dynamic properties are the result of larger-scale interactions. Classical molecular dynamics simulations provide a means to study some of these interesting properties in an efficient manner by disregarding the quantum properties of a system and describing the entire system using classical mechanics.

Classical molecular dynamics simulations solve Newton's equations of motion for a system of N particles. The mass of a nucleus is large enough that it may be treated classically, the electrons are described using point charges, and all bonded and non-bonded interactions are modelled using potentials. The position and momentum of every atom in the system is recorded at each discrete time step of the simulation. These quantities are then updated by solving Newton's second equation,[97]

$$-\frac{dV}{d\boldsymbol{r}} = m\frac{d^2\boldsymbol{r}}{dt^2} \tag{2.29}$$

where $\boldsymbol{r}$ is the coordinates of the given atom, and V is the potential energy at those coordinates.

The force on each atom is a combination of bonded and non-bonded interactions (Equation 2.30). A force field is used to set the parameters associated with bonded potentials between standard atom types. Such a methodology allows for the flexibility of bonds to be reproduced.

$$V_{\mathrm{total}} = V_{\mathrm{bonded}} + V_{\mathrm{non-bonded}} \tag{2.30}$$

$$V_{\text{bonded}} = V_{\text{bond}} + V_{\text{angle}} + V_{\text{dihedral}} + V_{\text{improper}} \tag{2.31}$$

$$V_{\text{non-bonded}} = V_{\text{electrostatic}} + V_{\text{vanderWaals}} \tag{2.32}$$

In this work, the OPLS all-atom (OPLS-AA) force field is used,[98] as it has been found to be accurate for organic semiconductors.[99] The torsional potentials in this force field were parametrised against Hartree-Fock quantum calculations, and bond and angle potentials were adapted from the Amber all-atom force field.[100]

Within the OPLS-AA force field, bond and angle potentials (V_{bond} and V_{angle}) are modelled using the following two equations:

$$V_{\text{bond}} = K_{\text{r}}(r - r_{\text{eq}})^2 \tag{2.33}$$

$$V_{\text{angle}} = K_{\theta}(\theta - \theta_{\text{eq}})^2, \tag{2.34}$$

where K_{r} and K_{θ} are force constants. For most of the polymer and all of the F4TCNQ dihedral interactions, a dihedral potential of the following form is used:

$$V_{\text{dihedral}} = \sum_{n=1}^{5} A_n \cos^{n-1}(\phi), \tag{2.35}$$

where the A_i terms are constants and ϕ is the dihedral angle. For the inter-monomer torsion potential, the following expression is used:

$$V_{\text{dihedral}} = \sum_{n=0}^{8} C_n \cos^{n}(\phi) \tag{2.36}$$

The parametrisation of this potential is based on quantum calculations.[101] Finally, a harmonic torsional potential was applied to maintain thiophene unit planarity, in accordance with the OPLS-AA force field:

$$V_{\text{dihedral}} = K_{\phi}[1 + d\cos(n\phi)]. \tag{2.37}$$

In this work, proper dihedral angles are described using Equations 2.35 and 2.36, while improper dihedral angles are described using Equation 2.37.

Long-range van der Waals interactions is described using a Lennard Jones (LJ) potential in the OPLS-AA force field

$$V_{\text{vanderWaals}} = 4\epsilon_{ij}\left[\left(\frac{\sigma_{ij}}{r_{ij}}\right)^{12} - \left(\frac{\sigma_{ij}}{r_{ij}}\right)^{6}\right], \tag{2.38}$$

and electrostatic interactions may be added to model charge interactions

$$V_{\text{electrostatic}} = \frac{q_i q_j}{4\pi\epsilon_0 r_{ij}}. \tag{2.39}$$

Here ϵ_{ij} and σ_{ij} are energy and distance constants characteristic of the i, j pairwise interaction, and here are taken from the OPLS-AA force field. The charges on particle i and j are represented by q_i and q_j, respectively, and r_{ij} is the distance between the i and j particles.

In principle, the non-bonded pairwise force interactions for each pair of particles in the system must be evaluated in order to realistically update the position of each atom. In practice, simplifications can be made. Dispersion interactions are subject to a cut-off, r_c, such that for pairs whose inter-atom distance exceeds this cut-off, no pairwise force is calculated. To avoid discontinuities at this cut-off point, a shifting function can be, and in this work is, applied.

Periodic boundary conditions are often used in MD simulations, because they remove the problem of edge effects, i.e. atoms in the system bumping into the edges of the simulation box. This is particularly important for small systems in which the surface area to volume ratio is quite large. They do this by requiring that if a particle passes through a wall of the box, it appears immediately directly on the other side of the simulation box (Figure 2.1). Where periodic boundary conditions are included, only nearest-image interactions are computed for short-range non-bonded interactions, that is, an atom only interacts with the closer of the particles, even if that particle is a periodic image of a particle in the true system. However, the long-range electrostatic interactions are generally computed using Ewald summation, which allow for accurate reproduction of these interactions for an infinite periodic system since electrostatic interactions cannot be cut off without an infinite error to the thermodynamics of the system.

In this work the particle-particle particle-mesh (PPPM) method[102] is used rather than Ewald summation. This method uses fast Fourier transform to evaluate the long-range electrostatic interactions, which are described using a periodic function and evaluated on a lattice.

The thermodynamic conditions of the system must also be specified. In this work, NPT simulations are performed, within which the number of particles, N, the pressure, P and the temperature T are all constant. A Nosé-Hoover barostat and thermostat are used, respectively, to enforce the latter two constraints.[103,104] This is done by including an additional fictitious coordinate with an effective mass within the system, one for the thermostat and one for the barostat. These coordinates undergo the equations of motion so that the system is consistent with the thermodynamic ensemble. Unless otherwise specified, all simulations presented in this work are performed in an isothermal-isobaric ensemble at an average temperature of 298 K and an average pressure of 0 atm. The latter constraint is, for all intents and purposes, equivalent to standard conditions of 1 atm, since the pressure fluctuations in molecular simulations are typically much larger than 1 atm. In this work the simulation timestep is set to 1 fs. The temperature is relaxed over 100 fs and the pressure is relaxed over 1000 fs.

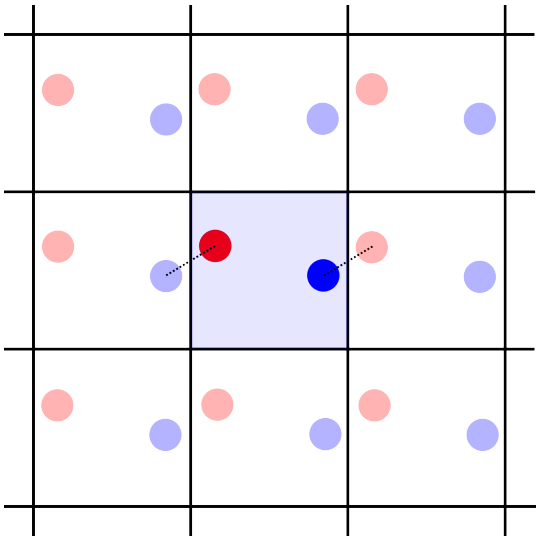

Figure 2.1: The true simulation box (shaded) is surrounded by periodic images of the same box in all directions. Short-range pairwise interactions are calculated between nearest-neighbour pairs, irrespective of whether the nearest neighbour is a periodic image, while long-range electrostatic interactions are evaluated using the PPPM method.

2.2.2 Steered molecular dynamics

It is sometimes of interest to study free energy changes along a reaction pathway. In this instance the efficiency of sampling of the trajectory of the system along this pathway to obtain the free energy can be substantially increased by using steered MD (SMD) simulations.[105] SMD simulations allow for the introduction of a steering force, which guides a simulation along the pathway of interest. When combined with Jarzynski's equality[106]

$$\mathrm{e}^{-\beta\Delta F} = \langle \mathrm{e}^{-\beta W} \rangle, \tag{2.40}$$

where $\beta = 1/k_{\mathrm{B}}T$, this technique is particularly powerful, as it makes it possible to obtain the equilibrium free energy of a process, ΔF, by averaging the work, W, obtained from a number of non-equilibrium simulations.[107,108]

The steering force is introduced by means of a harmonic spring potential. This potential constrains the reaction coordinate, $\xi(\mathbf{r})$, to be close to an external parameter λ by adding the following potential to the Hamiltonian:[107]

$$h(\mathbf{r};\lambda) = \frac{k}{2}[\xi(\mathbf{r}) - \lambda]^2. \tag{2.41}$$

λ is then varied over the course of the simulation, and the potential of mean force (PMF), $\Phi(\lambda_t)$, can be estimated.[108] The PMF is equal to ΔF in Equation 2.40. The PMF of a process provides a free energy profile of the system with respect to the changing value of λ, and by extension the reaction coordinate $\xi(\mathbf{r})$.

In Equation 2.40 the exponential of the work from a number of simulations is

averaged. However, the exponential average can give poor statistical error, and as such a common practice is to approximate it when obtaining the PMF with a cumulant expansion

$$\log\langle \mathrm{e}^{-\beta W}\rangle = -\beta\langle W\rangle + \frac{\beta^2}{2}(\langle W^2\rangle - \langle W\rangle^2) + \dots \,. \tag{2.42}$$

The second order cumulant expansion,

$$\Psi_M = \frac{1}{M}\sum_{i=1}^{M} W_i - \frac{\beta}{2}\frac{M}{M-1}\left[\frac{1}{M}\sum_{i=1}^{M} W_i^2 - \Big(\frac{1}{M}\sum_{i=1}^{M} W_i\Big)^2\right], \tag{2.43}$$

has been demonstrated to provide smaller statistical error for simulations with a small number of trajectories.[107] Both the second order cumulant expansion and the exponential average will be considered in this work.

In Chapter 6 SMD simulations are used to investigate the free energy change for separation of F4TCNQ dopant from P3HT polymer in chloroform. In these simulations, the reaction coordinate, $\xi(\mathbf{r})$, is the physical coordinates of the centre of mass of the F4TCNQ molecule within the simulation box. For simplicity, the F4TCNQ molecule is pulled, using the harmonic spring potential, from a separation of 30 Å to a separation of 5 Å from the centre of mass of the eight-unit 3-hexylthiophene, $(3HT)_8$, molecule used to represent P3HT. In these simulations λ represents the centre-of-mass (COM) separation of the $(3HT)_8$ and F4TCNQ molecules.

Exponential averaging is also applied in order to approximate the free energy of the process, ΔF_M,

$$\Delta F_M = -\frac{\beta}{2}\log\left[\frac{1}{M}\sum_{i=1}^{M} e^{-\beta W_i}\right], \tag{2.44}$$

along the PMF energy profile.

2.2.3 Alchemical free energy perturbation theory

Alchemical free energy perturbation (FEP) simulations[109] allow for the free energy of a process to be determined by estimating the energy change along an unphysical path in which atoms are created, destroyed or modified along the path. While it is possible to estimate the free energy of a process by taking an exponential average of the difference in energies of the end points. The accuracy of the result tends to be quite poor, particularly if the two states differ substantially in configuration. The free energy of the process relates to the difference in potential energy of the system calculated in its initial state configuration only. If states 0 and 1 (initial and final) differ substantially in configuration, the two are said to have poor phase space overlap and the resulting free energy does not well approximate the true free energy difference between the two states.

Phase space overlap can be improved by considering a series of $n-2$ intermediate states between the initial and final states that do not necessarily make chemical sense

and differ in configuration only slightly from one another. Because free energy is a state function, the total free energy change for the process, $\Delta F_{0,1}$, can then be related to the sum of the sequential changes in potential energy, $\Delta U_{i,i+1}$, where i is an intermediate state between states 0 and 1[97]

$$\Delta F_{0,1} = -k_{\mathrm{B}}T \sum_{i=1}^{n-1} \log\left\langle \mathrm{e}^{-\beta \Delta U_{i,i+1}} \right\rangle_i. \tag{2.45}$$

The similarity between sequential states now ensures that the change in potential energy is small between steps.

This methodology is applied in molecular dynamics simulations by introducing a coupling parameter λ, which is used to move the simulation between the n states of the system. The progression through these states may correspond to, for example, a change in non-bonded interaction potentials or atomic charges.

Care must be taken when scaling interaction potentials to or from zero, as singularities in the mathematical description of these potentials necessarily occur at this point. To circumvent the system exploding, a "soft" potential may be used to describe non-bonded interactions. The aforementioned Lennard-Jones potential with the additional Coulombic term can be corrected to a "soft" potential as follows:

$$V_{\mathrm{non-bonded}} = \lambda^2 4\epsilon_{ij} \left\{ \frac{1}{\left[\alpha_{\mathrm{LJ}}(1-\lambda)^2 + \left(\frac{r_{ij}}{\sigma_{ij}}\right)^6\right]^2} - \frac{1}{\left[\alpha_{\mathrm{LJ}}(1-\lambda)^2 + \left(\frac{r_{ij}}{\sigma_{ij}}\right)^6\right]} \right\} + \lambda^n \frac{q_i q_j}{4\pi\epsilon_0 \sqrt{\alpha_{\mathrm{C}}(1-\lambda)^2 + r_{ij}^2}}. \tag{2.46}$$

The additional parameters α_{LJ} and α_{C} are scaling factors only, and are set to the recommended values of 0.5 and 10.0, respectively, in this work. A value of $n = 1$ is also used in this work. The λ coupling parameter may be scaled between 1 and 0. When $\lambda = 1$, the potential behaves like the original potential, which is the sum of Equations 2.38 and 2.39. For $\lambda = 0$, the non-bonded interactions are switched off entirely, and for values between these end-points the potential scales smoothly (Figure 2.2).

In order to obtain realistic results from FEP simulations, a number of aspects of the simulations must be considered. Firstly, the process studied using FEP should be reversible, such that the free energy of the forward reaction is equal in magnitude and opposite in sign to the reverse reaction. This ensures that the system is in equilibrium and thus that the equilibrium free energy is being calculated. Secondly, two key parameters must be chosen: the number of intermediate states, and the simulation time in each of these intermediate states. In scaling λ between two states, the number of intermediate states determines the step size, $\Delta\lambda$, of the simulation. The full simulation time in each state is denoted t_λ. This quantity must be

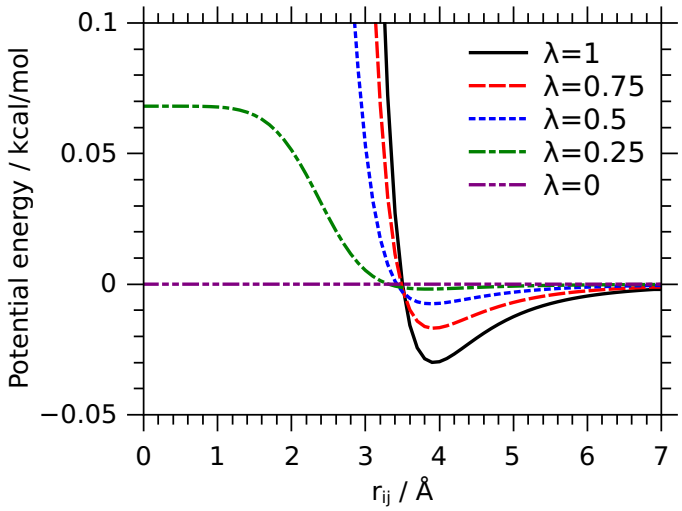

Figure 2.2: Non-bonded soft interaction potential for various values of λ, with $\sigma_{ij} = 3.5$ Å and $\epsilon_{ij} = 0.03$ kcal/mol.

sufficiently large so as to allow the system to re-equilibrate in the new state, as well as to provide ample sampling time of the potential energy of that state. The size of $\Delta\lambda$ must be chosen such that neighbouring states are sufficiently similar, i.e. good phase space overlap must be achieved.

In this work, FEP simulations are used to estimate the solvent contribution to the free energy change for separation of F4TCNQ from P3HT in chloroform. Four separate processes were considered in both explicit solvent and vacuum, and the free energies of each process were summed to provide the overall solvent contribution to the free energy of separating F4TCNQ from $(3HT)_8$, while accounting for the system changing from charge separated to charge neutral.

All simulations with explicit solvent were performed under the same conditions, and using the same system size, as the SMD simulations described above. Vacuum simulations were performed at constant volume. The change in Gibbs free energy for all FEP simulations was obtained using

$$\Delta G_{0,1} = -k_{\mathrm{B}}T \sum_{i=0}^{n-1} \log \frac{\left\langle V \exp\left(-\frac{U(\lambda_{i+1}) - U(\lambda_i)}{k_{\mathrm{B}}T} \right) \right\rangle_{\lambda_i}}{\langle V \rangle_{\lambda_i}}. \tag{2.47}$$

In this case, λ_i represents the intermediate states. As before, the positions of $(3HT)_8$ and F4TCNQ were specified using harmonic springs to set the centre of mass. All simulations were performed using LAMMPS and a locally modified version of the FEP package. This modification was necessary to ensure that charges could be modified by atom-ID, rather than by atom-type, as implemented.

3 | Ground-state properties of the P3HT/F4TCNQ dimer complex

Unsubmitted work written in manuscript style for submission to a peer-reviewed, international journal

Principal author (candidate): Sophia Ackling
Contribution: 85 %
Designed and carried out quantum calculations to investigate properties of interest in the model system. Collected, analysed and interpreted the data presented. Conceived and prepared the chapter as contained herein.

This chapter reports on original research conducted during the period of my Higher Degree by Research candidature and is not subject to any obligations or contractual agreements with a third party and would constrain its inclusion in this thesis. I am the primary author of this chapter. I hereby certify the statement of contribution is accurate.

26/10/16

Sophia Ackling Date

Contributing author: David Huang
Contribution: 15 %
Supervised quantum calculations, and assisted with interpretation of data and editing of the chapter.

I hereby certify that the statement of contribution is accurate and grant permission for the candidate to include work pertaining to the publication in their thesis.

26/10/16

David Huang Date

Abstract

The archetypal polymer/dopant system comprising poly-(3-hexylthiophene) (P3HT) and 2,3,5,6-tetrafluoro-7,7,8,8-tetracyanoquinodimethane (F4TCNQ) has been widely studied, both experimentally and computationally. However, factors affecting the charge transfer mechanism between the two species remain poorly understood. In particular, integer charge transfer occurs between P3HT and F4TCNQ, while only partial charge transfer occurs between quarterthiophene and F4TCNQ. This work uses density functional theory to demonstrate that charge transfer and spectral properties within the system are highly sensitive to both polymer structure and the surrounding environment. A systematic study of the length and substitution of the chain used to represent P3HT in an oligomer/F4TCNQ dimer complex is performed. An eight-unit-oligomer-based complex is found to better reproduce experimental spectral and electronic properties than a quarterthiophene-based complex as a result of better agreement with the conjugation length of P3HT. An increase in charge transfer upon methyl substitution of the oligomer reveals that the polymer side chains play an integral role in the charge transfer process between polymer and dopant. A dielectric medium is introduced to account for the experimental environment of the charge transfer unit and near-integer charge transfer is achieved, highlighting the importance of environment in the integer charge transfer process. Density functional impact on charge transfer is also considered and the amount of Hartree-Fock exact exchange is observed to dramatically affect electronic properties. The optimally-tuned range-corrected PBEh functional (LRC-ωPBEh) is found to provide the most realistic description of the experimental system, in terms of both spectral and charge transfer properties. This study illustrates how a number of physical characteristics of the P3HT/F4TCNQ system make it conducive to integer charge transfer, as well as the disparity in experimental accuracy that can occur without careful consideration of the chosen density functional.

3.1 Introduction

Organic electronic devices possess a number of attractive characteristics over traditional silicon devices. Reduced production costs and improved device flexibility are two key drivers in organic electronics research.[110] Applications for this technology exist within organic solar cells[111,112] and organic transistors,[113] as well as in device displays, which have already been commercialised.

Introducing molecular dopants into certain organic polymer systems has been demonstrated to improve the semiconducting properties of the polymer,[114] which is desirable for improved electronic behaviour. The addition of these dopants can be used to tune device properties through appropriate alignment of molecular orbitals.[115] Charge transfer occurs between polymer and dopant if the orbitals have suitable relative energies, resulting in charge separation. The magnitude of charge separation can be highly system dependent, and hence a solid understanding of the

electronics of the system of interest is crucial. Upon doping, a free charge is present on the polymer, which can migrate, resulting in the generation of current. The rate of this charge migration is a further consideration, and one that remains the subject of ongoing research.[36,116]

Morphology of polymer/dopant mixtures is known to play an important role in device efficiency and charge generation, and manipulation of morphology is paramount to efficient device production.[23,38,116,117] Recent experimental and computational work by Di Nuzzo *et al.* demonstrated that charge transfer within a copolymer/dopant system depends strongly on intermolecular separation between the two species.[118] This highlights the importance of polymer structure control, as manipulation of polymer morphology could lead to improved charge generation and mobility within the system. The dopant itself has also been observed to affect the morphology of the polymer. A number of studies on the archetypal poly(3-hexylthiophene) (P3HT) and 2,3,5,6-tetrafluoro-7,7,8,8-tetracyanoquinodimethane (F4TCNQ) polymer/dopant system have observed increased rigidity and planarity in the polymer backbone upon introduction of the dopant, demonstrating that charge transfer between the species has a measurable impact on polymer morphology.[26,44,119] Recent pioneering work by Jacobs *et al.* demonstrated highly specific light-induced polymer solubility control in this same system.[38] The team showed that irradiation of F4TCNQ-doped P3HT at 405 nm results in a reduction in polymer rigidity and subsequent dissolution of the polymer into solvent. It is likely that charge transfer between polymer and dopant plays a key role in this solubility change, but the mechanism of this light-induced reaction has yet to be clarified.

The key focus for this work is the nature of the charge transfer reaction that occurs between P3HT and F4TCNQ upon mixing. Experimental studies have shown that integer charge transfer occurs between polymer and dopant,[34–36] but the majority of DFT studies on this system have achieved only partial charge transfer.[44,45,120] Spectral properties have also been poorly reproduced in these studies due to simplifications in the structures modelled. A common simplification in DFT models of P3HT-based systems is the replacement of the polymer with a quarterthiophene molecule. Integer charge transfer has been demonstrated to occur over a small number of thiophene units in F4TCNQ-doped P3HT.[34,39] However, by studying F4TCNQ nitrile shifts in Fourier transform infra-red spectra and F4TCNQ anion peaks in ultraviolet/visible absorption spectroscopy, Méndez *et al.* recently found that in fact only partial charge transfer occurs between F4TCNQ and quarterthiophene. This result in particular highlights the importance of chain length and substitution in the charge transfer process, neither of which have previously been investigated computationally for this system.

In order to glean insight into factors that influence charge transfer between P3HT and F4TCNQ, this work presents a systematic investigation into the common simplifications of the structure of P3HT for quantum calculations. The impact of chain length and substitution on charge transfer in a F4TCNQ/oligothiophene complex

are considered, and an appropriate model for the P3HT polymer is described and justified based on both ground-state charge transfer and spectral properties. In seeking to further increase ground-state charge transfer, the surrounding environment of the system is introduced by means of a dielectric medium. Finally, the dependence of system properties on density functional is also reported, and results reveal the extent to which the choice of functional can impact agreement with experiment.

3.2 Computational details

All ground-state geometries were obtained by optimising initial guesses generated in GaussView 5.[121] Geometries were visualised using Avogadro.[122] Excited state energies for all systems were obtained using time-dependent DFT (TDDFT) and simulated absorption spectra were generated by convolution with a Gaussian of width 0.1 eV using Gabedit software.[123] All calculations were performed using Q-Chem 4.3.[96] The 6-31G(d) basis set was used in all cases, unless otherwise noted. Charge transfer was quantified as the charge on F4TCNQ as obtained using charges from the electrostatic potential on a grid (CHELPG)[124] population analysis.

3.2.1 Polymer structure dependence

Three dimer complexes were prepared: thiophene chains of four, eight and twelve units were constructed and an F4TCNQ molecule was placed with its centre-of-mass over the central bond in each chain. Such placement of the F4TCNQ molecule has previously been found to be the lowest energy geometry.[45] These complexes are denoted T4, T8 and T12 dimer. Three additional complexes with methyl substitution (M dimer) instead of hydrogen substitution were considered. Isolated oligomers from each dimer complex were also optimised.

Each complex was optimised using the optimally-tuned range-corrected PBEh (LRC-ωPBEh) functional.[70] The tuning procedure recently used by Zheng *et al.*[125] for an organic polymer/dopant complex was used to tune this functional for the model M8 dimer complex

$$J(\omega) = (E_{\mathrm{HOMO}} + IP)^2 + (E_{\mathrm{LUMO}} + EA)^2. \tag{3.1}$$

HOMO and LUMO energies are compared with the ionization potential (IP) and electron affinity (EA) of the complex and the difference between these values is minimised by minimising $J(\omega)$. The optimal value for ω was found for the M8 dimer complex to be $\omega = 0.065$ bohr^{-1} (see Appendix A, Table A.1). For comparison, each calculation was also repeated with the widely used Becke three parameter Lee-Yang-Parr (B3LYP) functional.[63] Grimme's D2 dispersion correction[67] was applied to all B3LYP calculations (denoted B3LYP-D), as it has been demonstrated to improve ground-state properties in organic systems.[45] These results may be found in Appendix A.

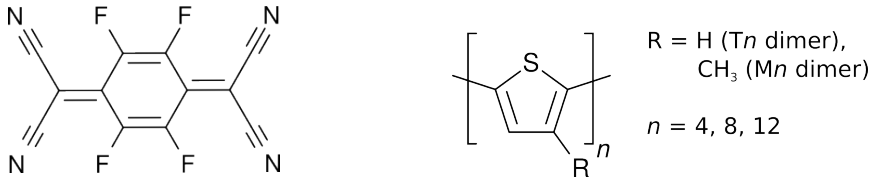

Figure 3.1: Structures of F4TCNQ (left) and the oligothiophenes (right) used in this study.

3.2.2 Dielectric dependence

Implicit solvent was introduced in select calculations using the conductor-like polarisable continuum model (CPCM),[89] and the integral equation formalised polarisable continuum model (IEFPCM)[90,91] as a way to represent the surrounding P3HT chains that are present in the experimental system. The IEFPCM results were essentially identical to those of the CPCM model (see Appendix A, Figure A.5 and Table A.2), and hence this latter model was used for all calculations presented here due to its improved efficiency.

3.2.3 Density functional dependence

The performance of a number of density functionals was investigated for the M8 dimer system. The ground-state geometry of this dimer and its isolated components was optimised using five functionals that varied in the amount of Hartree-Fock (HF) exchange included. These functionals were BP86,[64,126] B3LYP,[63] PBE0,[127,128] BHH-LYP,[129] and M06-HF.[130] Three functionals within which % HF varies with distance were also considered, and these were ωB97XD[131], CAM-B3LYP[132] and tuned LRC-ωPBEh[70]. The latter was tuned to the M8 dimer complex, with $\omega = 0.065$ bohr^{-1}. Grimme's D2 dispersion correction[67] was applied in all cases except for ωB97XD and LRC-ωPBEh, both of which already account for dispersion interactions.

3.3 Results and discussion

3.3.1 Polymer structure dependence

P3HT is often replaced with a short oligothiophene in DFT calculations. Experimental work by Pingel *et al.* studied the infra-red spectra of F4TCNQ mixed with polymers comprising 3-hexylthiophene substituted occasionally with tetrafluorobenzene in order to control the 3-hexylthiophene conjugation length. Based on C≡N stretches in F4TCNQ and the molar ratio of hexlythiophene units to F4TCNQ, the team concluded that each F4TCNQ molecule undergoes charge transfer with one quarterthiophene unit within the polymer.[39] The majority of previous computational studies of P3HT systems have simplified the polymer to a four unit thiophene chain.[44,45,49,133,134] However, the conjugation length for P3HT has been estimated to be greater than seven units,[135] which suggests that a four-unit chain may be insufficient for modelling the electronic properties of P3HT-based systems using DFT.

Moreover, the aforementioned experimental and computational studies by Méndez *et al.* showed that only partial charge transfer occurs between quarterthiophene and F4TCNQ.[34] The validity of reducing the polymer to a short oligomer chain is examined in this work.

Another common simplification in DFT studies of P3HT is the replacement of the hexyl side-chains with hydrogens. This method has been justified because the hexyl chains impact solubility, but not electronic behaviour.[136,137] The simplified structure has been used in the past to efficiently model many P3HT-based polymer/dopant systems.[44,45,120] However, some studies have used methyl substitution rather than hydrogen substitution when considering P3HT-based systems,[49,138] and it is possible that improved agreement with experiment may be obtained with such a model. While the impact of methyl substitution on isolated polythiophene has been investigated computationally,[47,139] no direct comparison has yet been examined for the P3HT/F4TCNQ system. The performance of methyl versus hydrogen substitution in the dimer complex is addressed in the following results.

Ground-state properties

As seen in Table 3.1, increasing the oligothiophene chain length was found to increase HOMO and LUMO energies of the complex, but decrease the HOMO-LUMO gap. Experimental studies of conjugated polymers have noted that this decrease in energy gap is a result of the increased conjugation length of the oligomer.[140]

A greater degree of ground-state charge transfer indicates a more physically realistic model for the P3HT/F4TCNQ system. The magnitude of charge transferred between oligothiophene and F4TCNQ in the ground state was also found to increase with increasing chain length (Table 3.2). However, no substantial difference is observed when increasing from eight to twelve units. This suggests that a twelve-unit chain is unnecessarily long for modelling P3HT in the polymer/dopant system, and that an eight-unit chain provides a more realistic description of the conjugation length in P3HT.

Experimental studies have demonstrated crystalline regions of polymer in the presence of sufficient doping concentrations of F4TCNQ,[26] and hence it may be concluded that the presence of dopant results in an increase in planarity of the local polymer backbone. In this work, inter-thiophene torsion angles increased for the terminal thiophene units as chain length and substitution increased, but did not exceed 30 degrees (M12 dimer). This twisting is likely due to long-range interactions between terminal thiophene units, the dopant and other parts of the chain, as a result of the long-range interactions modelled by the range-corrected functional. As the purpose of this work was to model one conjugation unit, the lack of significant twisting within the oligomer is promising, and suggests that all complexes provide a reasonable approximation to one conjugation unit in the experimental system. Modelling a much longer oligomer is likely to induce greater inter-thiophene twisting for the terminal thiophene units as a result of exceeding the conjugation length of

Table 3.1: Frontier molecular orbital energy levels for all complexes

	HOMO (eV)		LUMO (eV)		E_{GAP} (eV)	
Chain length	H sub.	CH_3 sub.	H sub.	CH_3 sub.	H sub.	CH_3 sub.
4	–6.48	–6.23	–3.73	–3.59	2.75	2.64
8	–5.96	–5.74	–3.57	–3.43	2.39	2.31
12	–5.80	–5.52	–3.57	–3.40	2.23	2.12

Table 3.2: Charge transfer (e) in all complexes

Chain length	H sub.	CH_3 sub.
4	0.37	0.44
8	0.44	0.54
12	0.45	0.55

the polymer. Likewise, modelling hexyl side chains on any of the oligomers studied in this work will induce greater twisting due to disruptive interactions between hexyl chains and the charge transfer unit of the complex.

Methyl substitution of the thiophene oligomers further increases both the HOMO and LUMO energies and ground-state charge transfer, and further decreases the HOMO-LUMO gap. The increase in ground-state charge transfer shows that methyl substitution is a necessary component of the model, as it provides a more physically realistic description of the experimental system, in which integer charge transfer occurs.

Simulated absorption spectra

Simulated absorption spectra for each of the oligothiophenes in isolation show that increasing chain length leads to progressively lower energy excitations (Table 3.3). All calculations were performed using the $\omega = 0.065$ bohr^{-1} value that was found to be optimal for the M8 dimer, for consistency. It is evident that the four-unit oligothiophenes vastly overestimate P3HT excitation energies, while the eight and twelve unit chains slightly over- and under-estimate, respectively. This is consistent with the previous assertion that the conjugation length for P3HT lies somewhere near eight thiophene units. Methyl substitution can be seen to only slightly increase excitation energies.

Spectra for each methyl-substituted oligomer-based complex (Figure 3.2) reveal that, like in the isolated oligothiophene case, increasing oligothiophene length red-shifts the spectra. This phenomenon has previously been observed for a similar P3HT-based complex,[141] and is a result of increasing conjugation length.[142] It is evident that the M4 and M12 spectra are substantially blue- and red-shifted, respectively, with respect to the experimental spectrum, while the M8 complex shows good agreement with the experimental spectrum. This once more supports the asser-

Table 3.3: Dominant excitation energies in hydrogen and methyl substituted oligomers of varying length

Thiophene units	H sub. (eV)	CH_3 sub. (eV)
4	3.05	3.10
8	2.41	2.43
12	2.21	2.21
P3HT	$\sim 2.3^a$	

[a]Spectra from Jacobs *et al.*[38]

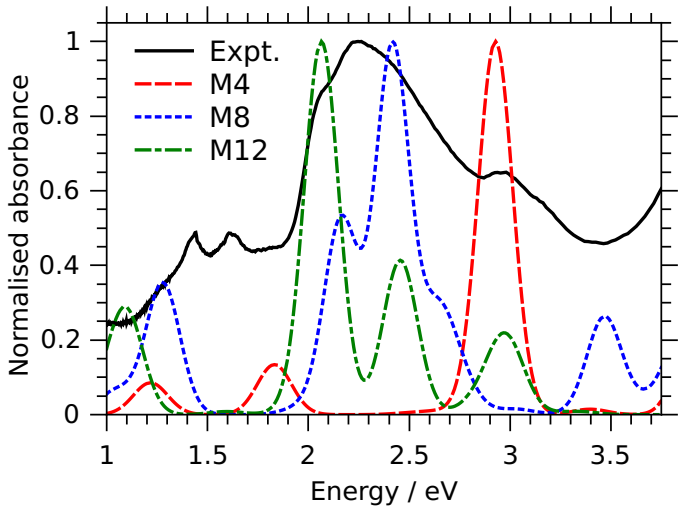

Figure 3.2: Normalised simulated absorption spectra for each methyl-substituted dimer shown with the normalised absorption spectrum of the P3HT/F4TCNQ film produced by Jacobs *et al.*[143] Experimental spectrum obtained from sequential doping of P3HT with F4TCNQ in acetonitrile, with a mole ratio of 96:4.

tion that an eight-unit oligomer provides the best description of the P3HT polymer. Methyl substitution on isolated oligomers was demonstrated to have minimal impact on excitation energies in isolation (Table 3.3). As such, only the methyl-substituted oligomer spectra are presented. Note that the B3LYP-D spectra show an identical trend (Appendix A, Figure A.1).

3.3.2 Dielectric dependence

The properties of the surrounding experimental environment and its impact on the model system can be included in DFT calculations by introducing a dielectric medium. In this study, a dielectric medium was introduced to represent the P3HT chains that surround the polymer/dopant unit in the experimental system. Such a model more accurately reproduces the experimental system.

The dielectric medium was introduced by setting the static and optical dielectric constants of the system to match experimental values for organic semiconducting polymers. The static dielectric constant, ϵ, for organic polymers is usually reported in the range of 2–5.[144–148] The optical dielectric constant, ϵ_∞, is equal to the square of

the refractive index of the material,[149,150] and for regio-regular P3HT the refractive index varies between 1.2 and 6.3,[149] as a result of the wavelength dependency. In a preliminary investigation, the M8 dimer complex was modelled using the B3LYP-D functional with ϵ equal to 3.0, 4.0 and 5.0 (with $\epsilon_\infty = 3.0$) and ϵ_∞ equal to 2.0, 3.0, 4.0 and 5.0 (with $\epsilon = 3.0$). Increasing ϵ increased the ground-state charge transfer, but ϵ_∞ did not greatly impact the excitation energies of the system (Appendix A, Table A.3 and Figure A.6). A value of 3.0 for each constant was chosen, as these values are close to experimental values.

With the growing popularity of optimally-tuned range-corrected functionals, the issue of tuning a system in a dielectric medium has arisen, with claims that such tuning yields unrealistically small values for ω.[72] However, Zheng *et al.* recently demonstrated improved agreement with experimental results when using an ω tuned in a polarisable continuum model (PCM) solvent, rather than a vacuum-tuned value with the dielectric medium, for the LRC-ωPBE functional.[125] In light of this finding, ω was tuned for the LRC-ωPBEh functional in a dielectric medium for this study, with ϵ and ϵ_∞ set to 3.0. The value of ω considered optimal once $J(\omega) < 3 \times 10^{-5}$, which gave $\omega = 0.005$ bohr^{-1}.

Ground-state properties

The inter-thiophene torsion angle for the terminal thiophene units decreased upon inclusion of an implicit solvent, from 27 to 15 degrees for the range-corrected functional results. This is due to the screening of favourable interactions between terminal thiophene units, the dopant and other parts of the chain.

The magnitude of ground-state charge transfer for the M8 complex (Table 3.4) was found to be substantially higher in the dielectric medium than in a vacuum for both the range-corrected functional and B3LYP, emphasising that environment plays an important role in charge transfer between P3HT and F4TCNQ. Single-point TDDFT calculations at the 6-31+G(d) level of theory, performed on the 6-31G(d) geometry (henceforth denoted 6-31G+(d)/6-31G(d)) also yielded an increase in charge transfer with respect to 6-31G(d) calculations (henceforth denoted 6-31G(d)/6-31G(d)). In the dielectric medium the degree of charge transfer approached integer values for both functionals. Diffuse functions are necessary to accurately describe long-range interactions as well as the properties of anionic species.[151,152] In this system, the F4TCNQ molecule has anionic properties as charge transfer increases. The observed increase in charge transfer with the larger basis set is thus likely a result of the diffuse functions providing a better description of the system. It should be noted that the range-corrected functional yields a slightly smaller degree of charge transfer than B3LYP. This may be due to the fact that B3LYP is known to overestimate electron delocalisation,[153,154] whereas the range-corrected functional does not.[154] In spite of this difference, the B3LYP functional shows strikingly similar behaviour to that of LRC-ωPBEh, suggesting that it may also be a viable functional for studying this system.

Table 3.4: Ground-state charge transfer (CT) in the M8 dimer with increasing basis set and in dielectric medium

Basis set	Dielectric medium	CT (e)	
		B3LYP-D	LRC-ωPBEh
6-31G(d)/6-31G(d)	no	0.65	0.54
	yes	0.82	0.76
6-31G+(d)/6-31G(d)	no	0.74	0.60
	yes	0.97	0.87

Simulated absorption spectra

TDDFT calculations were used to obtain simulated absorption spectra for the M8 dimer complex in vacuum and solvent, and using two different basis sets (Figure 3.3; Appendix A, Figure A.4 for B3LYP-D results). While introducing diffuse functions into the basis set leaves the spectrum essentially unchanged, the dielectric medium results in a substantial red-shift of excitation energies.

The observed red-shift in the solvated system is likely to be a result of a number of factors. Firstly, TDDFT calculations in a dielectric medium are red-shifted due to the dielectric medium being in equilibrium with the ground state of the system.[155] The excitation energies are also affected by the optimal ω values, which differ substantially between vacuum and solvated systems. The smaller dielectric-tuned ω value will result in 100 % Hartree-Fock exact exchange (HF) at a much larger distance than in the vacuum-tuned ω calculations, which is observed to affect molecular orbital energies of the dimer complex and its constituents. The energy spacing between molecular orbitals in the dimer is reduced upon the reduction in ω for inclusion of the dielectric medium (Figure 3.4). The dielectric medium on its own, without ω tuning, has only a minimal impact on molecular orbital energies (Appendix A, Figure A.3). The impact of ω and dielectric medium on molecular orbital energies has been previously observed in organic systems.[125] Because of the reduced ω value, the range-corrected functional performs like a local hybrid with 25 % HF in implicit solvent. Inspection of Figure A.2 (Appendix A) reveals the range-corrected spectrum to be comparable with the B3LYP-D (20 % HF) spectrum in the dielectric medium.

Finally, it is important to note that the change in ω and introduction of a dielectric medium changes the energy-level ordering between the M8 oligomer and F4TCNQ, with the LUMO of the latter lying below the HOMO of the oligomer in the presence of the dielectric medium (Figure 3.4). The increase in ground-state charge transfer can be ascribed to this reordering, as efficient electron transfer can occur between the HOMO of the oligomer and the LUMO of F4TCNQ. This reflects experimental orbital ordering, which give rise to the experimentally observed integer charge transfer.

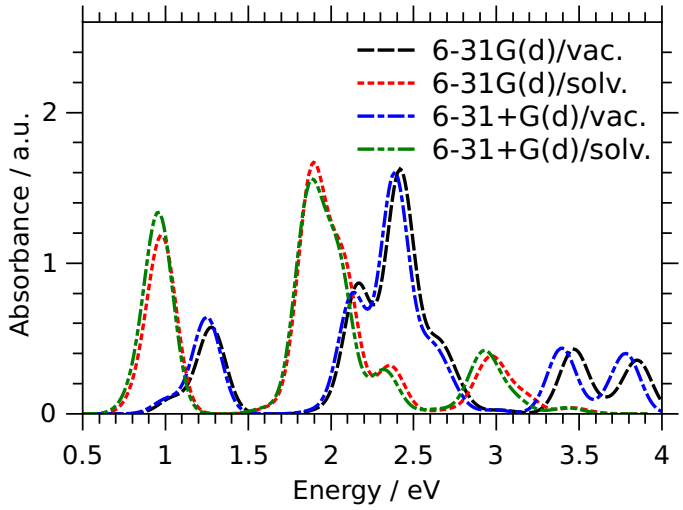

Figure 3.3: Simulated absorption spectra for the M8 dimer complex obtained using the LRC-ωPBEh functional with and without implicit solvent. In all cases the optimised 6-31G(d) geometry was used from vacuum and implicit solvent ground-state calculations, with either the 6-31G(d) or 6-31+G(d) basis set used in TDDFT calculations.

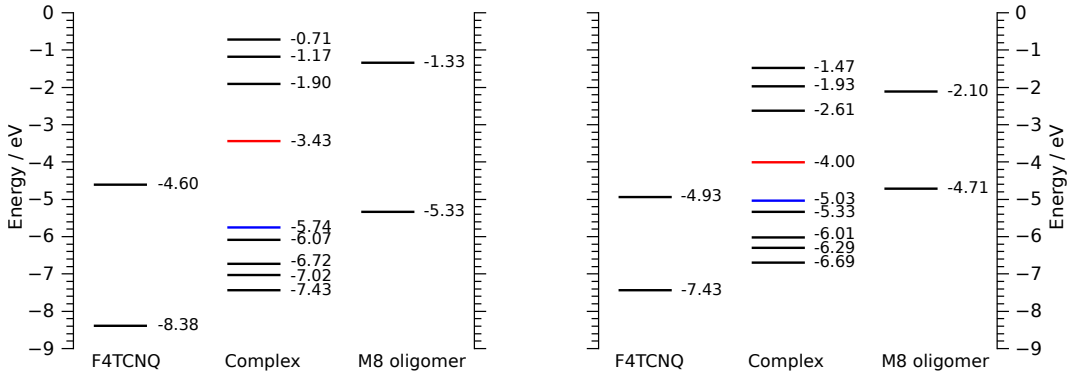

Figure 3.4: Calculated molecular orbital energies for the M8 dimer and its isolated fragments in vacuum (left; $\omega = 0.065$ bohr^{-1}) and in a dielectric medium (right; $\omega = 0.005$ bohr^{-1}).

3.3.3 Density functional dependence

Many previous DFT studies on the P3HT/F4TCNQ system have used the common B3LYP functional, citing reasonable replication of some physical parameters. However, its performance is not consistent between molecular systems. In particular it does not perform well for charge-transfer excited states and does not give consistently accurate reaction energies.[156,157] A number of new functionals have recently shown promise as alternatives.[157–160] In this work, both the LRC-ωPBEh and B3LYP functionals have been used. A number of recent studies have successfully used the related LRC-ωPBE functional, with 0 % HF at short range, for organic semiconductor systems.[71,154,161] The hybrid version, LRC-ωPBEh with 25 % HF at short range, was chosen for this work because of the apparent good performance of hybrid functionals with 20–30 % HF on this system. However, in order to validate the choice of functionals used in this study, a number of alternatives were investigated.

The amount of Hartree-Fock exact exchange (HF) included in the functional description can dramatically affect its performance. In this work, five common density functionals with varying amounts of HF are considered: BP86, B3LYP, PBE0, BHH-LYP and M06-HF, with 0, 20, 25, 50 and 100 % HF, respectively. These were selected as they cover the full range of % HF. Three popular range-separated functionals are also considered, all of which have variable HF: CAM-B3LYP[132], ωB97XD[131] and the aforementioned tuned LRC-ωPBEh, with $\omega = 0.065$ bohr^{-1}. These functionals possess 19–65 % HF, 22–100 % HF and 25–100 % HF, respectively. Both B3LYP and PBE0 have been widely used for organic systems,[47,48,141,162] and the M06-HF global hybrid functional has been popular in the past for its good performance with charge transfer states.[158] CAM-B3LYP and the ωB97XD were chosen because they have been shown to perform well for conjugated polymer systems.[118,160]

The performance of each functional was assessed in three ways: the accuracy and relative energies of the highest occupied and lowest unoccupied (HOMO and LUMO) molecular orbital energies of the M8 oligothiophene and F4TCNQ respectively; the degree of charge transferred from the M8 oligothiophene to F4TCNQ in the ground state of the dimer complex; and the simulated absorption spectra taken from TDDFT calculations.

Orbital energies and charge transfer

The HOMO energy of the M8 oligothiophene chain was found to decrease with increasing HF (Table 3.5), while the LUMO energy of the F4TCNQ molecule was found to increase with increasing HF. For functionals with less than 50 % HF the HOMO of the M8 oligothiophene was observed to be higher in energy than the LUMO of the F4TCNQ molecule. This is consistent with expectations based on experimental results: such ordering of orbitals would lead to efficient charge transfer from polymer to dopant. Additionally, the experimentally determined HOMO of

P3HT is greater than the electron affinity of F4TCNQ, which is generally accepted to be approximately equal to the LUMO.[42,163] As expected, given their popularity in past computational studies of this system, the B3LYP and PBE0 functionals provide good estimates for the M8 oligomer HOMO and F4TCNQ LUMO. However, for functionals with at least 50 % HF the molecular orbitals are reordered, so that the HOMO of the M8 oligothiophene is lower in energy than the LUMO of F4TCNQ. None of the range-corrected functionals, including the optimally-tuned LRC-ωPBEh functional, reproduce the experimental orbital ordering *in vacuo*, although the latter does do so upon inclusion of a dielectric medium (Figure 3.4). This orbital swapping behaviour has been observed previously for a different organic dimer complex.[159] For the M8/F4TCNQ complex the placement of M8 HOMO below F4TCNQ LUMO indicates that the range-corrected functionals, and hybrids with more than 50 % HF, do not realistically describe the experimental system.

The magnitude of ground-state charge transfer (Table 3.5) was found to decrease with increasing % HF. This is consistent with the relative orbital energies of the two dimer components observed for each functional. Even with zero % HF, integer charge transfer is not observed, which indicates that for this model system at this level of theory none of the functionals accurately describe the experimentally observed integer charge transfer. This further highlights the necessity for additional parameter considerations within the system, such as a dielectric medium.

Given their popularity in studying systems similar to that investigated here, the poor performance of ωB97XD and CAM-B3LYP is somewhat surprising. The magnitude of charge transfer observed for these functionals is very similar to that of the M06-HF (100 % HF) and BHHLYP (50 % HF) functionals, respectively. These data suggest that the dimer is being described by the "long range" component of the range-corrected functionals, with near-maximum % HF in both cases. The tuning of ω for the LRC-ωPBEh functional proved essential for its performance, and based on the trend in orbital energies and charge transfer observed, this functional performs as if it has less than 50 % HF for the dimer complex. This suggests that, unlike the two non-tuned range-corrected functionals, the properties of the dimer are still described by a large portion of the "short range" component of the exchange correlation functional.

Simulated absorption spectra

Previous density functional theory studies have found that excitation energies within oligothiophene are heavily impacted by the choice of functional.[160,164] A benchmarking study by Jacquemin *et al.* found that, in general, hybrid functionals with a small, but non-zero, amount of HF exchange provide the best TDDFT results for organic systems.[164] In this work, increasing the amount of HF was observed to blue-shift the simulated absorption spectra of the dimer complex (Figure 3.5). This is consistent with previous studies on organic molecules, including thiophene oligomers[156] and arises due to increased orbital spacing with increasing % HF.

Table 3.5: Ground-state charge transfer (CT) and intermolecular separation for the dimer complex, and HOMO and LUMO values for individual monomers obtained using various amounts of HF exchange

Functional	% HF	CT (e)	Dimer separation (Å)	M8 HOMO (eV)	F4TCNQ LUMO (eV)
BP86	0	0.69	3.06	–4.00	–5.72
B3LYP	20	0.65	3.10	–4.46	–5.25
PBE0	25	0.63	3.00	–4.68	–5.22
BHHLYP	50	0.52	3.03	–5.33	–4.43
M06-HF	100	0.35	2.92	–7.37	–3.40
CAM-B3LYP	19–65	0.48	3.04	–5.69	–4.25
ωB97XD	22–100	0.36	3.22	–6.59	–3.78
LRC-ωPBEh	25–100	0.54	3.31	–5.33	–4.60
Experimental		1[a]		–5.00[b]	–5.25[c]

[a]Wang *et al.*[35]

[b]P3HT HOMO from cyclic voltammetry, Sun *et al.*[163]

[c]Negative of F4TCNQ electron affinity from IPES measurements, Gao & Kahn[42]

The BP86, B3LYP and PBE0 functionals give similar spectra that differ only slightly in excitation energy and blue-shift. For the two functionals with at least 50 % HF, BHHLYP and M06-HF, spectra differ more significantly. Both demonstrate substantial blue-shifts with respect to the LRC-ωPBEh functional, which provides a good approximation to the experimental spectrum.

The two non-tuned range-corrected functional spectra demonstrate surprising similarities to that of the BHHLYP functional. Both spectra possess substantial blue-shifts with respect to the LRC-ωPBEh functional spectrum. Previous studies have demonstrated success when using both of these functionals to calculate excited states for polythiophene.[160] The poor agreement with experiment for the dimer complex suggests that while conjugated polymer properties can be accurately described by these functionals, properties of charge transfer dimer complexes cannot.

Figure 3.5 also displays simulated spectra obtained when the chosen functional is applied to the B3LYP-D optimised ground state. These spectra can be seen to differ, in some cases quite significantly, from those obtained from the ground state optimised with the same functional used for the excited-state calculation. This difference highlights the impact of ground-state geometry on excited state energies. Table 3.5 shows that the choice of functional also impacts intermolecular separation, which is then likely to impact molecular orbital energies and hence account for the observed difference in excitation energies. In particular, the M06-HF functional yields an intermolecular separation that differs by 0.18 Å compared with the B3LYP functional. This large difference in complex structure is a likely cause for the large difference in simulated absorption spectra obtained for the two geometries using the M06-HF functional.

According to the criteria for good performance, which here included relative orbital energies, charge transfer and spectral properties, both the B3LYP and PBE0 functionals are deemed appropriate for this system. Likewise, despite incorrect orbital ordering in the tuned LRC-ωPBEh functional in vacuum, the simulated ab-

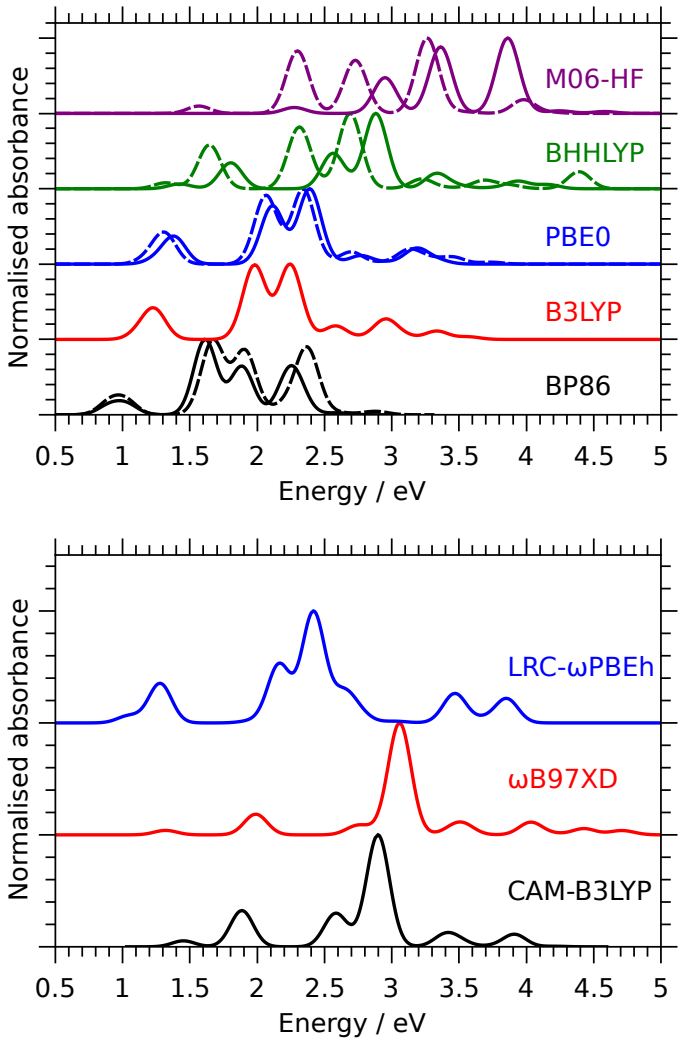

Figure 3.5: Simulated absorption spectra for each of the five functionals with varying % HF (top) and the three range-corrected functionals (bottom). The solid line represents TDDFT calculation on the ground-state structure optimised with that functional, and the dashed line represents TDDFT calculation on B3LYP-D optimised ground-state structure.

sorption spectrum matches very well with the experimental spectrum for P3HT/F4-TCNQ and the orbital ordering is known to be correct in implicit solvent. As such, this functional is also shown to be a good choice for studying this system. All other functionals considered here, however, fail to achieve accuracy in one or more of the criteria. The variability in performance highlights the importance of choosing an appropriate functional when studying the F4TCNQ-doped P3HT system.

3.4 Conclusions

This study aimed to provide insight into the charge transfer mechanism between P3HT and F4TCNQ, and in particular how structural and environmental features impact this mechanism. A model system was constructed and optimised using den-

sity functional theory, and a number of computational aspects of system design were considered in order to improve the charge transfer within the system.

When simplifying the P3HT polymer to an oligothiophene, it was shown that quarterthiophene is too short to accurately represent the P3HT polymer. In particular, the simulated absorption spectrum is a poor fit for the experimental spectrum and only a small degree of charge transfer was observed. Additionally, a twelve-unit thiophene chain does not perform any better than an eight-unit chain in terms of both ground-state charge transfer and spectral properties. This work has demonstrated that an eight-unit thiophene chain performs best for the P3HT/F4TCNQ system. Methyl substitution of this chain was found to provide a more realistic description of the ground-state electronic structure than hydrogen substitution.

Further improvement of the model has been demonstrated by including a dielectric medium within the system, which represents the experimental environment of the charge transfer unit. The dielectric medium was demonstrated to increase the magnitude of ground-state charge transfer substantially, and the introduction of diffuse functions in the basis set when calculating excited states of this dielectric medium system gives near-integer charge transfer. These results demonstrate the importance of considering the surrounding medium when modelling the charge transfer mechanism between P3HT and F4TCNQ.

The impact of density functional on model performance was also explored. A range of popular density functionals with various amounts of Hartree-Fock exact exchange (HF) were used to model the dimer comprising F4TCNQ and the eight-unit methyl-substituted thiophene chain. It was observed that functionals with more than 50 % HF give incorrect ordering of the oligothiophene HOMO and F4TCNQ LUMO, resulting in substantially reduced ground-state charge transfer occurs. Two commonly used range-corrected functionals were found to perform poorly for this particular system, but the tuned LRC-ωPBEh functional was found to give moderately accurate results. The B3LYP functional was also shown to perform well, both in terms of ground-state charge transfer and simulated absorption spectrum. It was hence concluded that the tuned LRC-ωPBEh functional is the best choice of the functionals investigated for modelling the P3HT/F4TCNQ system, but that the B3LYP functional can also provide a good description of the system.

In summary, this work highlights the importance of structural characteristics in oligothiophene when modelling the P3HT/F4TCNQ system, with particular application to the spontaneous charge-transfer reaction that occurs upon mixing. By considering some of these characteristics, as well as the impact of surrounding medium, a significantly improved understanding of how these features affect charge transfer was obtained. Application of this understanding to future computational studies on P3HT/F4TCNQ is likely to yield key insights into intrinsic charge-transfer-related properties within the system.

4 | Photo-induced charge-transfer mechanism

A portion of this work is presented in a publication, however this chapter presents a more comprehensive description of the work, and is written in manuscript style

Publication title: Optical Dedoping Mechanism of P3HT:F4TCNQ Mixtures
Journal: The Journal of Physical Chemistry Letters
Date of publication: 12 October, 2016
Citation details: Fuzell, J.; Jacobs, I. E.; Ackling, S.; Harrelson, T. F.; Huang, D. M.; Larsen, D. and Moulé, A. J. *The Journal of Physical Chemistry Letters*, **2016**, *7*, 4297-4303. DOI: 10.1021/acs.jpclett.6b02048

Principal author (candidate): Sophia Ackling
Contribution: Designed and carried out quantum calculations to provide insight into the proposed photo-induced charge back transfer mechanism, in addition to conceiving and preparing the chapter as contained herein.

This chapter reports on original research conducted during the period of my Higher Degree by Research candidature and is not subject to any obligations or contractual agreements with a third party and would constrain its inclusion in this thesis. I am the primary author of this chapter. I hereby certify the statement of contribution is accurate.

Sophia Ackling

26/10/16
Date

Author: Jack Fuzell
Contribution: Performed and analysed ultra-fast spectroscopy experiments, and wrote the first draft of the paper.

I hereby certify that the statement of contribution is accurate and grant permission for the candidate to include work pertaining to the publication in their thesis.

10/17/2016

✓Jack Fuzell Date

Author: Ian E. Jacobs
Contribution: Collected NMR and UV-vis spectra and performed the majority of the editing on the draft of the paper.

I hereby certify that the statement of contribution is accurate and grant permission for the candidate to include work pertaining to the publication in their thesis.

Oct 17, 2016

Ian Jacobs Date

Author: Thomas F. Harrelson
Contribution: Performed and analysed simulated NMR spectra obtained using density functional theory calculations.

I hereby certify that the statement of contribution is accurate and grant permission for the candidate to include work pertaining to the publication in their thesis.

10/19/16

Thomas Harrelson Date

Author: David M. Huang
Contribution: Supervised quantum calculations to investigate proposed photo-induced charge back transfer mechanism and wrote and edited sections of the manuscript describing these calculations.

I hereby certify that the statement of contribution is accurate and grant permission for the candidate to include work pertaining to the publication in their thesis.

26/10/16

David Huang Date

Author: Delmar Larsen
Contribution: Advisor to Jack Fuzell, and corresponding author for the paper.

I hereby certify that the statement of contribution is accurate and grant permission for the candidate to include work pertaining to the publication in their thesis.

10/17/2016

Delmar Larsen Date

Author: Adam J. Moulé
Contribution: Wrote a large portion of the paper. Also advisor to Ian Jacobs and Thomas Harrelson, and corresponding author for the paper.

I hereby certify that the statement of contribution is accurate and grant permission for the candidate to include work pertaining to the publication in their thesis.

10/17/2016

Adam Moulé Date

Abstract

In a recent study, photo-induced solubility control was demonstrated in poly(3-hexylthiophene) (P3HT) doped with 2,3,5,6-tetrafluoro-7,7,8,8-tetracyanoquinodimethane (F4TCNQ). Irradiation of the insoluble mixture at 405 nm was shown to result in dissolution of the polymer, and a photo-induced charge-transfer reaction from dopant to polymer was hypothesised. In this chapter, compelling computational evidence is provided against such a mechanism. Based on molecular and natural transition orbital analysis, time-dependent density functional theory calculations identify a possible charge-transfer excitation near 405 nm. However, the charge distribution of this excited state does not show charge neutrality, indicating that at the very least an energy barrier to spontaneous relaxation into the charge-neutral state is present. Furthermore, constrained density functional theory calculations show that the relaxed charge neutral state is not metastable. These results confirm that even if excitation were to cause charge transfer resulting in neutral dopant and polymer, the system would immediately relax back to the charge-separated ground state. It can thus be concluded that the photo-induced charge-transfer mechanism resulting in solvation of the neutral polymer is unlikely and an alternative mechanism must occur upon irradiation.

4.1 Introduction

Molecular doping has been demonstrated to vastly improve electronic properties within organic polymer systems.[117,145,165,166] Small molecular dopants, such as 2,3,-5,6-tetrafluoro-7,7,8,8-tetracyanoquinodimethane (F4TCNQ), have proven particularly successful for doping the poly(3-hexylthiophene) (P3HT) polymer.[37,120] These dopants have frontier molecular orbitals that interact favourably with those of the semiconducting polymer,[167] allowing charge transfer to occur between the two. The P3HT/F4TCNQ system is of particular interest as F4TCNQ has been demonstrated to undergo an integer charge-transfer reaction with the polymer upon mixing, resulting in the formation of F4TCNQ anions and cationic segments of P3HT chain.[35,36] There is some evidence to suggest that such a process results in more efficient charge transport than if partial charge transfer were to occur and form a charge-transfer complex.[168]

Charge-transfer reactions can heavily impact morphology in organic polymer systems. A number of studies have observed increased crystallinity upon increasing dopant concentration in F4TCNQ-doped P3HT films.[26,44] This has been attributed to the increased rigidity in P3HT chains upon charge transfer to F4TCNQ and the reduced solubility of the polymer as a result of the charge. Additionally, recent work by Jacobs et al. demonstrated that this increased crystallinity can in fact be reversed upon irradiation with 405 nm light.[38] Upon exposure, the insoluble polymer dissolves back into solvent, giving rise to a novel technique for polymer structure control, with applications in device fabrication.

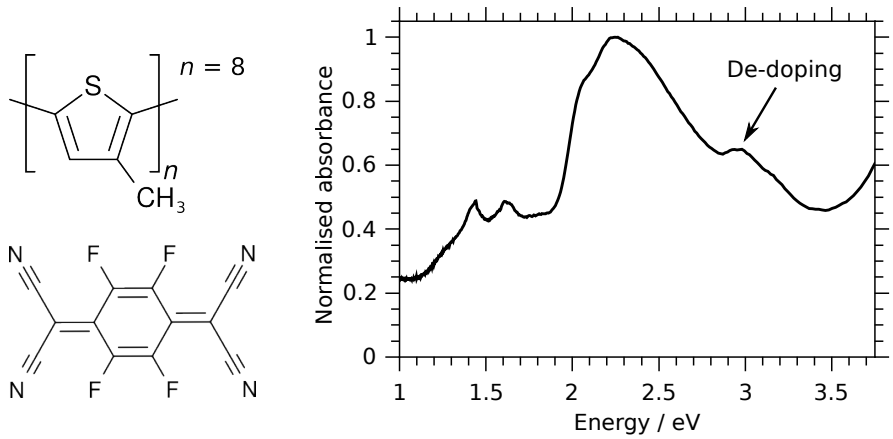

Figure 4.1: Top left: structure of the M8 oligomer used to represent P3HT. Bottom left: structure of F4TCNQ. Right: normalised experimental absorption spectrum of P3HT sequentially doped with F4TCNQ in acetonitrile in a 96:4 polymer:dopant mole ratio.[143] The wavelength associated with photo-induced de-doping is indicated.

The mechanism of this solubility change has yet to be fully characterised. An early hypothesis published the Moulé group suggested a photo-induced charge-transfer reaction, wherein which excitation at 405 nm causes the F4TCNQ anion to transfer its extra electron back onto the polymer, resulting in neutral and hence soluble polymer.[38] This mechanism is plausible as the F4TCNQ anion does indeed absorb near this wavelength.[169–172] However, in a recent study that combined experimental studies with computational work presented here, it was been demonstrated that an alternative mechanism takes place. Excitation is shown to result in a chemical reaction between F4TCNQ and the tetrahydrofuran (THF) solvent, which shifts the equilibrium between F4TCNQ and its anion, resulting in charge transfer from the anion back onto the polymer and subsequent dissolution of the polymer.[40]

This work presents a more comprehensive discussion of the computational evidence presented in the recent publication by Fuzell *et al.* against a simple photo-induced charge-transfer reaction being responsible for the change in solubility of the polymer under irradiation. Time-dependent density functional theory calculations are used to probe the properties of excited states in a model polymer/dopant system, and a combination of molecular and natural transition orbital analysis reveals that possible charge-transfer excitations from dopant to polymer do occur near 405 nm. Constrained density functional theory calculations are then applied to the complex in order to investigate the stability of the charge-neutral state, and conclusions are drawn regarding the feasibility of de-doping occurring as the result of a photo-induced charge-transfer reaction.

4.2 Computational details

The P3HT/F4TCNQ system was simplified to a dimer complex comprising one eight-unit methyl-substituted thiophene chain and one F4TCNQ molecule placed

over the central oligothiophene bond. Previous work (Chapter 3) has shown that this complex sufficiently replicates ground- and excited-state properties of the experimental system. The geometry of this structure was optimised from an initial guess generated in GaussView 5.[121] Molecular orbital plots were visualised in VMD,[173] and the charge transfer in the ground state was quantified by taking the sum of the Mulliken charges on the F4TCNQ molecule. A dielectric medium with static dielectric constant,ϵ, set to 3.0, was introduced in some calculations, using the conductor-like polarisable continuum model (CPCM),[89,174,175] to represent the excess P3HT chains that surround the charge-transfer complex in solution. Where a dielectric medium was included in time-dependent density functional theory (TDDFT) calculations, the optical dielectric constant, ϵ_∞, was set to 3.0. Both the static and optical dielectric constants replicate the experimental quantities for organic semiconductors.[144–149]

The 6-31G(d) basis set was used in all cases, and for comparison both the B3LYP[63] and optimally-tuned range-corrected LRC-ωPBEh[70] functionals were used. For the range-corrected functional, $\omega = 0.065$ bohr^{-1} and $\omega = 0.005$ bohr^{-1} in vacuum and dielectric medium, respectively. These values for ω were optimised using combined ionization potential and electron affinity tuning, as used by Zheng *et al.*[125] See Appendix A, Table A.1 for details of the parameters obtained with the optimal ω. Grimme's D2 dispersion correction was applied to all B3LYP calculations (B3LYP-D).[67]

TDDFT was applied to the optimised complex in order to obtain excitation energies and excited state charge populations. An excited state geometry optimisation was also performed using this technique. Simulated absorption spectra were generated by convolution with a Gaussian of width 0.1 eV using Gabedit software.[123] Natural transition orbital[86] plots were visualised using Molden (isodensity = 0.01).[176] Charge transfer in each excited state was quantified using the sum of Mulliken charges on F4TCNQ for the excitation.

To obtain the neutral state of the dimer complex, constrained density functional theory[78] was applied using the B3LYP-D functional with and without implicit solvent. The charge on the F4TCNQ fragment was constrained using Becke population constraints, with the spin on both fragments set to zero. All calculations were performed on Q-Chem 4.3.[96]

4.3 Results and discussion

4.3.1 Excited-state properties

Natural transition orbital analysis

Time-dependent DFT (TDDFT) calculations were performed on the M8 dimer complex and the simulated absorption spectra for both the B3LYP-D and LRC-ωPBEh functionals with and without solvent are shown in Figure 4.2. In this study, implicit solvent was used to represent the P3HT that surround the charge-transfer complex

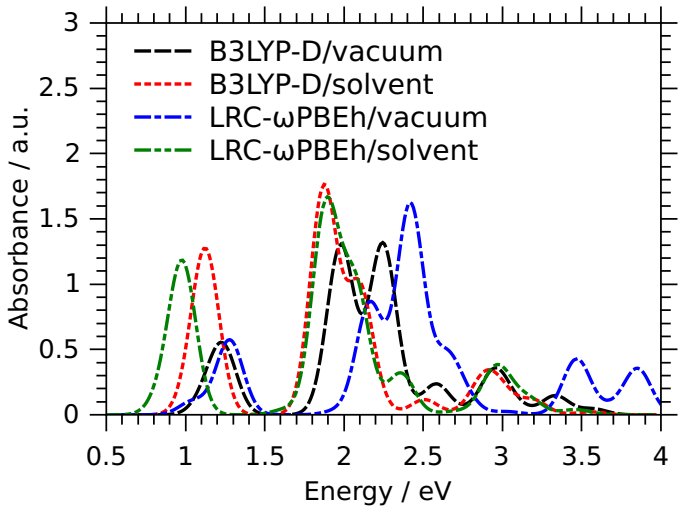

Figure 4.2: Simulated absorption spectra for the B3LYP-D and LRC-ωPBEh functionals in vacuum and implicit solvent

in the experimental system. The resulting excitation energies with intensity > 0.1 a.u. were extracted. Natural transition orbitals (NTOs) were used to visualise the movement of electron density upon excitation. NTOs are a unitary transform of the various Kohn-Sham (KS) orbitals involved in a transition, and provide qualitative information regarding the location of the particle (electron) and hole in a transition. Excitation can then be considered as the movement of electron density from the hole state to the particle state, and thus a description of the change in electron density during excitation can be elucidated. This data is tabulated in Figure 4.3.

If a photo-induced charge-transfer reaction does occur in the P3HT/F4TCNQ system, an orbital transition involving electron density moving from dopant to oligomer will be observed. Experimental studies suggest that such an excitation occurs close to 405 nm, or 3.1 eV (Figure 4.1). Criteria for a charge-transfer transition in the computational model hence include a reduction in electron density on F4TCNQ and an increase in the M8 oligomer; a decreased charge on the F4TCNQ molecule; and an excitation energy close to 3 eV. Inspection of Figure 4.3 reveals a number of excitations across each system that match these criteria.

It appears that a handful of states correspond to a decrease in electron density on the F4TCNQ molecule, and most of these have excitation energies close to 405 nm, or 3 eV. The 17th and 22nd excited states in the B3LYP-D/vacuum system both appear to exhibit back-transfer of charge from F4TCNQ onto P3HT, although the former excitation has less charge-transfer character. Likewise, in the corresponding solvated system the 16th, 20th and 22nd excited states appear to match the criteria, with the 16th and 20th states also having less dominant charge-transfer character. This transition is also present in the LRC-ωPBEh functional systems, occurring as the 21st excited state in the vacuum system and the 20th and 22nd excited states in the solvated system. It should be noted that TDDFT calculations are notorious for

Table 4.1: Calculated excitations proposed to correspond to experimental photo-induced charge-transfer excitations, with Mulliken charge change on F4TCNQ (positive indicates a decrease in electron density), orbital transition responsible for excitation and corresponding percentage molecular orbital contribution

Functional	Solvent	Exc. energy (eV)	Δq (e)	Transition	% contribution
B3LYP-D	No	3.33	0.10	H→L+3	53
	Yes	3.19	0.28	H→L+3	86
LRC-ωPBEh	Yes	3.17	0.25	H→L+3	71

producing spurious transitions. Here a large number of excited states with near-zero intensity are observed as a result of this behaviour, which is why the excited states of interest appear as such high numbered transitions.

Molecular orbital analysis

Inspection of each excitation revealed the Kohn-Sham (KS) orbital transitions responsible for the excitation. A number of KS orbital transitions may contribute to one excitation, and hence the qualitative information gleaned about an excitation is a little more ambiguous than that obtained from NTOs. Nonetheless, molecular orbitals are regularly used in the literature to derive a description of electron density movement upon excitation.[44,49,141] In this work, they are used in conjunction with NTOs to provide an elementary understanding of the movement of electron density upon excitation of the complex. The transition that contributed the most to each excitation is tabulated in Figure 4.4. In some cases, the dominant KS orbital transition accounted for less than 50 % of the total transition (See Appendix B, Table B.1 for contributions).

The dominant orbitals for each transition in all four systems are qualitatively consistent for the most part. In particular, given the consistency of dominant transitions irrespective of functional and dielectric medium, it is possible to conclude that the first five excited states arise from HOMO→LUMO, HOMO–1→LUMO, HOMO→LUMO+1, HOMO–3→LUMO and HOMO–4→LUMO excitations, respectively. Furthermore, orbital shape is qualitatively consistent irrespective of functional and solvent. Of particular note is the fact that the HOMO and LUMO are both entirely delocalised over the dimer complex, rather than being localised on one molecule or the other. Most transitions involve electron density changes across the entire molecule, rather than from one molecule to the other.

Analysis of the Mulliken charge population on the F4TCNQ molecule for each vertical excitation was used to quantify the degree of charge transfer in the corresponding excited state. This value was compared with the ground-state charge to give the change in charge on F4TCNQ during excitation. These values are recorded for each transition in Figure 4.4, where a negative value indicates a decrease in charge density on F4TCNQ. Considering the degree of change in charge on F4TCNQ as a criterion for a photo-induced charge-transfer excitation, the 22nd excited state in

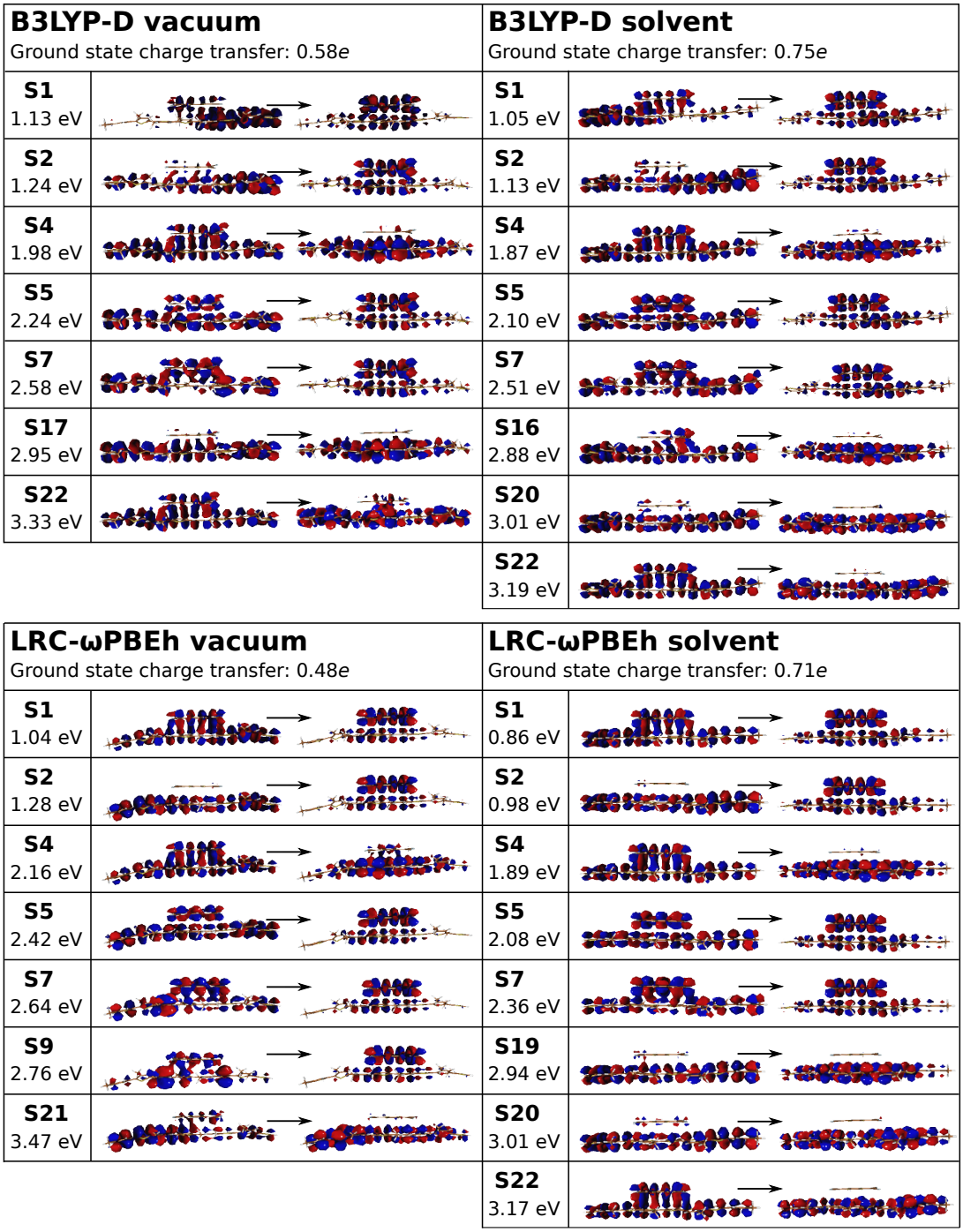

Figure 4.3: Dominant natural transition orbitals for excited states corresponding to excitations with intensity $>$ 0.1 a.u. for the M8 dimer. Excitation energies and singlet transition number are also listed.

both B3LYP-D systems and the 22nd excited state in the LRC-ωPBEh system with implicit solvent are potential candidates. In each of these three cases the excited state corresponds to a HOMO→LUMO+3 transition. For the LRC-ωPBEh/vacuum system the peak displaying the expected behaviour for photo-induced charge back-transfer, i.e. the 21st excited state, is actually the result of an almost even mixing of the HOMO-1→LUMO+2 and the HOMO→LUMO+3 transition. The charge density is essentially the same between ground and excited states for this excitation, suggesting that it is not a charge-transfer excitation. Interestingly, no excitation in the range-corrected vacuum system matches the photo-induced charge-transfer criteria, which highlights the importance of the dielectric medium for modelling experimental charge transfer behaviour.

With respect to the proposed charge-transfer mechanism, it is of key importance to note that while a decrease in charge density on F4TCNQ does occur for each of the transitions listed in Table 4.1, the vertical excited state in each instance is not charge neutral. To investigate how the charge separation in the excited state changes as the geometry is allowed to relax to its equilibrium state, an excited-state geometry optimisation was performed on the 22nd excited state in the B3LYP-D/solvent system. The resulting geometry was not charge neutral, and in fact relaxation of the excited state yielded a greater charge density on F4TCNQ compared with vertical excitation (Table 4.2). This result shows that the 22nd excited state is not charge-neutral and that relaxation to a charge-neutral state may be blocked by an energy barrier. This behaviour is likely to be consistent between the two functionals in the presence of implicit solvent due to the similarity in TDDFT results between the two and the similar amount of Hartree-Fock exact exchange at short range as a result of the small ω value in the tuned functional.

The B3LYP-D functional, in spite of its documented problems with accurately describing charge-transfer states,[156,158] gives surprisingly comparable results to the range-corrected functional, both in terms of excitation energies and nature of the natural transition orbitals. A smaller degree of charge transfer occurs in the excited state of interest for the vacuum system compared with the solvent system (Table 4.1), which highlights the necessity of considering the environment of the system. However, in terms of excitation energy of the B3LYP functional compared with the range-corrected functional, the results are essentially the same in solvent. This fact suggests that, as B3LYP is known to perform poorly for charge-transfer excitations, the excited states of interest may not be charge-transfer excited states in the truest sense. In particular, the electron density is delocalised over the complex in the initial state and localised on the oligomer in the final state. This incomplete charge transfer may account for the good performance of the B3LYP-D functional.

4.3.2 Charge-neutral state

To establish whether the charge-neutral state of the dimer complex is metastable with respect to relaxation into the ground charge-separated state, a series of con-

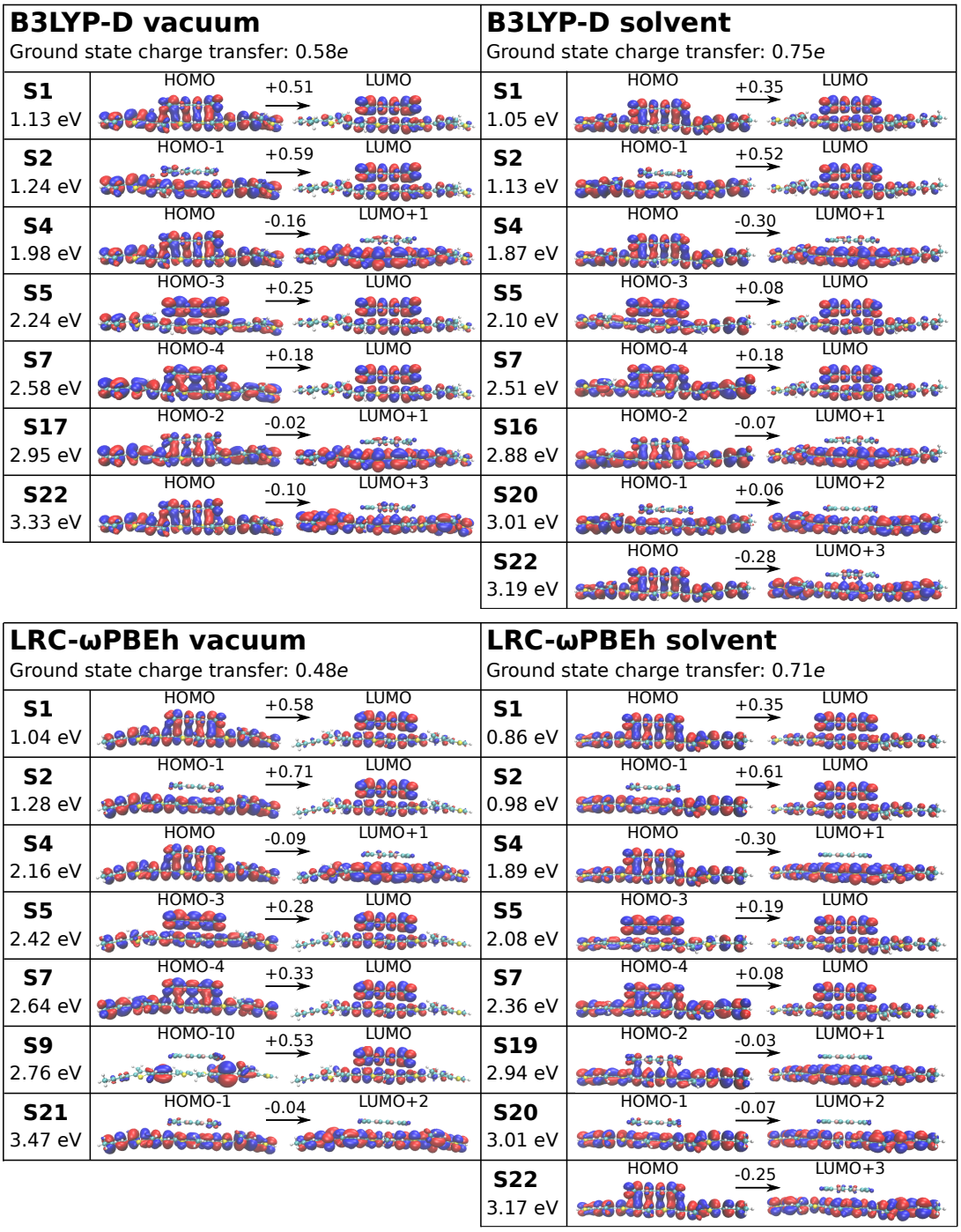

Figure 4.4: Dominant molecular orbital transitions for excited states corresponding to excitations with intensity $>$ 0.1 a.u. for the M8 dimer, as well as the change in electron density on F4TCNQ (e). A negative value indicates a decrease in electron density. Excitation energies and singlet transition number are also listed.

Table 4.2: Ground, excited and neutral state properties for the M8 dimer complex calculated at the B3LYP-D/6-31G(d) level of theory in implicit solvent ($\epsilon = 3.0$)

State	Separation (Å)	Charge (e)
Ground	3.1	0.75
22nd exc. (vertical)	3.1	0.47
22nd exc. (relaxed)	3.5	0.80
Neutral	3.2	0.0

strained DFT calculations were performed for the B3LYP-D complex in vacuum. Charge constraints ranging from zero to one electron constrained on the F4TCNQ molecule, at $0.25e$ intervals, were applied. The ground charge-separated state corresponds to roughly half an electron on the F4TCNQ molecule in vacuum, and around $0.75e$ in implicit solvent.

The geometry of the charge-neutral state was compared with that of the optimised excited-state geometry and the ground-state geometry. The excited-state geometry showed an increase in intermolecular separation of 0.4 Å compared with the ground state, and 0.3 Å compared with the charge-neutral state (Table 4.2). The substantial difference in geometries between excited and neutral states suggest the presence of a considerable energy barrier to relaxation from excited to neutral states.

The energy difference between the charge-neutral state and each of the charge-constrained states was measured. If the charge-neutral state were metastable, increasing the charge density on F4TCNQ from zero would increase the energy of the system, and an energy barrier to relaxation from neutral to charge-separated states would be present. However, the results do not indicate the presence of an energy barrier. Energy difference with respect to the charge-neutral state was plotted against fraction of charge constrained to the F4TCNQ molecule (Figure 4.5). The resulting energy profile shows a smooth curve downwards from the neutral state to the $0.5e$ constraint state, which as previously noted is roughly equivalent to the ground state of the system for the functional used. The energy difference between neutral and ground states is around 0.20 eV, or 19 kJ/mol. The integer charge-separated state is also higher than the charge neutral state by around 0.07 eV (6.7 kJ/mol).

The above calculations were then repeated for the B3LYP-D/solvent system in order to investigate whether accounting for the surrounding polymer chains present in the experimental system results in increased stability of the charge neutral state. In this case, the CDFT calculations reveal a minimum energy near $0.75e$ on F4TCNQ, which is expected as CPCM solvent has already been demonstrated to increase ground-state charge transfer. Again, no energy barrier is observed between charge-neutral and ground states. The energy difference between the ground and charge-neutral states is 0.33 eV (32 kJ/mol). Because the ground state corresponds to a greater degree of charge transfer in the solvated system compared with the vacuum system, the integer-charge-separated state lies only 0.07 eV (6.7 kJ/mol)

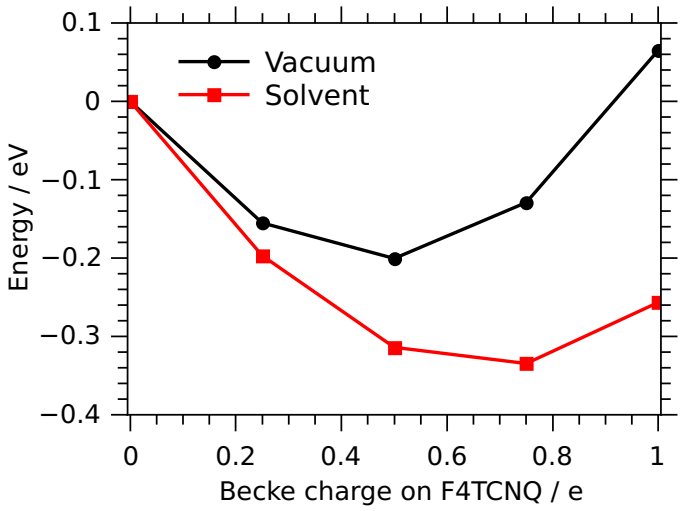

Figure 4.5: Energy difference between charge neutral and charge-separated states with increasing charge density constrained to F4TCNQ for the B3LYP-D/vacuum and solvent systems.

above the ground state and is 0.26 eV (25 kJ/mol) lower than the charge-neutral state.

The smooth energy profile observed both in vacuum and in the presence of implicit solvent provide strong evidence against the charge-neutral state being metastable. This result implies that if relaxation of the excited state into the charge-neutral state does occur as a result of photo-induced charge transfer from dopant to polymer, the system is unlikely to persist in this neutral state. Given the lack of an energy barrier between the two states, relaxation is likely to be essentially instantaneous.

4.4 Conclusions

The likelihood of a photo-induced charge-transfer reaction between dopant and polymer resulting in a charge-neutral state was evaluated using density functional theory. Comprehensive analysis of the excited states obtained from time-dependent DFT calculations revealed the presence of a possible charge-transfer state near 3 eV, which is consistent with the energy of the light used to optically control solubility in the work by Jacobs *et al.* Geometry optimisation of this state revealed that it was not, in fact, charge neutral, suggesting that relaxation of the excited state into the charge-neutral state is not a likely pathway. Furthermore, a series of constrained DFT calculations with a varying degree of charge constrained on F4TCNQ yielded a smooth curve with no energy barrier between the charge-neutral and ground charge-separated state. This result reveals that no energy barrier exists to relaxation to a charge-separated state.

Physically, this result is of interest for the solubility change mechanism in the P3HT/F4TCNQ system. It was originally hypothesized that a charge-transfer exci-

tation results in charge-neutral components, which display increased solubility in a set of given solvents. The calculations performed here suggest that such a mechanism is unlikely. Firstly, excitation to a charge-neutral state does not appear possible, as no such excited state was found to exist in the systems studied. Furthermore, the charge-neutral state into which the system is proposed to transfer is not metastable. This indicates that, even if the system does enter a charge-neutral state, such a state would not persist and the system would almost instantaneously relax back into the charge-separated ground state. It is reasonable to conclude, therefore, that an alternative mechanism is responsible for the photo-induced de-doping of F4TCNQ from P3HT at 405 nm.

5 | Molecular mobility of F4TCNQ in P3HT systems

Unpublished work written in manuscript style

Principal author (candidate): Sophia Ackling
Contribution: 85 %
Designed and carried out quantum calculations to investigate energy barriers in the system of interest. Collected, analysed and interpreted the data presented. Conceived and prepared the chapter as contained herein.

This chapter reports on original research conducted during the period of my Higher Degree by Research candidature and is not subject to any obligations or contractual agreements with a third party and would constrain its inclusion in this thesis. I am the primary author of this chapter. I hereby certify the statement of contribution is accurate.

Sophia Ackling — 26/10/16 Date

Contributing author: David Huang
Contribution: 15 %
Supervised quantum calculations, and assisted with mathematical interpretation of data and editing of the chapter.

I hereby certify that the statement of contribution is accurate and grant permission for the candidate to include work pertaining to the publication in their thesis.

David Huang — 26/10/16 Date

Abstract

A limiting factor in the ability of popular p-type dopant 2,3,5,6-tetrafluoro-7,7,8,8-tetracyano-quinodimethane (F4TCNQ) to dope the poly(3-hexylthiophene) (P3HT) polymer is the solubility of the dopant in solvents commonly used for P3HT. Recent work has demonstrated improved solubility of the dopant by substitution of one or more of the cyanide groups with an ester group. It is also anticipated that diffusion mechanisms of the dopant within the polymer system will be affected by this substitution, potentially resulting in a more stable doped polymer system. Understanding how substitution affects diffusion could lead to better dopant design in future studies. Preliminary experimental studies using quasi-elastic neutron scattering (QENS) have measured two diffusion processes for the substituted dopant, and this work seeks to interpret the experimental observations and identify the processes responsible. Density functional theory calculations are used to investigate the impact of replacing one cyanide group with a methyl-ester group on F4TCNQ, with particular focus on mobility of the dopant along the polymer backbone as a proxy for mobility of the dopant in the polymer film. Charge transfer between dopant and a short methyl-substituted oligothiophene is observed to decrease by 25 % upon substitution with the ester group as a result of a higher energy LUMO. Energy barriers to translation along the oligomer backbone by both the F4TCNQ and substituted F4TCNQ dopants, and methyl rotation in the substituted dopant, are quantified. The activation energy for methyl rotation is found to be in very good agreement with one of the experimentally measured diffusion processes. The charge on both dopants is observed to vary by as much as $0.2e$ during translation, highlighting the importance of considering quantum effects when studying diffusion processes in doped polymer systems. The energy profiles for translation are essentially the same for both dopants except for the point at which the methyl group on the substituted F4TCNQ molecule is in close proximity with the methyl groups on the oligomers, at which point a large energy barrier is present. Analytical equations are used to describe diffusion coefficients in each of the two systems, and the functional group substitution of F4TCNQ is found to approximately halve the diffusion coefficient. The diffusion coefficients are approximated and found to be two orders of magnitude smaller than experimental measurements for the second diffusion process, indicating that an alternative diffusion mechanism is likely to be occurring within the system.

5.1 Introduction

Organic semiconducting polymers present a viable alternative to inorganic-based electronics, with the potential for cheaper production and greater diversity of applications as a result of improved flexibility. The semiconducting properties of organic polymers can be improved by introducing a dopant, which serves to increase the number of charge carriers available for conduction within the system.[14,37,114,115,165] Charge transfer between organic polymer and dopant has been shown to induce

aggregation and crystalline regions in some polymer/dopant systems.[26] However, the stability of the resulting film can vary. For the purpose of commercial products, degradation of organic devices must be considered.[177,178] While a number of degradation pathways can be removed by using careful production techniques and conditions,[179] diffusion of the device components, including polymer, dopant and metal components, between layers can lead to a reduction in performance and lifetime of the device.[180,181]

Early doping studies used halogen atoms such as iodine[12] or metals atoms[13] to dope semiconducting polymers. Despite inducing vast improvements in thin-film conductivities, these dopants readily diffused from the system due to their small size. Such behaviour is less than ideal if widespread commercial adoption of the technology is to be realised. Improvements in device stability have been realised by using small molecules as dopants, such as the strong electron acceptor 2,3,5,6-tetrafluoro-7,7,8,8-tetracyano-quinodimethane (F4TCNQ), to dope popular polymers such as poly(3-hexylthiophene) (P3HT).

F4TCNQ is a small aromatic molecule, and its increased stability in polymer films can be attributed to π-stacking with the polymer backbone, as well as its bulk when compared to atomic dopants. In spite of this increased stability and considerable popularity as a dopant for organic polymers and organic molecules, numerous studies have observed diffusion of this dopant in such systems. This behaviour is exacerbated by higher temperatures.[182] To address this issue, a variety of alternative dopants displaying similar electron affinities but reduced diffusion rates have been reported.[31,56–59] It has been demonstrated that increasing the polarity of the thiophene ring within the polymer, for example by replacing hexyl chains with ether-based chains, decreases F4TCNQ diffusion at elevated temperatures.[183] However, it is also possible that small modifications to the original F4TCNQ dopant could equally reduce diffusion.

A systematic investigation by Li *et al.* recently reported a number of modified F4TCNQ dopants with improved solubility in non-polar solvents.[60] The motivation for this work was to address the problem of poor solubility of F4TCNQ in solvents regularly used for solution processing of P3HT. By improving dopant solubility, solution processing of P3HT/F4TCNQ mixtures becomes a plausible way to produce polymer films on a commercial scale. In the aforementioned study, the solubility of the F4TCNQ dopant was improved by replacing one or more cyano groups with ester groups. In all cases, the electron affinity of the modified dopant was only slightly smaller than that of F4TCNQ, ensuring that the modified dopants maintain the ability to p-dope P3HT. However, the addition of ester groups introduces steric bulk onto the dopant, and removes its planarity. As a result, diffusion of the dopant in the polymer film is likely to be affected. These modified dopants thus have the potential to not only display improved solubility, but also a reduced diffusion rate in P3HT.

Preliminary experimental studies using quasi-elastic neutron scattering (QENS)

have measured two diffusion processes within methyl-ester mono-substituted F4-TCNQ (mF4TCNQ). One of these processes, a "fast" process, is hypothesised to arise due to methyl hydrogen rotation as the energy barrier to rotation is consistent with literature on such a process. The slower process is thought to be the result of translation of the dopant along the polymer backbone.

This study presents a preliminary computational investigation into how functional group substitution of F4TCNQ impacts dopant mobility. Density functional theory calculations are used to model the experimental system using a dimer complex representing the polymer/dopant charge transfer unit. Charge transfer is shown to decrease with substitution of a cyanide group with a methyl-ester group as a result of less favourable orbital overlap compared with the original dopant. A simplified sandwich structure is then modelled, with each dopant placed between two short substituted thiophene chains. Two different inter-chain separations are considered. The energy barrier to rotation of the substituted dopant methyl group is quantified and compared with experimental measurements. The energy barrier to translation of each dopant between the two thiophene chains is also quantified and compared, and the charge on the dopant is monitored during translation. The impact of functional group substitution on dopant mobility is elucidated.

5.2 Computational details

A dimer complex comprising one dopant molecule placed over the central inter-thiophene bond in an eight-unit methyl-substituted oligothiophene was constructed. Previous work by this author has revealed the necessity for methyl side chains on the thiophene oligomer in order to accurately model electronic properties in the P3HT/F4TCNQ system (see Chapter 3). Furthermore, an eight-unit chain has been demonstrated to be necessary to model the conjugation length of the polymer. This length is also sufficient such that the translated dopant will not progress beyond the end of the oligomer. Hence, eight-unit methyl-substituted thiophene (M8) oligomers were used to represent P3HT in all calculations. Both F4TCNQ and its methyl-ester-substituted version (mF4TCNQ) were considered, with the latter placed such that its methyl group was on the opposite side to the nearest oligothiophene methyl group (Figure 5.1). Geometry optimisations were performed in the presence of a dielectric medium used to represent the P3HT chains that surround the explicitly modelled molecules in the experimental system. This medium was introduced using the conductor-like polarisable continuum model (CPCM),[89,174,175] with a dielectric constant of 3.0. This value is deemed appropriate for organic semiconductors.[144–148] Charge transfer was assessed based on charge distributions using charges from the electrostatic potential on a grid (CHELPG).[124] Similar calculations were performed on the isolated dopant molecules and oligomer in the dielectric medium in order to extract molecular orbital energies.

In order to accurately model the translation of the dopant molecule along the

polymer backbone, a "sandwich" geometry was constructed, in which the dopant molecule was placed between two parallel M8 oligomers. The M8 chains were held fixed at an inter-chain separation of 6.30 Å and the mF4TCNQ (or F4TCNQ) molecule was allowed to relax. The geometry of both chains was taken from calculations on the molecule in isolation, because fully relaxed optimisation of the system resulted in the chains bending around the dopant molecule and would have hence created a spurious energy barrier to translation. The large system size resulted in poor convergence of the geometry optimisation in both cases, and so convergence was considered reached once the energy difference between sequential optimisation steps fell below 0.01 kJ/mol. For the substituted dopant, two geometries were considered, in which the mF4TCNQ methyl group was either on the same side as the M8 methyl groups, or on the opposite side (Figure 5.1). The opposite side geometry was found to be the lower in energy by around 12 kJ/mol, and so was used for subsequent calculations.

Having established a starting geometry, each dopant was progressively translated between the two chains to obtain a potential energy profile. Two inter-chain separations were considered for this translation: 6.30 Å and 6.96 Å. These values correspond to twice the optimal M8/F4TCNQ dimer complex separation optimised using B3LYP with and without Grimme's D2 dispersion correction,[67] respectively. Using these two separations gave a lower and upper boundary on the energy barriers to rotation and translation due to van der Waals interactions, while also allowing for the impact of inter-chain separation on system properties to be examined. The dopant molecule was placed equidistant from each chain, with its ring over the central inter-thiophene bond. Charge population was monitored during translation using Mulliken charge population analysis.

Because of its good performance for ground-state properties of organic semiconducting systems, the B3LYP functional[63] was used with the 6-31G(d) basis set. Grimme's D2 dispersion correction was applied in all cases.[67] All calculations were performed using Q-Chem 4.3,[96] and the initial guess for the mF4TCNQ molecule geometry was generated using GaussView 5.[121]

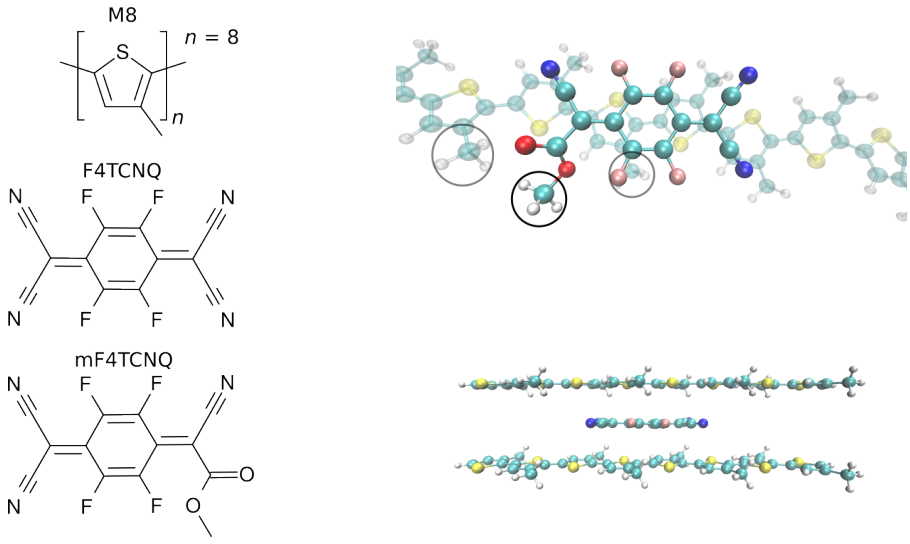

Figure 5.1: Left: structures of the simplified P3HT polymer and the F4TCNQ and mF4TCNQ dopants used in this study. Top right: lowest energy configuration of the mF4TCNQ molecule in the dimer or sandwich complex maximises the distance between dopant and oligomer methyl groups (circled). Bottom right: an example of the "sandwich" structure comprising oligomers and dopant.

5.3 Results and discussion

5.3.1 Charge transfer

The performance of the original F4TCNQ dopant was compared to that of methyl-ester-substituted F4TCNQ (mF4TCNQ) by investigating the degree of charge transfer upon mixing. Each dopant was modelled in a dimer complex with an M8 molecule, and the optimised charge distribution was inspected. The substituted dopant was revealed to induce a smaller degree of charge transfer from the oligothiophene (Table 5.1). This decrease in charge transfer can be attributed to molecular orbital alignment. Charge transfer occurs efficiently in the P3HT/F4TCNQ system as a result of the lowest unoccupied molecular orbital (LUMO) of F4TCNQ being lower in energy than the highest occupied molecular orbital (HOMO) of P3HT (Figure 5.2). An electron can then be efficiently transferred from polymer to dopant. The calculated highest occupied molecular orbital (HOMO) of the M8 oligomer is found to be -4.52 eV, while cyclic voltammetry measurements suggest it lies close to -5 eV.[184] Differences between calculated and experimental values are likely the result of the level of theory used. Nonetheless, calculations qualitatively model the relative molecular orbital energies of dopants and oligomer. The calculated LUMO of F4TCNQ is 0.41 eV lower in energy than the HOMO of the oligomer and hence efficient charge transfer occurs between the two. Functional group substitution of F4TCNQ with a methyl-ester group increases its LUMO to an energy that is iden-

Table 5.1: Calculated and experimental[60] (in parentheses) LUMO energies and charge transfer (CT) for the two dopants

	LUMO (eV)	CT (e)
F4TCNQ	-4.93 (-5.23)	0.82
mF4TCNQ	-4.52 (-5.14)	0.64

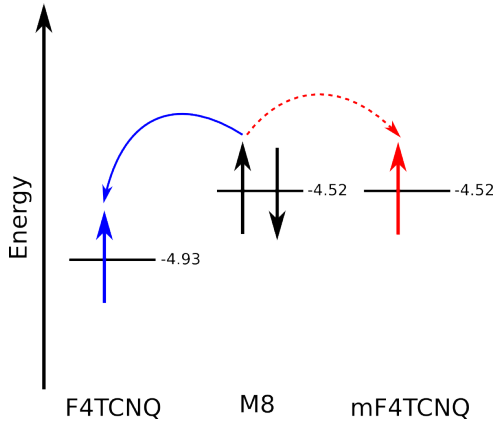

Figure 5.2: Charge transfer process proceeds more readily for F4TCNQ than mF4TCNQ due to the greater energy difference between M8 HOMO and F4TCNQ LUMO energies.

tical to the HOMO of the M8 oligomer. The efficiency of charge transfer between the two is hence reduced. This observation is consistent with the experimental observation that substitution decreases the electron affinity of the dopant.[60]

5.3.2 mF4TCNQ methyl rotation

Methyl rotation in the mF4TCNQ molecule is a diffusion process that is likely to occur within the P3HT/mF4TCNQ system. In order to quantify the energy barrier to rotation, DFT calculations were performed. Using the optimised geometry of the M8 sandwich complex described above, with the two inter-chain separations, the entirety of the complex was held fixed except for the three hydrogens on the mF4TCNQ ester methyl group. The hydrogens were allowed to relax subject to a set of dihedral angle constraints on one of the hydrogen atoms. These constraints yielded energies for the system with a methyl rotation of 0, 30, 60, 90 and 120 degrees from equilibrium geometry.

From the resulting energies, an activation energy, E_A, of methyl rotation was found to be around 8 kJ/mol for the closer separation and around 11 kJ/mol for the larger separation (Table 5.2; for plot of this data see Appendix C, Figure C.1). The difference in energies for the two inter-chain separations highlights the fact that the proximity of the P3HT chains has a small but significant effect on methyl rotation. In these calculations, this increase in separation lowers the energy of the ground state of the system more substantially than that of the transition state, leading to a greater energy barrier to methyl rotation in the system with larger inter-chain

Table 5.2: Calculated model parameters for methyl rotation in mF4TCNQ

Inter-chain separation (Å)	Rotation energy (kJ/mol)	Jump length (Å)
6.30	7.8	1.8
6.96	10.7	1.8

separation. Because the dopant molecule remains almost entirely fixed in these calculations, the change in steric repulsion results in a counter-intuitive increase in energy barrier with increasing separation. These values both match reasonably well to experimental results, which have measured a "fast" diffusive process with an energy barrier estimated to be $E_{\mathrm{A}} = 9 - 12$ kJ/mol.[185] Increasing the inter-chain separation reduces repulsive steric interactions within the system, and hence the energy of the system.

The jump length associated with this diffusion process is the distance travelled by the hydrogen atoms between each barrier-crossing event in this process. The experimental jump length was estimated to be around 2.5 Å [185] which is quite a bit longer than the calculated physical distance a methyl hydrogen would move during a rotation through zero to 120 degrees (1.8 Å linearly, 2.1 Å arc length). However, these calculations were performed at a fairly low level of theory and with necessary physical constraints on oligomer flexibility. Overall, the DFT calculations provide evidence that methyl rotation is indeed responsible for the experimentally observed "fast" process. The energy barrier to rotation is only a little larger than the thermal energy at room temperature, $k_{\mathrm{B}}T$, and so this process proceeds freely under such conditions.

5.3.3 Dopant translation

Using the optimised geometry of the sandwich model described above as a starting point, both dopant molecules were translated along the plane between the two M8 oligomers, through half a thiophene unit in each direction (1.97 Å) at the smaller inter-chain separation of 6.30 Å. While the atom positions in the oligomer chains were once again fixed, in these optimisations the dopant molecule was free to relax, with one atom fixed so that the molecule remained in the necessary translated position relative to its optimal geometry.

The energy profile for each dopant molecule reveals an energy barrier roughly one Ångstrom from the optimal geometry in both directions. A local minimum appears to be present at half a thiophene unit (close to 2 Å) translation in either direction. This corresponds to the point at which the rings of the dopant molecule are in line with those of the thiophene chains. This stabilisation is likely the result of π-π stacking. The lower energy barriers in mF4TCNQ could be the result of slight stabilisation from interactions between the methyl oxygen and the fixed hydrogens on the oligomers, as these overlap at the energy maximum. Such stabilisation is not present in F4TCNQ as the nitrogen does not come into close contact with these

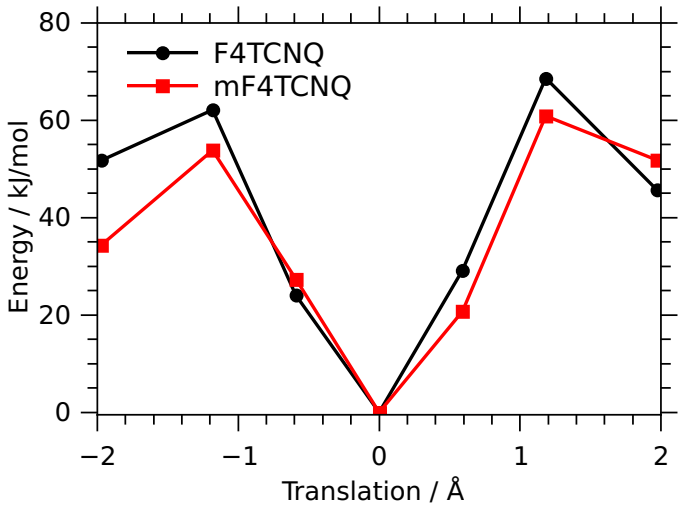

Figure 5.3: Energy profile for the translation of two dopant molecules between planar M8 oligomers over one thiophene unit for an inter-chain separation of 6.30 Å.

same hydrogens and instead sits between thiophene carbons on the oligomers. It is interesting to note the size of the energy barriers and the energy of the local minima: both are quite high in energy. In fact, the energy barrier to translation in both dopants is more than 20 times thermal energy, suggesting that both systems are very stable to translation. It is possible that these energy barriers are overestimated as a result of steric interactions between dopant and oligomers, and that in the experimental system the inter-chain separation is larger than 6.30 Å.

The same calculations were then performed at an inter-chain separation of 6.96 Å. The two inter-chain separations considered in this work aim to replicate the dynamic and varied nature of inter-polymer separation in the experimental system. In order to account for the asymmetry in the methyl-substituted thiophene rings, translation was extended to include one full thiophene ring in each direction from the equilibrium geometry (3.94 Å). The energy profile for this process for both dopants is displayed in Figure 5.4. The degree of charge transfer was also quantified by considering the Mulliken population of charge on the dopants. Figure 5.5 displays how charge transfer varies with dopant position, and it is evident that substantial fluctuation in charge transfer of up to $0.2e$ occurs during dopant translation. This result highlights the importance of quantum considerations when modelling diffusion in polymer/dopant systems and discussing their stability, and suggests that a classical description of diffusion in this system, with fixed charge distributions, would be unrealistic.

All energy barriers at the larger inter-chain separation are substantially smaller than those in Figure 5.3 for the smaller inter-chain separation. This is likely the result of reduced steric repulsion between dopant and chains. Unlike in the methyl rotation calculations, in this case the dopant molecule is free to relax between the chains, and can thus reduce the steric interactions to a greater degree. This results

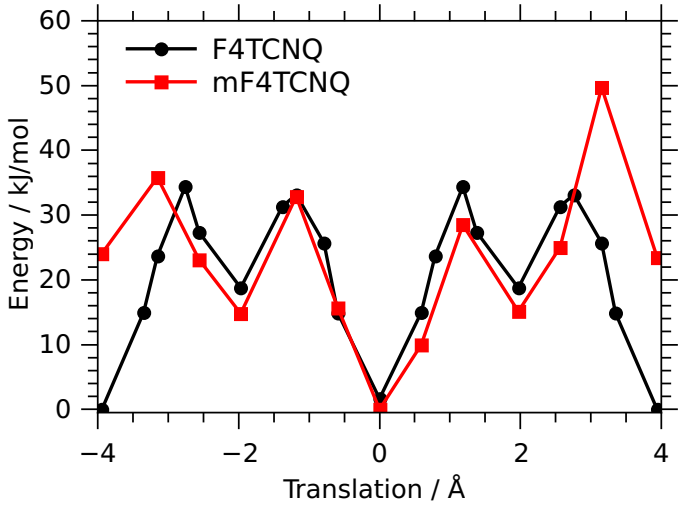

Figure 5.4: Energy profile for the translation of two dopant molecules between planar M8 oligomers over two thiophene units for an inter-chain separation of 6.96 Å.

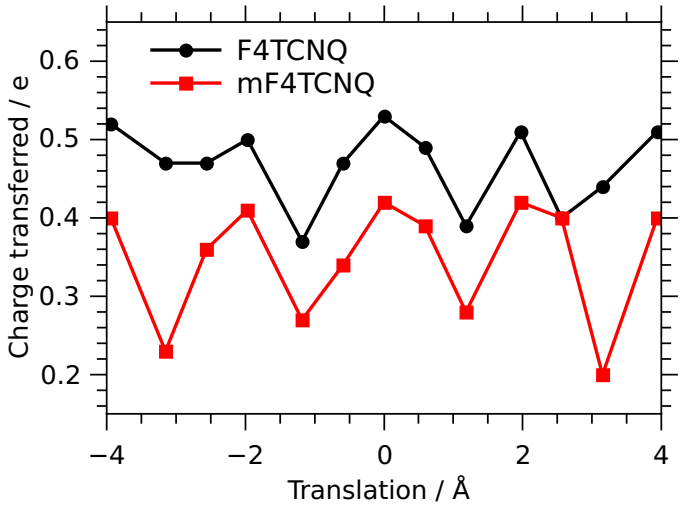

Figure 5.5: Charge transfer profile for the translation of two dopant molecules between M8 oligomers over two thiophene units at an inter-chain separation of 6.96 Å.

in a more intuitive change in energy barrier heights. It is evident that inter-chain separation dramatically affects translation of the dopant throughout the polymer system. In order to reduce dopant diffusion, it may be possible to design polymers with shorter stacking distances and hence produce more stable polymer/dopant mixtures.

Considering first the F4TCNQ dopant, it is clear that translation yields a symmetric energy profile with two energy barriers. The activation energies for the two barriers in F4TCNQ are 18 and 34 kJ/mol, and the system returns to a global minimum upon translation through one thiophene unit. Although the energy was evaluated at the same 13 points as in mF4TCNQ, because of the symmetry in F4TCNQ, the data points for each direction were combined to give 21 points. The repeat unit in the energy profile for mF4TCNQ involves translation over two thiophene units, as shown in Figure 5.4, wherein the energy at ±4 Å (or ±1 thiophene unit) is equivalent. This is a result of the asymmetry in the dopant molecule and the thiophene units in the oligomers. This potential energy profile involves four barriers to translation, with activation energies of 15 (two barriers), 31 and 35 kJ/mol.

It is possible to approximate the impact of functional group substitution on the diffusion coefficient, D, by considering the activation energies to translation for each dopant. A naïve approach may be to consider just the maximum energy required for each dopant to traverse two thiophene units and consider each of these to be the activation energy, E_{A}, in the Arrhenius relation,

$$D = D_0 \exp\left(\frac{-E_{\mathrm{A}}}{RT}\right) \tag{5.1}$$

where D_0 is a prefactor that will likely be similar for both systems. Taking a ratio of diffusion coefficients for F4TCNQ versus mF4TCNQ, with $E_{\mathrm{A}} = 34$ kJ/mol for F4TCNQ and $E_{\mathrm{A}} = 50$ kJ/mol for mF4TCNQ, yields a very large value of 640. However, given the complex nature of the multi-barrier diffusion processes observed in both systems, such a simplification is unlikely to be a realistic approach. A better description of the system can be obtained by considering a one-dimensional model of multi-step diffusion.

Kramers' theory states that the hopping rate between energy wells, h, can be calculated using

$$h = \nu \mathrm{e}^{-E_{\mathrm{A}}/k_{\mathrm{B}}T}, \tag{5.2}$$

where ν is the jump attempt frequency and E_{A} is the activation energy. The jump attempt frequency may be approximated as the effective vibrational frequency for the dopant molecules in a harmonic potential fit to the energy well of interest:

$$\nu = \frac{1}{2\pi}\sqrt{\frac{k}{m}}. \tag{5.3}$$

Here k is obtained from the harmonic fit, and m is the mass of the dopant molecule. In this work, the curvature of the energy wells is essentially equivalent for each well and for both dopants. Likewise, the mass of the dopants differs only slightly. Hence it is reasonable to assume that the difference between ν in each system is negligible and will not greatly affect the calculated hopping rate. In order to quantify the frequency factor, ν, energy values for translation between ± 1 Å for F4TCNQ were plotted and a quadratic fit was applied to the data (Appendix C, Figure C.2). From this fit, ν was found to be on the order of 10^{11} s^{-1} using Equation 5.3.

Theoretical methods for estimating the diffusion coefficient in a multiple-barrier system have recently been reported by Yang *et al.*[186] Here the same methodology will be applied to F4TCNQ (a two-barrier system extending over one thiophene unit) and mF4TCNQ (a four-barrier system extending over two thiophene units). Firstly, consider the barriers to translation in the F4TCNQ energy profile. The equation for the diffusion coefficient in a two-barrier system is

$$D = \left(\frac{l}{2}\right)^2 \sqrt{h_1 h_2 f\left(\frac{h_2}{h_1}\right)}, \tag{5.4}$$

where l is the jump length and f is a function of the ratio of the two hopping rates, determined by Monte Carlo simulations. In this case the ratio of hopping rates, which depend on the two energy barriers, is on the order of 0.001. This results in a simple analytical form of f, which is then equal to $\frac{4h_1}{h_2}$. Defining $h_1 = h_{\mathrm{F4TCNQ}}$, which is equal to the slower hopping rate, and substituting f into Equation 5.4 yields

$$D_{\mathrm{F4TCNQ}} = \frac{l^2}{2} h_{\mathrm{F4TCNQ}}. \tag{5.5}$$

Yang *et al.* did not generalise their method explicitly to n-barrier systems, and in order to determine the form of f in such a system where $n > 2$, Monte Carlo simulations would be required. In light of this, the "worst-case scenario" for the lower bound of the diffusion coefficient for mF4TCNQ is considered. In this case, the dopant molecule sees four energy barriers, all with the height equal to the highest energy barrier in the system, which is around 30 kJ/mol, during translation through two thiophene units. It is then possible to consider that, during translation over one thiophene unit (4 Å), the dopant molecule will undergo a two-barrier diffusion process, where the barriers have equal height. In contrast to this situation, F4TCNQ encounters two energy barriers of different height over the same translation length. Yang *et al.* found that when $h_1 = h_2 = h_{\mathrm{mF4TCNQ}}$, as in the case of mF4TCNQ due to the equivalent barrier heights, f can be found analytically and is equal to one. Substituting $f = 1$ into Equation 5.4 then gives

$$D_{\mathrm{mF4TCNQ}} = \frac{l^2}{4} h_{\mathrm{mF4TCNQ}}. \tag{5.6}$$

To provide a qualitative description of the ratio of diffusion coefficients for the

two dopants, the larger energy barrier encountered by F4TCNQ is assumed to be close to 30 kJ/mol. Given that ν is likely to be on the same order for both dopants and that the dominant energy barriers in both systems are equivalent in energy, it is then possible to assume that the hopping rates for both dopants are equivalent (i.e. $h_{\mathrm{mF4TCNQ}} = h_{\mathrm{F4TCNQ}}$). Because the jump length is the same for both systems, the ratio of the two diffusion coefficients is found to be 2. This result is consistent with the intuitive assumption that a system with two energy barriers of roughly equivalent height will result in diffusion at roughly half the rate of a system with one barrier of the same height. Variations in barrier heights and frequency factors may modify this value in a small way, but overall this worst-case scenario highlights that in fact the functional group substitution of F4TCNQ with a methyl-ester group does not have a significant impact on the stability of the dopant to translation in the P3HT polymer system.

It is possible to quantify the diffusion coefficient for the two dopants, assuming the worst-case scenario as described above, by setting the jump length to $l = 2$ Å and the activation energy to 30 kJ/mol. The diffusion coefficient for F4TCNQ is then found to be on the order of $D_{\mathrm{F4TCNQ}} = 1 \times 10^{-10}$ cm^{2}s^{-1}, and for mF4TCNQ $D_{\mathrm{mF4TCNQ}} = 0.5 \times 10^{-10}$ cm^{2}s^{-1}. This is roughly four orders of magnitude smaller than the preliminary experimental data for the "slow" process for mF4TCNQ, which has a diffusion coefficient on the order of 10^{-6} cm^{2}s^{-1}.[185] On the other hand, the jump length of 2 Å, equal to the distance between potential energy wells, is roughly equal to that of the experimental process, which has a jump length of around 2.1–2.3 Å. These calculations suggest that the measured diffusion process is not the result of dopant translation along the polymer backbone. An alternative diffusion process may be responsible for the experimental observations, for example diffusion between aligned chains rather than along the chain axis.

5.4 Conclusions

Density functional theory calculations were applied in order to investigate how functional group substitution of the common F4TCNQ dopant affects doping efficiency and translational diffusion within a P3HT polymer system. Geometry optimisations of the dimer complexes comprising a short oligothiophene and each dopant revealed decreased charge transfer by around 25 % within the modified dopant system as a result of modified molecular orbital energies. Using a simple "sandwich" model comprising the dopant surrounded by two oligothiophenes, the energy barrier to methyl rotation on the methyl-ester-substituted F4TCNQ molecule, denoted mF4TCNQ, was found to be 8–11 kJ/mol, with a jump length of 1.8 Å. This result matches well with an experimentally measured diffusion process for this system.

A second experimentally measured diffusion process has been hypothesised to be the result of dopant translation along the polymer backbone. The energy barrier to translation of mF4TCNQ and F4TCNQ between two oligothiophenes over half

a thiophene unit was found to be around 55–65 kJ/mol for a 6.30 Å interchain separation. A small local energy minimum was present in both systems at half a thiophene unit from the global minimum. Increasing interchain separation to 6.96 Å and translating over two thiophene units gave similar energy profiles for the two dopants, with the exception of an additional large energy barrier for mF4TCNQ. This barrier is attributed to unfavourable interactions between the dopant methyl group and the methyl groups on the oligothiophenes. The charge density on both dopants was found to vary by as much as $0.2e$, indicating that quantum relaxation and charge transfer play a major role in dopant stability to diffusion processes.

Both dopants display multi-barrier diffusion and so an Arrhenius relation based on the highest energy barrier could not be used to quantify the difference in diffusion coefficients between the two. An analytical model for multi-barrier diffusion was used, assuming both dopants undergo two-barrier diffusion, with two energy barriers of different heights for F4TCNQ and two energy barriers of equivalent for mF4TCNQ. The diffusion coefficient for mF4TCNQ was found to be approximately half that of F4TCNQ, indicating that this particular functional group substitution has a minimal impact on dopant stability in P3HT. Applying a quadratic fit to an energy well in the F4TCNQ energy profile yielded a frequency factor on the order of $\nu = 10^{11}$ s^{-1} for both dopants. The diffusion coefficients for F4TCNQ and mF4TCNQ were then found to be on the order of 1×10^{-10} cm^2s^{-1}, and 0.5×10^{-10} cm^2s^{-1}, respectively. These values are roughly four orders of magnitude smaller than the second experimentally measured diffusion process, and hence it was concluded that an alternative diffusion mechanism is likely to be responsible for the experimental measurements, such as the diffusion of the dopant between aligned polymer chains.

6 | Quantifying Charge-Transfer-Induced Solubility Control

Unpublished work written in manuscript style

Principal author (candidate): Sophia Ackling
Contribution: 85 %
Performed necessary calculations using a mixture of classical and quantum techniques. Collected, analysed and interpreted the data presented. Conceived and prepared the chapter as contained herein.

This chapter reports on original research conducted during the period of my Higher Degree by Research candidature and is not subject to any obligations or contractual agreements with a third party and would constrain its inclusion in this thesis. I am the primary author of this chapter. I hereby certify the statement of contribution is accurate.

Sophia Ackling — 26/10/16 — Date

Contributing author: David Huang
Contribution: 15 %
Supervised quantum and classical calculations, and assisted with statistical interpretation of data and editing of the chapter.

I hereby certify that the statement of contribution is accurate and grant permission for the candidate to include work pertaining to the publication in their thesis.

David Huang — 26/10/16 — Date

Abstract

It is important to understand how molecular charge distributions affect the solubility of semiconducting polymer/dopant mixtures, as charges are quite mobile in these materials and aggregation and nanoscale structure play an important role in organic electronic device performance. This chapter presents a computational investigation into how solubility changes with charge. Using steered molecular dynamics, the impact of the molecular charge distribution on the free energy of separation of an eight-unit poly(3-hexylthiophene) (P3HT) chain and an 2,3,5,6-tetrafluoro-7,7,8,8-tetracyano-quinodimethane (F4TCNQ) molecule in the presence of explicit chloroform is investigated. The "neutral" distribution, in which the total charge on each molecule sums to zero, yields a free energy change of around 4 kJ/mol. For the "charged" distribution, in which the total charge on F4TCNQ sums to -1 and on P3HT sums to +1, yields a free energy change of around 29 kJ/mol. These results reveal that the charge distribution is a key factor dictating the solubility of the system. However, these results do not account for quantum effects for the process of separation. An energy decomposition analysis calculation performed using density functional theory (DFT) reveals that quantum relaxation and charge transfer dominate the free energy of separation, and so the binding energy of the complex is calculated using DFT calculations instead of classical simulations. A thermodynamic correction is included, as well as the change in solvation free energies obtained by including a continuum model to represent chloroform, giving a total free energy change of 40.6 kJ/mol. To more accurately model the effect of the solvent, alchemical free energy perturbation simulations are performed to investigate the explicit solvent contribution to the free energy change of separation. Using the explicit solvent contribution, the free energy of separation was found to be 22.6 kJ/mol. This value is in very good agreement with experimental measurements, and highlights the importance of the explicit treatment of the solvent for the solvent contribution.

6.1 Introduction

Molecular doping of organic semiconducting polymers has been demonstrated to vastly improve the semiconducting properties of these polymers.[17,117,165] Efficient doping occurs as a result of comparable frontier molecular orbital energies within the dopant and polymer, allowing charge transfer to occur between the two.[31] However, physical properties can also be affected by introducing sufficient quantities of dopant. Aggregation has been demonstrated to occur as a result of integer charge transfer between small molecular dopant 2,3,5,6-tetrafluoro-7,7,8,8-tetracyano-quinodimethane (F4TCNQ) and semiconducting polymer poly(3-hexylthiophene) (P3HT) upon sufficient doping concentrations.[26,38,44] The formation of holes within the polymer upon doping reduces the solubility of the polymer in the surrounding solvent, causing crystalline regions to occur within thin films of this mixture. Furthermore, optical control over this aggregation has recently been reported by Jacobs *et al.*, who

demonstrated that irradiation of the aggregated system at 405 nm results in disaggregation, with the polymer once more soluble in the chosen solvent.[38] This technique has far-reaching applications in efficient production of patterned organic electronic devices, and hence understanding the nature of the photo-induced solubility control is paramount. In particular, the role of charge transfer on aggregation must be investigated. It is also of interest to quantify the stability of the aggregated, doped system.

Recent work by Sweetnam *et al.* investigated aggregation in the P3HT/PCBM system, using a mixture of experimental and theoretical techniques.[50] The team concluded that van der Waals interactions provide the predominant driving force for aggregation in this system. However, only minimal charge transfer occurs between the polymer and dopant in this system.[50] In the P3HT/F4TCNQ system, integer charge transfer is known to occur.[34–36] It is thus reasonable to assume that the integer charge transfer doping process plays some role in the solubility of the polymer, and alternative interactions may dominate the aggregation observed within this particular system.

In order to realistically investigate how charge distributions affect solubility and quantify the free energy associated with aggregation, explicit solvent molecules must be modelled. Such calculations cannot feasibly be performed using quantum mechanical calculations due to the size of the resulting solvated system. Classical molecular dynamic simulations, on the other hand, can provide invaluable insight into thermodynamic properties of molecular systems and can efficiently model explicit solvent surrounding the system of interest. While a number of MD simulation studies have provided important insight into semiconducting polymer properties in solvent,[52,53,187] polymer/dopant interactions in solution have not previously been studied. This study seeks to use MD simulations to compare the free energy of disaggregation in the P3HT/F4TCNQ system for different charge distributions corresponding to initial and final states of the integer charge transfer doping mechanism.

Quantum calculations can also provide insight into the thermodynamic properties of a system. Density functional theory has been shown to provide experimentally realistic binding free energies, free energies of association and solvation for a large number of molecular systems, as well as energy barriers to a variety of processes.[188–193] In such studies, solvent contributions to free energy changes are often considered by introducing a continuum solvent model[194,195] to implicitly represent the solvent of interest. This methodology has been used successfully in recent years.[188–190,196,197] However, it has been shown that when solute-solvent interactions are strong, an implicit model is incapable of modelling the solvent contribution to the free energy change during nucleophilic substitution reactions.[196,197] Likewise, it is possible that when considering properties like solubility these implicit solvents may show severe limitations. In this work, the previous quantum methodology is tweaked so as to include the explicit solvent contribution to disaggregation of F4TCNQ from P3HT using molecular dynamics simulations.

The impact of the molecular charge distribution, and by extension the charge transfer reaction between polymer and dopant, on polymer solubility is investigated using complementary computational techniques. Classical molecular dynamics simulations are used to probe the free energy change for separation of polymer and dopant before and after integer charge transfer. Steered molecular dynamics (SMD) simulations of a P3HT oligomer and an F4TCNQ molecule in explicit chloroform are used to quantify the free energy change upon separation for a fixed charge distribution in the molecules. To address the problem of unrealistic charge distribution due to the static nature of the charges, as well as quantum relaxation upon dimerisation, density functional theory (DFT) calculations are used to quantify the binding energy and the entropic contribution to this process. The solvent contribution to this process is included by means of a continuum model. To improve on the accuracy of the results, free energy perturbation (FEP) simulations are performed in explicit solvent and in a vacuum in order to extract the solvent contribution to this process.

6.2 Computational details

6.2.1 Density functional theory calculations

In order to obtain molecular charge distributions, bond lengths and angles for the molecular dynamics simulations, density functional theory (DFT) calculations were performed at the B3LYP/6-31+G(d) level of theory,[63] with Grimme's D2 dispersion correction.[67] This functional was chosen because it has been shown to perform well for ground state properties of oligothiophenes, both in this body of work and elsewhere.[198] A dielectric medium was used to represent chloroform by setting the dielectric constant to $\epsilon = 4.8$.[199] This was introduced by means of the conductor-like polarisable continuum model (CPCM)[89,174,175] and was included in order to improve the accuracy of the charge distributions. Geometry optimisations were performed on a chloroform molecule, F4TCNQ and an eight-unit methyl-substituted (M8) oligomer in isolation, as well as on the dimer complex composed of M8 and F4TCNQ. Previous DFT calculations have shown that the M8 oligomer accurately reproduces experimental properties of the P3HT polymer in the P3HT/F4TCNQ system (see Chapter 3). Atomic partial charges were obtained from CHELPG calculations.[124]

A number of additional DFT calculations were also performed on the isolated fragments and dimer complex. An energy decomposition analysis (EDA) calculation was performed on the optimised B3LYP-D/6-31G(d) dimer complex geometry, at the same level of theory. A frequency calculation was performed on each of the optimised molecules and the optimised dimer, also at the B3LYP-D/6-31G(d) level of theory, to obtain thermodynamic corrections to the binding energy. In order to obtain the binding energy of the complex, the energy difference between dimer and molecules was computed, for structures calculated at the B3LYP-D/6-31+G(d) level of theory in implicit chloroform solvent. Isolated molecule energies *in vacuo*

were counterpoise corrected to remove basis set superposition error (BSSE) using the method of Boyes and Bernardi.[200] The BSSE present in the solvated isolated molecule energies was assumed to be equivalent to that of the *in vacuo* calculations. The solvent contribution to the free energy of separation was computed by taking the difference between the electrostatic contribution to the free energy of solvation of the isolated molecules and the dimer complex. All DFT calculations were performed using Q-Chem 4.3.[96]

6.2.2 Molecular dynamics simulations

Classical molecular dynamics simulations were prepared, with one F4TCNQ molecule and one M8 oligomer with the hexyl side chains included (denoted $(3HT)_8$) in a box of explicit chloroform molecules at a density of 1.49 g/cm^3. Bond lengths, angles and dihedrals of each molecule were set to match those from the aforementioned B3LYP-D/6-31+G(d) DFT calculations in implicit chlorofrm, and charge distributions were mapped directly on a per-atom basis from these same DFT calculations. Charges on the hexyl chains of $(3HT)_8$, which replaced the methyl chains in the DFT calculations, were modified such that the overall charge on the fragment summed to either zero or one, depending on the simulation. In order to ensure that the two molecules could be sufficiently separated without interacting with each other through periodic boundary conditions, a box length of 82 Å was prepared and populated with 3850 chloroform molecules.

All bonded dihedral and non-bonded parameters were taken from the OPLS-AA force field, as this force field has been previously shown to accurately model structure and thermodynamics of organic semiconductors.[201] A non-standard dihedral potential was used for inter-monomer dihedrals for the $(3HT)_8$ chain.[202] Electrostatic and van der Waals interactions were modelled using a Lennard-Jones potential, and the long-range dispersion interactions were shifted and truncated at 12 Å. Long-range Coulombic interactions were calculated using the particle-particle particle-mesh (PPPM) method. Simulations were performed in a cubic simulation box with periodic boundary conditions. Unless noted otherwise, a Nośe-Hoover thermostat and barostat were used to simulate an isothermal-isobaric (NPT) ensemble. The temperature was set to 298 K and the pressure set to 0 atm, which is essentially equivalent to 1 atm in molecular simulations, so that standard conditions were reproduced.

All simulations were performed using LAMMPS[203–206] (`http://lammps.sandia.gov`), and trajectories were visualised using VMD.[173]

6.2.3 Steered molecular dynamics parameters

Two key parameters were set within the SMD simulations: the spring constant and the pulling velocity for the moving component. Previous work by Park *et al.* has demonstrated that the choice of spring constant does not have a considerable

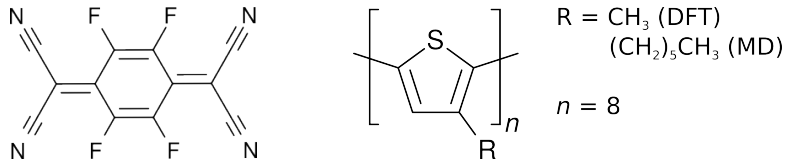

Figure 6.1: Structure of F4TCNQ (left) and oligothiophene. The methyl-substituted oligomer is used in DFT calculations, and the hexyl-substituted oligomer is used in MD simulations.

impact on the results.[107] However, they note that the spring constant should not be made arbitrarily large. A spring constant of k_{SMD}=20 kcal/mol·Å^2 was chosen for all simulations, which is on a similar order to values used in previous studies.[107,207] Each simulation was initialized from the same system configuration and equilibrated for 1 ns with various initial velocity seeds, giving rise to independent simulation trajectories. A pulling speed of 1 Å/ns was used in all cases, as this value allowed for a balance to be struck between necessary sample size for acceptable error bars and sampling efficiency. The centre of mass of the $(3HT)_8$ oligomer was fixed via a stiff spring to the centre of the box, with a spring constant of k_{COM}=20 kcal/mol·Å^2. The F4TCNQ molecule was then pulled at a constant velocity towards the centre of the box from a separation of 30 Å.

6.2.4 Free energy perturbation simulation set-up

The charged system was equilibrated in explicit chloroform with the centre of mass of $(3HT)_8$ fixed at the centre of the simulation box and the centre of mass of F4TCNQ fixed 5 Å from the centre of the simulation box. Using a modified version LAMMPS, the charges on each atom in the F4TCNQ and $(3HT)_8$ molecules were linearly scaled from the charged to the neutral distribution. The free energy change for this process was measured. The neutral system was also equilibrated as described above, with F4TCNQ fixed 5 Å away from $(3HT)_8$. The charges on F4TCNQ were linearly scaled to zero while the inter- and intramolecular interaction potential on each atom was simultaneously scaled to zero. This resulted in the free energy of annihilation of F4TCNQ. A second neutral system was equilibrated in the same way, except with F4TCNQ fixed 30 Å away from the centre of the simulation box. F4TCNQ was once more annihilated, as per the method described. A diagrammatic summary of the three FEP simulations is illustrated in Figure 6.2. Each of these processes was then repeated with the dopant and oligomer in vacuum. Vacuum simulations were performed under constant volume and temperature (NVT ensemble), with the box length equal to that of the explicit solvent simulations.

The soft version of the Lennard-Jones potential with the long-range Coulombic term was used in all FEP simulations to avoid discontinuities associated with annihilating or creating molecules.

The accuracy of FEP simulations depends on good phase-space overlap, which can be achieved by choosing a sufficiently small λ window, $\Delta\lambda$, with which to scale

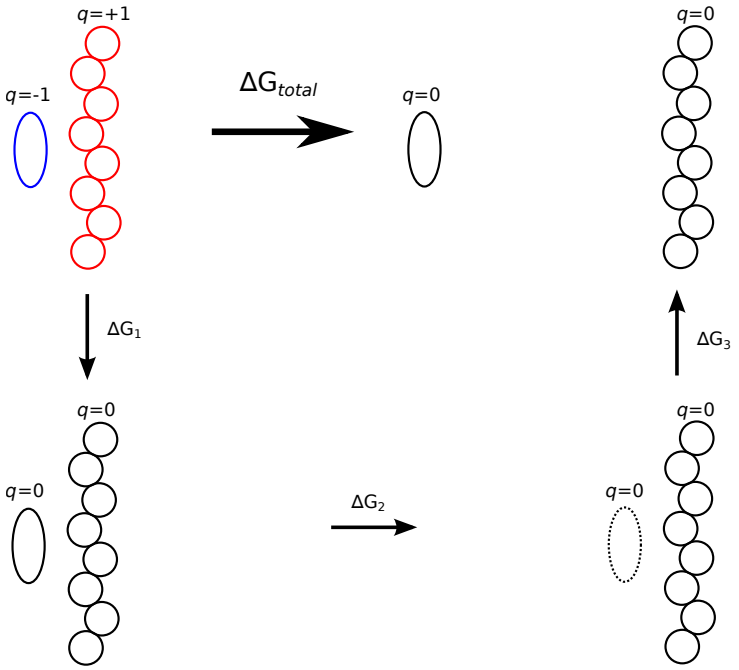

Figure 6.2: Diagramatic representation of the three alchemical processes simulated. Integer-charge-separated species are indicated in colour (blue for a charge of $-1e$ and red for a charge of $+1e$). The chain of circles represents the P3HT chain, while the oval represents F4TCNQ. Dotted lines represent an annihilated molecule. The free energy of the overall process is the sum of the individual free energies for each separate process.

the interactions. Additionally, sufficient equilibration time in each window is required in order to obtain reliable results. The time spent at each λ is here defined as t_λ. A number of values for $\Delta\lambda$ and t_λ were considered for the annihilation of F4TCNQ at small and large separations and the results are summarised in Appendix D, Table D.11. For simulation results presented in this study, $\Delta\lambda = 0.05$ and $t_\lambda = 400,000$ fs, of which the last 100,000 fs are used to calculate the free energy. In order to ensure reversibility of the FEP simulations, the charges and potential on F4TCNQ were gradually scaled from zero, to replicate the process of creating F4TCNQ. The free energy of this process was found to be consistent to within 3 % of the annihilation process, and hence reversibility was assumed for the chosen $\Delta\lambda$ and t_λ.

6.3 Results and discussion

6.3.1 Steered molecular dynamics simulations

A set of ten independent simulations were performed on the $(3HT)_8$/F4TCNQ pair for two molecular charge distributions, corresponding to a charge-neutral molecular pair and oppositely integer-charged molecules. These simulations were performed in

explicit chloroform, because the P3HT/F4TCNQ mixture cast from chloroform has been shown to provide better charge transport than casting from other similar solvents, such as chlorobenzene.[208] The steering force, introduced as a harmonic spring potential $\xi(\mathbf{r})$, was constrained to be close to an external parameter λ. Exponential averaging of the work, W, obtained from each of the simulations was performed in order to obtain the potential of mean force (PMF), Φ, using

$$\Phi(\lambda_t) = \Phi(\lambda_0) - \frac{1}{\beta}\log\langle e^{-\beta W}\rangle. \tag{6.1}$$

where $\beta = 1/k\mathrm{B}T$. Because exponential averaging is notoriously poor, a second-order cumulant expansion

$$\log\langle e^{-\beta W}\rangle = -\beta\langle W\rangle + \frac{\beta^2}{2}(\langle W^2\rangle - \langle W\rangle^2) + ... \tag{6.2}$$

was also applied to the data for comparison in order to obtain an approximation to the PMF. The PMF is the free energy for bringing together the two molecules from a large to a small separation. Both calculation methods indicate a free-energy well at a small molecular distance, confirming that there is a free energy cost for separating the molecules in chloroform solvent. This energy well can be used to quantify the free energy change of separating the molecules.

For the charge distribution taken from DFT calculations on the isolated monomers in implicit chloroform solvent ("neutral" system), the results indicated relatively weak interactions between the two components. For separations less than 15 Å, variation in potential energy was observed. In all simulations the $(3\mathrm{HT})_8$ molecule was constrained only by its centre of mass, leaving its ends free to move within the system. Dips in the free energy profile as F4TCNQ approached the centre of the box are likely due to variations in the position of the chain with respect to the F4TCNQ molecule. Because the $(3\mathrm{HT})_8$ molecule was not perpendicular to the direction of approach of F4TCNQ, the ends of the chains were free to favourably interact with the dopant molecule. A free energy difference between close and separated molecules was found to be $\Delta G = 4 \pm 4$ kJ/mol for the charge-neutral system. Given that this value is only a little larger than $k_\mathrm{B}T$ (2.5 kJ/mol), this result is sufficiently small so as to indicate minimal "sticking" of the F4TCNQ to the P3HT; that is, thermal energy at room temperature is sufficient to separate the two species and the free energy difference between bound and unbound states is small.

For the "charged" system, the charge distribution was taken from DFT calculations on the M8 dimer complex at the B3LYP-D/6-31+G(d) level in implicit chloroform solvent. This distribution demonstrated integer ground state charge transfer, i.e. the total charge on the F4TCNQ molecule was $q = -1.04e$, and the total charge on the oligomer was $q = +1.04e$. This distribution gave a free energy profile that demonstrated substantial interaction between the two components of the system. A free energy difference between close and separated components of $\Delta G = 29 \pm 8$ kJ/mol was observed, which is roughly $12k_\mathrm{B}T$. This shows that

the charge distribution has a significant impact on aggregation of the P3HT and F4TCNQ components, as by changing from a charge-neutral to an integer-charge-separated system results in an sevenfold increase in free energy well depth, and equally a sevenfold increase in the free energy change for separation of the components. For the charge-separated system, it is therefore reasonable to conclude that thermal energy at room temperature will not allow for separation of the components, and they will remain aggregated.

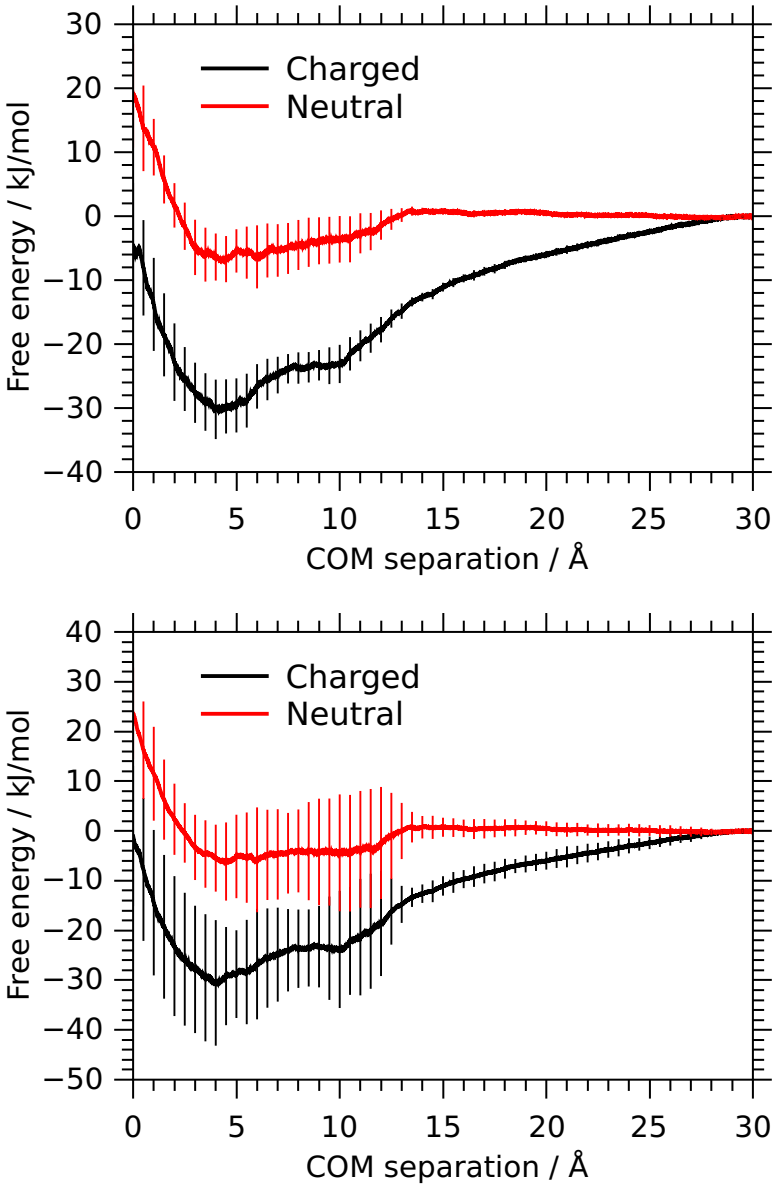

Figure 6.3: Potential of mean force for the neutral and charge-separated distribution systems obtained via cumulant expansion (top) and exponential averaging (bottom) with error bars indicating two times the standard error.

6.3.2 Free energy of separation

Implicit solvent

The static nature of the charge distribution as the molecules are separated in the SMD simulations is experimentally unrealistic. While these simulation results do provide an indication of the role that charge distribution plays in aggregation, they cannot be used to quantify the free energy of separation of dopant from oligomer. Upon separation, the oligomer and dopant will no longer interact, and return to a neutral, isolated, charge distribution. Clearly the classical description of the system cannot account for changes in charge distribution, nor the quantum relaxation that occurs when the molecules are in close proximity. On the other hand, density functional theory (DFT) calculations cannot be used to explicitly describe the solvent surrounding the system because the system size would be infeasible. Thus, an alternative approach is proposed in which a mixture of classical and quantum calculations are used to provide an accurate quantitative description of the separation process.

An energy decomposition analysis calculation on the dimer complex at a low level of theory reveals that the stability of the bound complex is due in most part to quantum relaxation and charge transfer between oligomer and dopant. The energy contribution from bringing the two molecules together from infinite separation, in the absence of quantum relaxation (denoted "frozen" in Table 6.1), is less than half that of the contribution from quantum relaxation and charge transfer (-52 vs -134 kJ/mol). This validates the assertion that quantum effects play an important role in the system and hence a purely classical description is inadequate.

The free energy associated with separating F4TCNQ from $(3HT)_8$ can be broken down into the sum of the binding energy, the thermodynamic correction due to translational, rotational and vibrational degrees of freedom at finite temperature, and the solvent contribution using

$$\Delta G_{\text{total}} = \Delta E_{\text{bind}} + \Delta G_{\text{thermo}} + \Delta G_{\text{solvent}}. \tag{6.3}$$

The binding energy of the M8 dimer complex was calculated at the B3LYP-D/6-31+G(d) level in implicit chloroform, for consistency with the charge distribution used in molecular dynamics simulations. The thermodynamic correction was calculated using frequency calculations on the complex and isolated fragments with a

Table 6.1: Contributions to the energy of the dimer complex obtained from an energy decomposition analysis calculation at the B3LYP-D/6-31G(d) level of theory

Energy term	ΔE (kJ/mol)
Frozen	–52.9
Intramolecular relaxation	–13.2
Intermolecular relaxation (CT)	–133.8

Table 6.2: Electrostatic contribution to solvation free energy in chloroform at the B3LYP-D/6-31+G(d) level of theory

	ΔG_{elec} (kJ/mol)
F4TCNQ	–64.1
M8 oligomer	–50.1
Complex	–114.2

Table 6.3: Contributions to the total free energy to separate F4TCNQ from the thiophene oligomer from DFT calculations using a dielectric medium to represent the solvent

Contribution	E (kJ/mol)
ΔE_{bind}	+111.7
ΔG_{thermo}	–71.1
$\Delta G_{\text{solvent}}$	~ 0
ΔG_{total}	+40.6

smaller basis set and no solvent, as these are not expected to greatly impact the resulting correction.[194,195] The solvent contribution was initially approximated using the implicit solvent and was taken to be the difference between the electrostatic contribution to solvation energy of the complex and the isolated fragments (Table 6.2). This term was also calculated using the larger basis set. The total free energy to separate the two components was found to be $\Delta G_{\text{total}} = 40.6$ kJ/mol.

While the binding energy is the dominant term contributing to the free energy of separation, the thermodynamic correction can be seen to be substantial. In particular, this term accounts for the change in entropy upon transforming one complex into two fragments. The solvent contribution, on the other hand, appears to be negligible. This result is somewhat surprising, given that recent work by Ho and Ertem found that using the methodology described in Equation 6.3 can provide experimentally realistic free energies for a large number of organic and inorganic molecules.[190] Such a small solvent contribution is unlikely to be a realistic representation of the free energy change in the solvent as the molecules are separated. In order to validate this assertion, the classical (and hence explicit) solvent contribution was evaluated using free energy perturbation simulations.

Explicit solvent

Thermodynamic integration, using[209]

$$\Delta G = -kT \sum_{i=0}^{n-1} \ln \frac{\left\langle V \exp\left(-\frac{U(\lambda_{i+1}) - U(\lambda_i)}{kT} \right) \right\rangle_{\lambda_i}}{\langle V \rangle_{\lambda_i}}, \tag{6.4}$$

where λ is the coupling parameter, was applied to each of the three processes shown in Figure 6.2, and the free energies in explicit chloroform solvent were summed as per Hess's law to provide the total free energy to separate the molecules while accounting

Table 6.4: Solvent contribution to free energies obtained by application of alchemical free energy perturbation in classical MD simulations

Process	Free energy (kJ/mol)
ΔG_1	+23.4
ΔG_2	+2.1
ΔG_3	–43.5
$\Delta G_{\text{solvent}}$	–18.0

for changing charge distribution during separation. These simulations provide a free energy that is more realistic than the steered MD simulations because they account for this change in charge distribution upon separation. The same simulations were then performed in the absence of the solvent, and the free energies obtained from these simulations were subtracted from those obtained for the solvent system, in order to obtain the solvent contribution for each of the processes.

The solvent contributions to each of the processes is tabulated in Table 6.4. Here ΔG_1 corresponds to the process of changing the charge distribution from charge-separated to charge-neutral, ΔG_2 corresponds to the process of annihilating F4TCNQ close to $(3HT)_8$, and ΔG_3 corresponds to the process of creating F4TCNQ at a large distance from $(3HT)_8$. $\Delta G_{\text{solvent}}$ corresponds to the total free energy difference for the process considering purely solvent contributions. The small magnitude of ΔG_2 is likely a result of the fact that few solvent molecules will be present between F4TCNQ and $(3HT)_8$ when the two are at such a small separation, and hence there is not a large rearrangement of solvent molecules upon annihilation of the dopant molecule. ΔG_1 is a larger contribution due to a large change in the Coulombic interaction strength between solvent molecules and the atoms in the dimer complex. Similarly, ΔG_3 is also a large contribution due to the substantial rearrangement of solvent molecules upon creation of F4TCNQ at a large distance from $(3HT)_8$. The overall solvent contribution to this process is observed to be $\Delta G_{\text{solvent}} = -18.0$ kJ/mol, which is substantially larger than the value obtained with the continuum model.

The total free energy to separate the dimer complex, i.e. the reverse of the process shown in Equation 6.5, was calculated by using the same binding energy and thermodynamic correction as listed in Table 6.3, except with the explicit solvent free energy contribution of $\Delta G_{\text{solvent}} = -18.0$ kJ/mol. This gave a value of $\Delta G_{\text{total}} = 22.6$ kJ/mol.

Using a Langmuir isotherm model fit to UV-vis data for various % doping of P3HT with F4TCNQ from acetonitrile, Jacobs *et al.* experimentally estimated the free energy of solvation of F4TCNQ into amorphous P3HT (Equation 6.5) to be around $\Delta G = -22.2$ kJ/mol.[143] This value is in excellent agreement with the results obtained here using the mixed DFT/FEP methodology. The difference in solvent polarity is unlikely to have a large impact on the free energy of separation because in the bound state there will be very little solvent between the charge-separated

species, and at large separation the species are neutral and so a change in dielectric will not greatly impact the properties of the system.

$$P_3HT_{CH_3CN} + F_4TCNQ_{CH_3CN} \rightleftharpoons P_3HT^+ + F_4TCNQ_{P3HT}{}^- \tag{6.5}$$

6.4 Conclusions

Classical molecular dynamics simulations were used to investigate the change in polymer solubility in the P3HT/F4TCNQ polymer/dopant system upon mixing. In particular, the impact of charge transfer on solubility was explored. Steered molecular dynamics simulations were used to investigate how the free energy for separation of F4TCNQ from P3HT in chloroform changes with changes in the molecular charge distribution. In the case of neutral molecules, a small free energy cost for separation of approximately 4 kJ/mol was found. The size of this free energy cost is such that thermal energy at room temperature would be sufficient to induce disaggregation, resulting in the polymer dissolving back into solution. When a charge-separated distribution was used for the complex, in which the charge on F4TCNQ summed to -1e and the charge on the P3HT segment summed to +1e, the free energy of separation was found to be around 29 kJ/mol. This is roughly equal to 12 k_BT, which suggests that disaggregation at room temperature will not occur and the aggregated complex is highly stable. The large difference in free energies of separation as a result of modifying the charge distribution from charge-separated to charge neutral indicates that Coulombic interactions do play an important role in aggregation of the F4TCNQ-doped P3HT system.

Energy decomposition analysis of the dimer complex revealed that quantum relaxation and charge transfer dominate the stability of the bound complex. The steered MD simulations could not account for these contributions to the free energy of separation, nor the dynamic nature of the charges upon separation. Hence density functional theory calculations were used to quantify the free energy of separation in F4TCNQ-doped P3HT. The binding energy of the complex was quantified and a thermodynamic correction was applied. The solvent contribution was first quantified using an implicit solvent model, and the free energy of separation was found to be $\Delta G = 40.6$ kJ/mol. In order to more realistically include the solvent contribution, alchemical free energy perturbation simulations were used. These simulations yielded the solvent contribution to the free energy of separation of F4TCNQ from the thiophene oligomer while accounting for the change in charge distribution. Using this explicit solvent contribution gave a total free energy of separation of $\Delta G = 22.6$ kJ/mol, which is in excellent agreement with experimental results. In this way, explicit solvent was demonstrated to play an important role in accurately quantifying the free energy of separation in this complex, and the shortcomings of the implicit solvent model were revealed.

7 Conclusions and future directions

7.1 Conclusions

An in-depth investigation into a number of physical and electronic properties of the polymer/dopant system comprising poly(3-hexylthiophene) (P3HT) and molecular dopant 2,3,5,6-tetrafluoro-7,7,8,8-tetracyano-quinodimethane (F4TCNQ) has been performed. Quantum and classical calculations have provided key insight into charge transfer processes, dopant diffusion and charge-mediated solubility.

The work presented in Chapter 3 sought to investigate the structural and environmental properties of the P3HT/F4TCNQ system that make it conducive to an integer charge-transfer doping mechanism, rather than the partial charge-transfer mechanism observed when the polymer is replaced with quarterthiophene. The system was modelled using density functional theory (DFT) and the magnitude ground-state charge transfer was used in conjunction with the accuracy of simulated absorption spectra to evaluate the performance of a number of models with different structural characteristics. An optimal chain length was elucidated, and side-chain substitution was observed to play an important role in the doping mechanism. Even more important is the environment of the system, with solvent effects increasing the ground-state charge transfer to near-integer. A range of density functionals were then used to model the optimal system, and each one demonstrated shortcomings in their ability to reproduce experimental properties. Overall, this systematic investigation revealed how structural properties of the polymer affect the doping mechanism in the P3HT/F4TCNQ system. Furthermore, this study reports a best practice for modelling this system such that experimentally quantitative results may be achieved.

Chapter 4 extended the work of Chapter 3 by using the optimised model to investigate the experimentally observed photo-induced solubility change reported by Jacobs *et al.*[38] The plausibility of a photo-induced charge back-transfer from dopant to polymer at 405 nm was investigated. Time-dependent density functional theory calculations indicated that excitation at 405 nm does produce excited states that could plausibly be related to back-transfer of charge. Optimisation of one of these states did not indicate charge neutrality, however. Furthermore, progressively

increasing the charge from zero to one electron on the dopant revealed that the charge neutral state is not metastable. In the absence of a stable charge-neutral state, it is highly unlikely that charge neutrality in the P3HT/F4TCNQ system could be responsible for the observed solubility of the irradiated system. Thus it was concluded that the hypothesised photo-induced charge transfer mechanism is implausible.

Diffusion mechanisms in F4TCNQ-doped P3HT were investigated in Chapter 5. A methyl-ester-substituted F4TCNQ dopant (mF4TCNQ) was placed between two oligothiophene chains and optimised using DFT. The energy barrier to methyl rotation was quantified and found to be in very good agreement with an experimentally measured "fast" diffusion process. A second, slower diffusion mechanism has been measured experimentally, and hypothesised to result from translation of the dopant along the polymer backbone. DFT calculations replicating this translational diffusion process for F4TCNQ and mF4TCNQ between two oligothiophenes revealed that both dopant molecules undergo multi-barrier diffusion across one to two thiophene units. The energy barriers and diffusion coefficients calculated for both dopants are not in agreement with experimental results, suggesting that an alternative diffusion process may be responsible for the experimental measurements. Substitution of F4TCNQ with a methyl-ester functional group was not observed to greatly reduce the diffusion rate of the dopant along the polymer backbone, which suggests that the modified dopant is unlikely to produce a more stable doped polymer film.

The final study, presented in Chapter 6, investigated the solubility change of F4TCNQ-doped P3HT as a result of charge transfer, and presented a mixture of classical molecular dynamics simulation and density functional theory results. Steered MD simulations, in which F4TCNQ was gradually pulled towards the eight-unit 3-hexylthiophene oligomer in chloroform, revealed that the free energy of separation when both components possess a neutral charge is only a little greater than the thermal energy at room temperature. In stark contrast, the free energy change when each component possesses integer charge (negative on dopant, positive on oligomer) is roughly twelve times the thermal energy at room temperature. It was concluded that the molecular charge distribution strongly affects aggregation in the P3HT/F4TCNQ system. In order to quantify the free energy change of separation while accounting for quantum relaxation and dynamic charge distribution, DFT calculations were performed on the dimer complex described in Chapter 3. Initially the free energy was quantified in implicit solvent and found to be quite large as a result of a negligible solvent contribution. Free energy perturbation simulations were then performed to quantify the explicit solvent contribution to the free energy of separating F4TCNQ from the thiophene oligomer. Accounting for this explicit contribution in the DFT calculations yielded a free energy change that is in excellent agreement with experimental results. This study highlighted both the impact of charge transfer on aggregation in F4TCNQ-doped P3HT, and also the importance of considering the solvent explicitly when quantifying the free energy change of a

process related to solubility.

Collectively, this body of work provides a comprehensive study of important physical and electronic properties of the P3HT/F4TCNQ system. Structural properties of the polymer and the environment surrounding the charge transfer unit were shown to affect charge transfer in the system. Photo-induced charge back-transfer from dopant to polymer was found to be an infeasible mechanism for the observed change in solubility. The stability of F4TCNQ-doped P3HT was investigated and compared to a methyl-ester substituted F4TCNQ analogue. The latter was not found to be a better candidate for doping P3HT on the grounds of dopant diffusion. And finally, the stability of the charge transferred system was compared with that of the charge neutral system and the free energy of to separation of polymer and dopant was quantified.

7.2 Future directions

While each of the studies presented in this work represents a comprehensive investigation into the property of interest, additional calculations and simulations may provide further insight. The exception to this is the work presented in Chapter 4, which confirmed that the mechanism of interest is not possible. In fact an entirely different mechanism for solubility change has recently been elucidated.[40]

7.2.1 Ground state properties of the P3HT/F4TCNQ dimer complex

Chapter 3 presented a study of how certain structural and environmental properties can affect charge transfer in the P3HT/F4TCNQ system. However, extending the system beyond the dimer complex may present new and interesting properties that are hitherto unexplored. While it seems unlikely that increasing the side chain length will increase the accuracy of the model,[47,139] it would be interesting to evaluate the properties of a trimer or tetramer comprising stacked oligothiophenes and F4TCNQ molecules. Such a model would provide a more accurate model of a highly-doped system. At present this may, however, be beyond the size limits of DFT calculations. Density functional tight-binding (DFTB) calculations may be applicable, subject to the accuracy of the parameter files for organic semiconductors. Such calculations could also be extended using molecular mechanics methodology in order to study how the system charges change when modelled with explicit solvent molecules.

7.2.2 Diffusion in the P3HT/F4TCNQ system

Experimental investigation into diffusion processes within the methyl-ester-substituted F4TCNQ (mF4TCNQ) doped P3HT system has quantified two diffusion processes. The first was ascribed to methyl rotation, which was accurately modelled in this work. The second experimentally measured process is much slower, but presented a similar energy barrier to the methyl rotation. Calculations used to model the translation of the dopant along the polymer backbone yielded an energy barrier

that was far too high to be related to the experimental slow process, and the associated diffusion coefficient was roughly four orders of magnitude smaller than the experimental process. It is possible that this alternative diffusion process is instead the result of mF4TCNQ rotating out of the plane of the P3HT chain, such that it lies at 90 degrees to the direction of the chain, or due to translation between aligned chains rather than along the chain backbone. Such processes were not modelled in this work, as in order to obtain an accurate description of the process, hexyl chains would need to be modelled on the oligothiophene. Unfortunately such a calculation remains beyond the realms of DFT. However, DFTB calculations may be able to provide an approximation to the energy barrier to this dopant rotation. With such a result it may be possible to assign the observed experimental process to this diffusion mechanism. For an even more realistic description, quantum mechanics/molecular mechanics (QM/MM) calculations could be performed, in which the oligomer backbone and dopant are treated quantum mechanically, while the hexyl side-chains on the oligomers are treated classically. Such calculations are likely to provide a reasonably realistic description of the experimental system. Likewise, this technique could be used to model a large number of classical P3HT chains around the central backbones in the sandwich configuration, which may reduce the warping observed when these chains were not held fixed. This would allow for more flexibility in the quantum chains during translation of the dopant molecule, and hence a more experimentally realistic description of the system.

Translation of both the original and substituted dopants along the oligomer backbone resulted in very high energy barriers, and it is possible that these energy barriers were overestimated with respect to the experimental process. The B3LYP functional was used because the results of Chapters 3 and 4 showed that it performs quite well for the M8/F4TCNQ model system. However, it is possible that this functional over-estimated the binding energy of the system and hence the energy barrier to translation.[153] For comparison, these calculations could be performed with a range-corrected functional. However, the results of Chapter 3 showed that only the optimally tuned range-corrected functional LRC-ωPBEh gave a realistic description of the model system, with the other alternatives performing quite poorly. It would thus be necessary to tune this functional for the sandwich system studied in Chapter 5, which would be feasible but time consuming due to the large system size.

One final way in which this study could be extended is by performing Monte-Carlo simulations of a particle hopping along the calculated potential energy profile for translation of each dopant. These simulations would provide important parameters relating to the hopping of the dopant along the polymer backbone, such as the diffusion coefficient, in a multi-barrier system.[186] From this data it would be possible to better compare the calculated and experimental results, as well as more accurately quantify how functional group substitution affects translational diffusion in the doped polymer system.

7.2.3 Quantifying charge-transfer-induced solubility control

The results of Chapter 6 provide novel insight into the free energy of separation of dopant from polymer for two different molecular charge distributions in chloroform. It would be interesting to investigate how these barriers to separation change for different solvents. For example, tetrahydrofuran is regularly used as a solvent for P3HT. Investigating chlorobenzene would be particularly pertinent as work by Müller *et al.* indicates that this solvent elicits different stacking behaviour compared with chloroform.[208]

In studying the energy barrier to separation, a very simplified model was used: only one dopant molecule and one oligomer were present in the system. This quantified the free energy of separating dopant from polymer, but it is of equal interest to quantify the free energy of separating polymer from doped polymer. These simulations present only a minor extension of those already performed, in which two polymer chains are stacked with the dopant adjacent to one chain. The polymer/dopant unit could then be separated from the remaining chain. The binding energy in this system may be challenging to quantify with DFT due to the large system size, and so once more QM/MM calculations could be used. QM/MM calculations have recently been used to accurately quantify ligand binding energies using free energy perturbation, and a similar methodology could be applied to this system.[210] This approach is particularly attractive as it allows for the free energy change for the separation process to be quantified using one technique, rather combining free energy contributions from different calculations.

It appears that, barring this work, no classical MD simulations studies on F4-TCNQ-doped P3HT have been published. A number of important properties could be explored using this technique, including properties of the solid-phase system, after evaporation of the solvent. Solid-state simulations of P3HT with fullerene revealed how fullerene interacts with and disrupts interdigitation in the polymer side chains. It has been proposed that a "weak" doping process, which occurs at low dopant concentrations, results in the F4TCNQ molecules interacting with the hexyl chains of the polymer, rather than binding to the backbone.[24] Simulations of such a system could provide evidence for or against this assertion.

A | Ground state properties of the P3HT/F4TCNQ dimer complex

Optimally-tuned range-corrected functionals, such as LRC-ωPBEh, have demonstrated improved performance over their non-tuned counterparts as a result of the optimal tuning process. In this process, the system of interest is modelled with a range of values of ω. The energy difference between the HOMO of the system and its ionization potential is evaluated for each ω, and the optimal value is chosen such that this energy difference is minimised. For a more sophisticated tuning procedure, the LUMO of the system can simultaneously be compared with the electron affinity of the system and this gap also minimised, as per Equation 3.1. Using this procedure, the optimal value for ω was found to be 0.065 bohr^{-1} in vacuum, and 0.005 bohr^{-1} in a dielectric medium with a dielectric constant of 3.0. The frontier molecular orbital energies, ionization potential and electron affinity are presented in Table A.1.

The popularity of the B3LYP functional is diminishing in the face of a new family of optimally tuned range-corrected functionals, such as the LRC-ωPBEh functional used in Chapter 3, due to their improved performance. However, for comparison and to evaluate the performance of B3LYP for this dispersion-bound complex, all calculations in the work discussed in Chapter 3 were performed with both the range-corrected functional and the B3LYP functional. Grimme's D2 dispersion correction was added to the latter, and will be denoted B3LYP-D. In all cases the same trends were observed using both functionals.

Simulated absorption spectra for the B3LYP-D functional are red-shifted with

Table A.1: Parameters (in eV) obtained from tuning the LRC-ωPBEh functional for the dimer complex in vacuum and in a dielectric medium

	Vacuum ($\omega = 0.065$ bohr^{-1})	Solvent ($\omega = 0.005$ bohr^{-1})
HOMO	5.74	5.03
IP	5.76	5.00
LUMO	3.43	3.97
EA	3.47	4.10

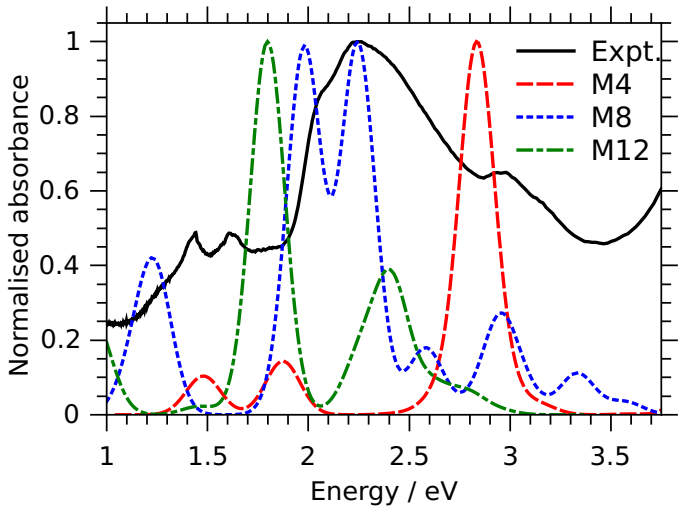

Figure A.1: Normalised simulated absorption spectra for each methyl-substituted dimer shown with the normalised simulated absorption spectrum of the P3HT/F4TCNQ film produced by Jacobs *et al.* Calculations performed at the B3LYP-D/6-31G(d) level of theory.

respect to both the range-corrected results and the experimental spectrum in vacuum (Figures A.1 and A.2). However, in solvent the two simulated spectra show very good agreement, indicating that the range-corrected functional experiences a greater red-shift under the influence of solvent than the hybrid functional. As discussed in Chapter 3, this is attributed to the greater spatial extent of electron density for the solvated LRC-ωPBEh functional due to the small ω value. Figure A.3 confirms that the dielectric medium itself does not affect molecular orbital energies, rather it is the choice of ω in the solvent that causes them to change. Finally, Figure A.4 shows the same trend as Figure 3.3 in that the addition of diffuse functions results in only a very slight red-shift of the spectrum.

The integral equation formalised polarisable continuum model (IEFPCM) model has been proposed to perform better than the conductor-like polarisable continuum model (CPCM) for low dielectric constant solvents, such as the P3HT solvent implicitly introduced in the work presented in Chapter 3. However, it is more computationally expensive than the CPCM model. In order to evaluate the performance of these two solvent models, the M8 dimer was optimised in the presence of each, at the B3LYP-D/6-31G(d) level of theory. Table A.2 shows that frontier molecular orbital energies are largely unchanged, and the amount of charge transferred onto F4TCNQ is essentially consistent between the two. Furthermore, the simulated absorption spectra in Figure A.5 are almost identical. It was hence concluded that the difference between the two solvent models was minimal, and due to its improved efficiency, CPCM was chosen for the remainder of the study.

For accurate performance from an implicit solvent model, the static, ϵ, and optical, ϵ_∞, dielectric constants must be chosen to match the experimental values for the solvent of interest. For organic polymers, ϵ lies between 3 and 5. An investiga-

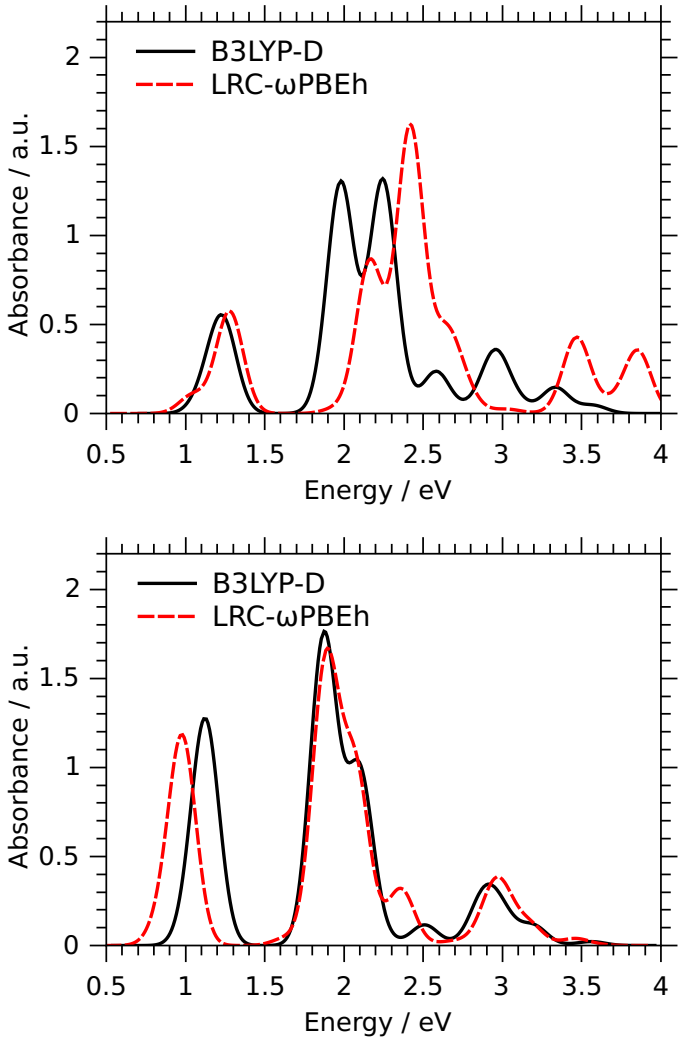

Figure A.2: Simulated absorption spectra for the M8 dimer complex in vacuum (top) and solvent (bottom) for the B3LYP-D and LRC-ωPBEh functionals with the 6-31G(d) basis set.

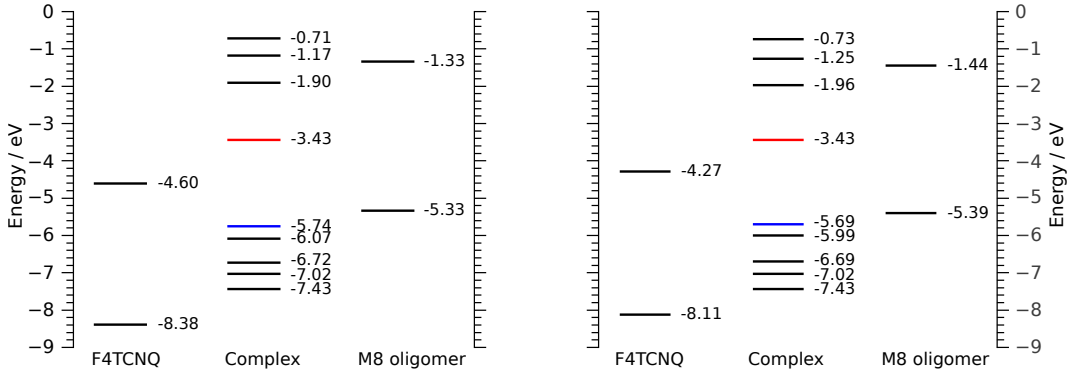

Figure A.3: Calculated molecular orbital energies obtained using the LRC-ωPBEh functional for the M8 dimer and its isolated fragments in vacuum (left; ω = 0.065 bohr^{-1}) and in a dielectric medium with ω equal to the optimal vacuum value (right; $\omega = 0.065$ bohr^{-1}).

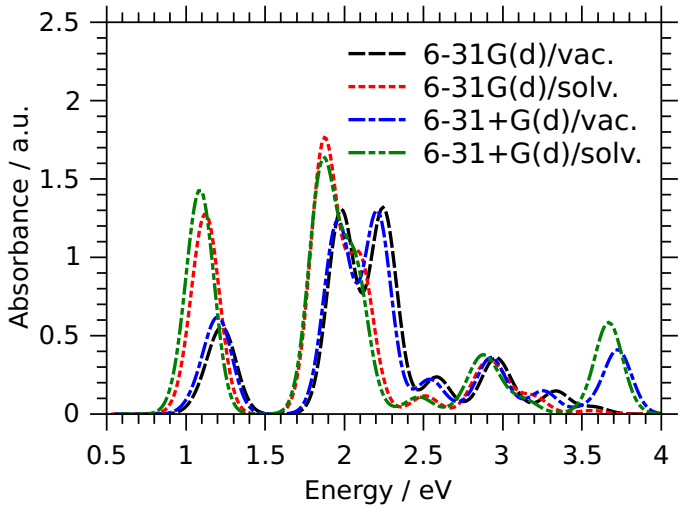

Figure A.4: Simulated absorption spectra for the M8 dimer complex obtained using the B3LYP-D functional with and without implicit solvent. In all cases the optimised 6-31G(d) geometry was used from vacuum and implicit solvent ground state calculations, with either the 6-31G(d) or 6-31+G(d) basis set used in TDDFT calculations.

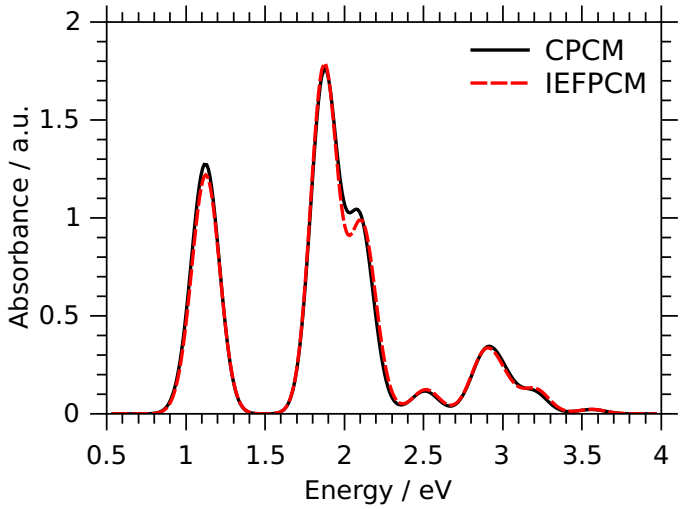

Figure A.5: Simulated absorption spectra for the M8 dimer complex, obtained using CPCM and IEFPCM solvent models. Calculations performed at the B3LYP-D/6-31G(d) level of theory.

Table A.2: Frontier molecular orbital energies and CHELPG charge transfer in the M8 dimer complex optimised in two solvent models (ϵ = 3.0) using B3LYP-D/6-31G(d)

Model	HOMO (eV)	LUMO (eV)	Charge (e)
CPCM	–4.98	–3.81	0.82
IEFPCM	–4.95	–3.78	0.81

Table A.3: Charge transfer (CT) for the M8 dimer at the B3LYP-D/6-31G(d) level of theory for a range of static dielectric constants, ϵ

Dielectric constant	CT (e)
1.0	0.65
3.0	0.82
4.0	0.86
5.0	0.89

tion was performed into the impact of static dielectric constant by optimising the ground-state geometry of the M8 dimer with ϵ set to 3.0, 4.0 and 5.0. Calculations were performed at the B3LYP-D/6-31G(d) level of theory. Table A.3 shows how increasing ϵ increases the degree of ground-state charge transfer. While a static dielectric constant of 4.0 and 5.0 give a greater degree of charge transfer, these values approach the upper limit of acceptable values for organic polymers, and hence a value of 3.0 was chosen as the most appropriate value.

The value of ϵ_∞ is equal to the square of the refractive index, which for regioregular P3HT values over a range of 1.1–2.5, giving an optical dielectric constant somewhere between 1.2 and 6.3. In this work, a range of intermediate values, equal to 2.0, 3.0, 4.0 and 5.0, were used to obtain simulated absorption spectra of the M8 dimer, with ϵ set to 3.0. Figure A.6 shows that only small differences in peak intensities were observed when ϵ_∞ was increased. An intermediate value of 3.0 was chosen for this study.

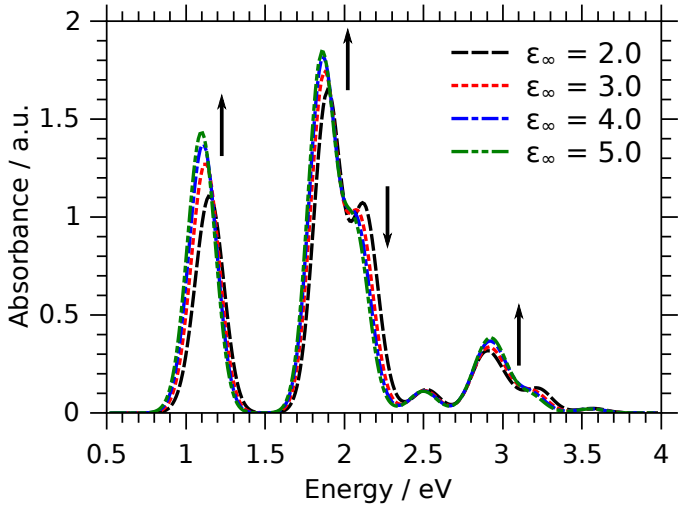

Figure A.6: Simulated absorption spectra for the M8 dimer in a dielectric medium ($\epsilon = 3.0$) obtained with various ϵ_∞ at the B3LYP-D/CPCM level. Arrows indicate increasing ϵ_∞.

B | Photo-induced charge-transfer mechanism

Time-dependent density functional theory (TDDFT) calculations revealed a large number of excited states in the M8 dimer complex. Molecular orbitals and natural transition orbitals associated with the dominant transitions may be seen in Chapter 4. For each excitation, the dominant molecular orbital transition is displayed in Figure 4.4. The contribution percentage for each of these transitions is listed in Table B.1.

Table B.1: Dominant molecular orbital contribution percentage for each excited state with intensity > 0.1 a.u.

State	B3LYP-D/vac.	B3LYP-D/solv.	LRC-ωPBEh/vac.	LRC-ωPBEh/solv.
1	92	88	100	100
2	76	84	94	98
4	80	91	66	90
5	82	86	58	77
7	79	94	70	82
9			46	
16		57		
17	60			
19				57
20		57		57
21			47	
22	53	86		71

C | Molecular mobility of F4TCNQ in P3HT systems

Geometry optimisations were performed wherein the entire system was constrained in its equilibrium geometry except the hydrogens on the methyl group on mF4-TCNQ. The hydrogens were rotated through 120 degrees at 30 degree increments and allowed to relax. The position of one hydrogen was fixed at each rotation to prevent relaxation back into the ground-state geometry. The energies of rotation for the two inter-chain separations are recorded in Figure C.1.

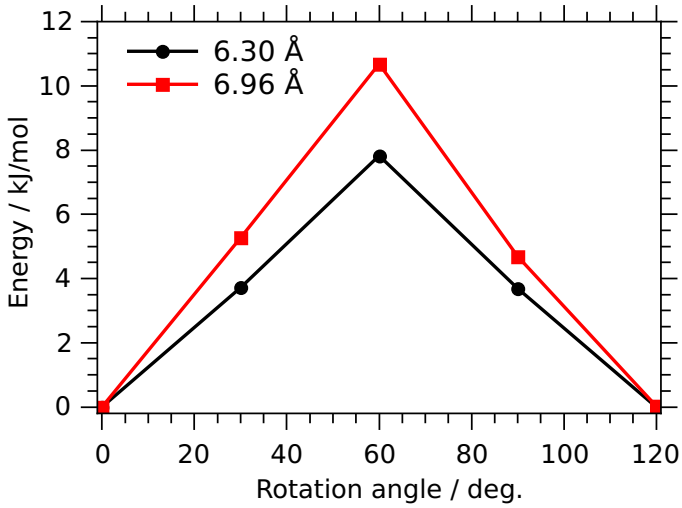

Figure C.1: Rotation energy of the mF4TCNQ ester group for the smaller and larger inter-chain separations.

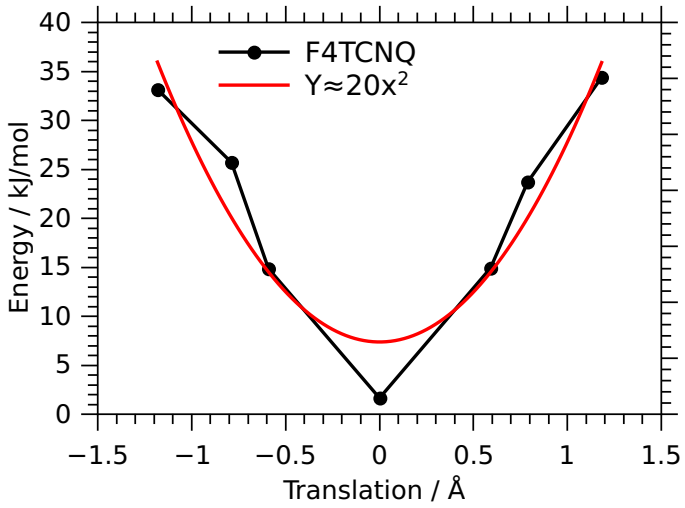

Figure C.2: Quadratic fit to potential energy data from F4TCNQ, in order to approximate a harmonic fit to the data.

D | Quantifying Charge-Transfer-Induced Solubility Control

All parameters used in this work to describe P3HT and F4TCNQ in molecular dynamics simulations are listed below. Atom parameters were taken from the OPLS-AA force field. Bond and angle parameters were taken from the OPLS-AA force field, but the equilibrium bond lengths and angles were set to values taken from DFT calculations at the B3LYP-D/6-31+G(d) level of theory in implicit chloroform solvent (conductor-like polarisable continuum model, $\epsilon = 4.8$). Dihedral and improper dihedral parameters were taken from the OPLS-AA force field. For the potentials used to describe bonded and non-bonded parameters please see Chapter 2.

When performing free energy perturbation calculations, a small $\Delta\lambda$ is required such that good phase space overlap is achieved. The choice of t_λ is also important as it must allow for sufficient equilibration time at each λ window. A set of values for each of these parameters were prepared, and the free energy of annihilating neutral F4TCNQ at a small and large separation from $(3HT)_8$ were quantified (Table D.11). The difference between these two free energies was observed to decrease with both increasing the time at each step and decreasing the step size $\Delta\lambda$. The change in energies and energy difference was determined to be sufficiently small in going from 200,000 fs to 400,000 fs at $\Delta\lambda = 0.05$ and so the latter t_λ was chosen with a step size of $\Delta\lambda = 0.05$ for all subsequent simulations.

Table D.1: Atom parameters for the F4TCNQ molecule

Atom	Atom type	Mass (amu)	σ_{ii} (Å)	ϵ_{ii} (kcal/mol)
1	F	18.9984	2.85	0.0607
2	CA	12.0110	3.55	0.0698
3	CA	12.0110	3.55	0.0698
4	CA	12.0110	3.55	0.0698
5	CZ	12.0110	3.30	0.0657
6	NZ	14.0067	3.20	0.1693

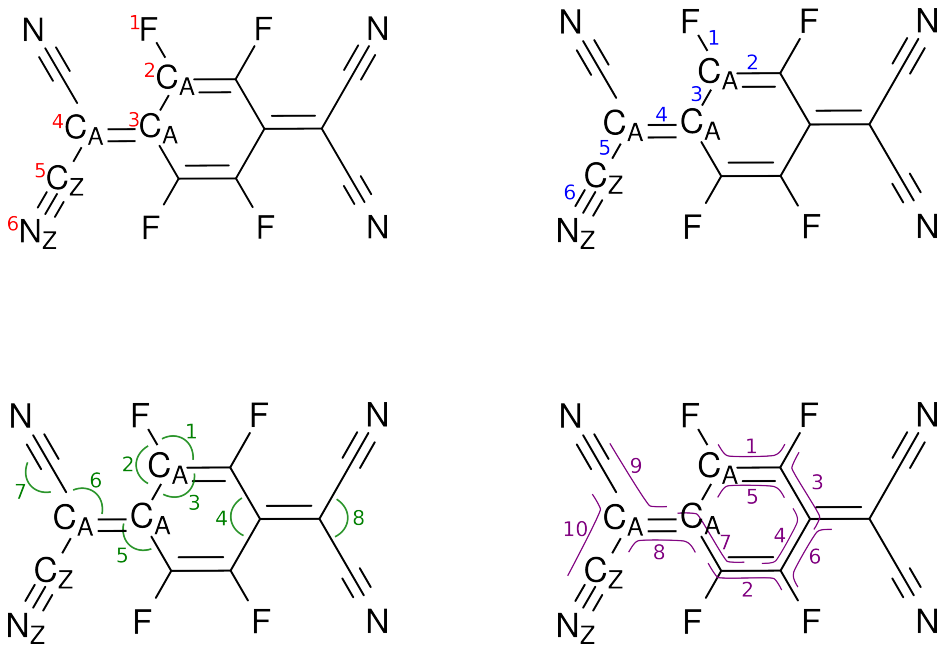

Figure D.1: Atoms, bonds, angles and dihedrals for the F4TCNQ molecule.

Table D.2: Bond parameters for the F4TCNQ molecule taken from the charged distribution (neutral parameters shown in parentheses)

Bond	Bond type	r_{eq} (Å)	K_r (kcal/mol·Å^2)
1	F–CA	1.35 (1.34)	418.4
2	CA–CA	1.37 (1.36)	467.2
3	CA–CA	1.42 (1.45)	467.2
4	CA–CA	1.42 (1.39)	467.2
5	CA–CZ	1.17 (1.16)	647.5

Table D.3: Angle parameters for the F4TCNQ molecule taken from the charged distribution (neutral parameters shown in parentheses)

Angle	Angle type	θ_{eq} (deg.)	K_θ (kcal/mol·rad^2)
1	F–CA–CA	117.4 (118.4)	79.70
2	F–CA–CA	117.9 (118.8)	79.70
3	CA–CA–CA	123.4 (122.9)	62.76
4	CA–CA–CA	113.3 (114.3)	62.76
5	CA–CA–CA	123.4 (122.9)	62.76
6	CA–CA–CZ	123.6 (124.0)	69.73
7	CA–CZ–NZ	175.8 (175.6)	149.40
8	CA–CA–CZ*	112.7 (113.2)	69.73

*No parameters exist in the OPLS-AA force field for a CZ–CA–CZ angle

Table D.4: Dihedral parameters for the F4TCNQ molecule

Dihedral	Dihedral type	Coefficients (kcal/mol)
1	F–CA–CA–F	7.220, 0.000, -7.220, 0.000, 0.000
2	F–CA–CA–CA	7.220, 0.000, -7.220, 0.000, 0.000
3	F–CA–CA–CA	7.220, 0.000, -7.220, 0.000, 0.000
4	CA–CA–CA–CA	7.220, 0.000, -7.220, 0.000, 0.000
5	CA–CA–CA–CA	7.220, 0.000, -7.220, 0.000, 0.000
6	F–CA–CA–CA	7.220, 0.000, -7.220, 0.000, 0.000
7	CA–CA–CA–CA	7.220, 0.000, -7.220, 0.000, 0.000
8	CA–CA–CA–CZ	7.220, 0.000, -7.220, 0.000, 0.000
9	CA–CA–CZ–NZ	0.000, 0.000, 0.000, 0.000, 0.000
10	CZ–CA–CZ–NZ	0.000, 0.000, 0.000, 0.000, 0.000

Table D.5: Improper dihedral parameters for the F4TCNQ molecule

Dihedral	Dihedral type	ϕ (deg.)	Coefficient (kcal/mol)
1	Z–CA–X–Y	0.0	1.0958
2	Z–CA–X–Y	0.0	1.0958
3	Z–CA–X–Y	2.1	1.0958

Table D.6: Atom parameters for the $(3HT)_8$ molecule

Atom	Atom class	Mass (amu)	σ_{ii} (Å)	ϵ_{ii} (kcal/mol)
1	CA	12.0110	3.55	0.07
2	S	32.0650	3.55	0.25
3	CA	12.0110	3.55	0.07
4	CA	12.0110	3.55	0.07
5	CA	12.0110	3.55	0.07
6	HA	1.0080	2.42	0.03
7	CT	12.0110	3.55	0.07
8	CT	12.0110	3.55	0.07
9	HA	1.0080	2.42	0.03
10	HA	1.0080	2.42	0.03
11	CT	12.0110	3.50	0.066
12	CT	12.0110	3.50	0.066
13	CT	12.0110	3.50	0.066
14	CT	12.0110	3.50	0.066
15	CT	12.0110	3.50	0.066
16	CT	12.0110	3.50	0.066
17	HC	1.0080	2.50	0.03
18	HC	1.0080	2.50	0.03

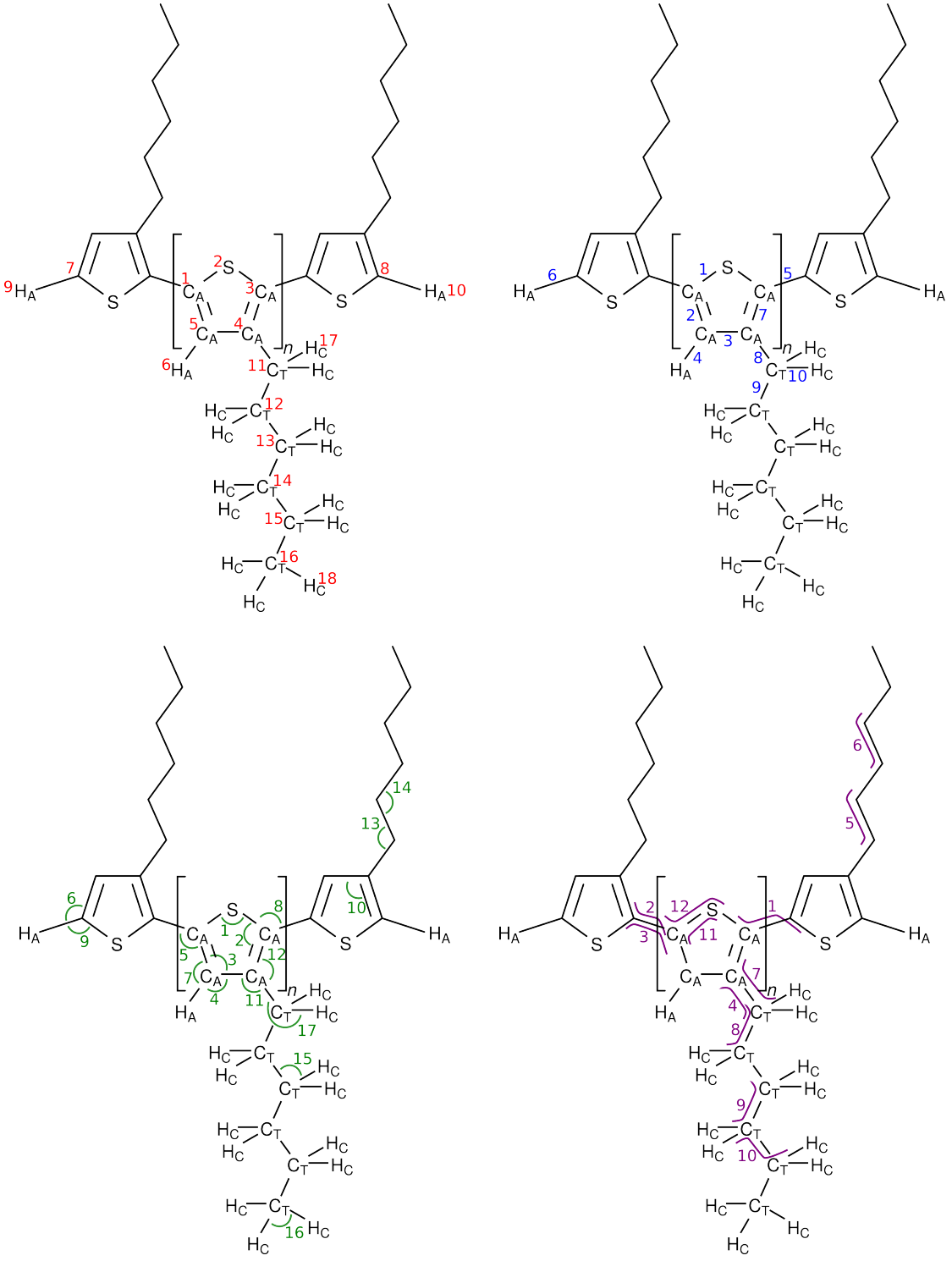

Figure D.2: Atoms, bonds, angles and dihedrals for the $(3HT)_8$ molecule.

Table D.7: Bond parameters for the $(3HT)_8$ molecule taken from the charged distribution (neutral parameters shown in parentheses)

Bond	Bond type	r_{eq} (Å)	K_r (kcal/mol·Å^2)
1	CA–S	1.76 (1.76)	291.3
2	CA–CA	1.39 (1.38)	514.3
3	CA–CA	1.41 (1.42)	453.1
4	CA–HA	1.09 (1.09)	370.63
5	CA–CA	1.43 (1.45)	392.3
6	CA–HA	1.08 (1.08)	370.6
7	CA–CA	1.40 (1.39)	514.4
8	CA–CT	1.50 (1.51)	317.0
9	CT–CT	1.53 (1.53)	268.0
10	CT–HC	1.09 (1.09)	340.0

Table D.8: Angle parameters for the $(3HT)_8$ molecule taken from the charged distribution (neutral parameters shown in parentheses)

Angle	Angle type	θ_{eq} (deg.)	K_θ (kcal/mol·rad^2)
1	CA–S–CA	92.0 (92.3)	86.36
2	S–CA–CA	110.4 (110.2)	86.36
3	CA–CA–CA	115.1 (115.1)	39.58
4	CA–CA–HA	122.1 (122.0)	35.26
5	CA–CA–CA	128.3 (129.2)	54.69
6	CA–CA–HA	128.0 (128.2)	35.26
7	CA–CA–HA	122.8 (123.0)	35.26
8	S–CA–CA	121.2 (120.9)	41.74
9	S–CA–HA	120.0 (120.0)	28.79
10	CA–CA–CA	112.1 (112.4)	39.58
11	CA–CA–CT	122.8 (122.0)	70.00
12	CA–CA–CT	125.0 (125.7)	70.00
13	CA–CT–CT*	114.0 (114.0)	63.00
14	CT–CT–CT*	112.7 (112.7)	58.35
15	CT–CT–HC*	110.7 (110.7)	37.50
16	HC–CA–HC*	107.8 (107.8)	33.00
17	CA–CT–HC*	109.5 (109.5)	35.00

*Default parameters from the OPLS-AA force field

Table D.9: Dihedral parameters for the $(3HT)_8$ molecule

Dihedral	Dihedral type	Potential	Coefficients (kcal/mol)
1	S–CA–CA–S	Eq. 2.36	1.686, -0.155, -0.767, 0.885, -4.549, -1.890, 7.980, 1.099, -4.412
2	CA–CA–CA–CA	Eq. 2.36	1.686, -0.155, -0.767, 0.885, -4.549, -1.890, 7.980, 1.099, -4.412
3	CA–CA–CA–S	Eq. 2.36	1.686, 0.155, -0.767, -0.885, -4.549, 1.890, 7.980, -1.099, -4.412
4	CA–CA–CT–CT	Eq. 2.35	0.000, 0.000, 0.000, 0.000, 0.000
5	CA–CT–CT–CT	Eq. 2.35	0.700, 0.350, 0.050, 0.400, 0.000
6	CT–CT–CT–CT	Eq. 2.35	0.700, 0.350, 0.050, 0.400, 0.000
7	CA–CA–CT–HC	Eq. 2.35	0.000, 0.000, 0.000, 0.000, 0.000
8	CA–CT–CT–HC	Eq. 2.35	0.231, -0.693, 0.000, 0.924, 0.000
9	CT–CT–CT–HC	Eq. 2.35	0.150, -0.405, 0.000, 0.600, 0.000
10	HC–CT–CT–HC	Eq. 2.35	0.150, -0.450, 0.000, 0.600, 0.000
11	X–CA–S–X	Eq. 2.37	3.625, -1.000, 2.000
12	X–CA–CA–X	Eq. 2.37	3.625, -1.000, 2.000

Table D.10: Improper dihedral parameters for the $(3HT)_8$ molecule

Dihedral	Dihedral type	Coefficient (kcal/mol)	d	n
1	CA–CA–CA–CT	1.1	-1.0	2.0

Table D.11: Calculated free energies for the annihilation of neutral F4TCNQ at small (5 Å) and large (30 Å) separation from neutral $(3HT)_8$

$\Delta\lambda$	t_λ	ΔG_{small} (kcal/mol)	ΔG_{large} (kcal/mol)
0.1	200,000	38.94	35.08
0.05	200,000	35.82	34.35
0.05	400,000	34.35	33.08

References

[1] Yang, S.; Shin, K.; Park, C. *Advanced Functional Materials* **2005**, *15*, 1806–1814.

[2] Green, M. A.; Emery, K.; Hishikawa, Y.; Warta, W.; Dunlop, E. D. *Progress in Photovoltaics: Research and Applications* **2016**, *24*, 3–11.

[3] Reineke, S. *Nature Materials* **2015**, *14*, 459–462.

[4] Adhikari, B.; Majumdar, S. *Progress in Polymer Science* **2004**, *29*, 699 – 766.

[5] Onorato, J.; Pakhnyuk, V.; Luscombe, C. K. *Polymer Journal* **2016**, 1–20.

[6] Sekitani, T.; Someya, T. *Advanced Materials* **2010**, *22*, 2228–2246.

[7] Noriega, R.; Rivnay, J.; Vandewal, K.; Koch, F. P. V.; Stingelin, N.; Smith, P.; Toney, M. F.; Salleo, A. *Nature Materials* **2013**, *12*, 1038–1044.

[8] Mei, J.; Bao, Z. *Chemistry of Materials* **2014**, *26*, 604–615.

[9] Babel, A.; Jenekhe, S. A. *Synthetic Metals* **2005**, *148*, 169–173.

[10] Liu, J.; Zhang, R.; Sauvé, G.; Kowalewski, T.; McCullough, R. D. *Journal of the American Chemical Society* **2008**, *130*, 13167–13176.

[11] He, M.; Li, J.; Sorensen, M. L.; Zhang, F.; Hancock, R. R.; Fong, H. H.; Pozdin, V. A.; Smilgies, D.-M.; Malliaras, G. G. *Journal of the American Chemical Society* **2009**, *131*, 11930–11938.

[12] Shirakawa, H.; Louis, E. J.; MacDiarmid, A. G.; Chiang, C. K.; Heeger, A. J. *Journal of the Chemical Society, Chemical Communications* **1977**, 578–580.

[13] Parthasarathy, G.; Shen, C.; Kahn, A.; Forrest, S. R. *Journal of Applied Physics* **2001**, *89*, 4986–4992.

[14] Walzer, K.; Maennig, B.; Pfeiffer, M.; Leo, K. *Chemical Reviews* **2007**, *107*, 1233–1271.

[15] Singh, M.; Haverinen, H. M.; Dhagat, P.; Jabbour, G. E. *Advanced Materials* **2010**, *22*, 673–685.

[16] Teichler, A.; Perelaer, J.; Schubert, U. S. *Journal of Materials Chemisry C* **2013**, *1*, 1910–1925.

[17] Kang, K.; Watanabe, S.; Broch, K.; Sepe, A.; Brown, A.; Nasrallah, I.;

Nikolka, M.; Fei, Z.; Heeney, M.; Matsumoto, D.; Marumoto, K.; Tanaka, H.; Kuroda, S.; Sirringhaus, H. *Nature Materials* **2016**, *15*, 896–902.

[18] DeFranco, J. A.; Schmidt, B. S.; Lipson, M.; Malliaras, G. G. *Organic Electronics* **2006**, *7*, 22–28.

[19] Taylor, P. G.; Lee, J.-K.; Zakhidov, A. A.; Chatzichristidi, M.; Fong, H. H.; DeFranco, J. A.; Malliaras, G. G.; Ober, C. K. *Advanced Materials* **2009**, *21*, 2314–2317.

[20] Ouyang, S.; Xie, Y.; Zhu, D.; Xu, X.; Wang, D.; Tan, T.; Fong, H. H. *Organic Electronics* **2014**, *15*, 1822–1827.

[21] Love, J. A.; Proctor, C. M.; Liu, J.; Takacs, C. J.; Sharenko, A.; van der Poll, T. S.; Heeger, A. J.; Bazan, G. C.; Nguyen, T.-Q. *Advanced Functional Materials* **2013**, *23*, 5019–5026.

[22] Sharenko, A.; Kuik, M.; Toney, M. F.; Nguyen, T.-Q. *Advanced Functional Materials* **2014**, *24*, 3543–3550.

[23] Zalar, P.; Kuik, M.; Ran, N. A.; Love, J. A.; Nguyen, T.-Q. *Advanced Energy Materials* **2014**, *4*, 1400438.

[24] Duong, D. T.; Phan, H.; Hanifi, D.; Jo, P. S.; Nguyen, T.-Q.; Salleo, A. *Advanced Materials* **2014**, *26*, 6069–6073.

[25] Albrecht, S.; Vandewal, K.; Tumbleston, J. R.; Fischer, F. S. U.; Douglas, J. D.; Fréchet, J. M. J.; Ludwigs, S.; Ade, H.; Salleo, A.; Neher, D. *Advanced Materials* **2014**, *26*, 2533–2539.

[26] Duong, D. T.; Wang, C.; Antoni, E.; Toney, M. F.; Salleo, A. *Organic Electronics* **2013**, *14*, 1330–1336.

[27] Abdou, M. S. A.; Orfino, F. P.; Son, Y.; Holdcroft, S. *Journal of the American Chemical Society* **1997**, *119*, 4518–4524.

[28] Castro, H.; Sowade, E.; Rocha, J.; Alpuim, P.; Machado, A.; Baumann, R.; Lanceros-Méndez, S. *Organic Electronics* **2015**, *22*, 12–19.

[29] Gardonio, S.; Gregoratti, L.; Melpignano, P.; Aballe, L.; Biondo, V.; Zamboni, R.; Murgia, M.; Caria, S.; Kiskinova, M. *Organic Electronics* **2007**, *8*, 37–43.

[30] Gao, Z. Q.; Mi, B. X.; Xu, G. Z.; Wan, Y. Q.; Gong, M. L.; Cheah, K. W.; Chen, C. H. *Chemical Communications* **2008**, 117–119.

[31] Qi, Y.; Sajoto, T.; Barlow, S.; Kim, E.-G.; Brédas, J.-L.; Marder, S. R.; Kahn, A. *Journal of the American Chemical Society* **2009**, *131*, 12530–12531.

[32] Salzmann, I.; Heimel, G.; Duhm, S.; Oehzelt, M.; Pingel, P.; George, B. M.; Schnegg, A.; Lips, K.; Blum, R.-P.; Vollmer, A.; Koch, N. *Physical Review Letters* **2012**, *108*, 035502.

[33] Méndez, H.; Heimel, G.; Opitz, A.; Sauer, K.; Barkowski, P.; Oehzelt, M.; Soeda, J.; Okamoto, T.; Takeya, J.; Arlin, J.-B.; Balandier, J.-Y.; Geerts, Y.; Koch, N.; Salzmann, I. *Angewandte Chemie International Edition* **2013**, *52*, 7751–7755.

[34] Méndez, H.; Heimel, G.; Winkler, S.; Frisch, J.; Opitz, A.; Sauer, K.; Wegner, B.; Oehzelt, M.; Rothel, C.; Duhm, S.; Többens, D.; Koch, N.; Salzmann, I. *Nature Communications* **2015**, *6*, 8560.

[35] Wang, C.; Duong, D. T.; Vandewal, K.; Rivnay, J.; Salleo, A. *Physical Review B* **2015**, *91*, 085205.

[36] Pingel, P.; Neher, D. *Physical Review B* **2013**, *87*, 115209.

[37] Ma, L.; Lee, W. H.; Park, Y. D.; Kim, J. S.; Lee, H. S.; Cho, K. *Applied Physics Letters* **2008**, *92*, 063310.

[38] Jacobs, I. E.; Li, J.; Burg, S. L.; Bilsky, D. J.; Rotondo, B. T.; Augustine, M. P.; Stroeve, P.; Moulé, A. J. *ACS Nano* **2015**, *9*, 1905–1912.

[39] Pingel, P.; Zhu, L.; Park, K. S.; Vogel, J.-O.; Janietz, S.; Kim, E.-G.; Rabe, J. P.; Brédas, J.-L.; Koch, N. *The Journal of Physical Chemistry Letters* **2010**, *1*, 2037–2041.

[40] Fuzell, J.; Jacobs, I. E.; Ackling, S.; Harrelson, T. F.; Huang, D. M.; Larsen, D.; Moulé, A. J. *The Journal of Physical Chemistry Letters* **2016**, *7*, 4297–4303.

[41] Jacobs, I. E.; Aasen, E. W.; Nowak, D.; Li, J.; Morrison, W.; Roehling, J. D.; Augustine, M. P.; Moulé, A. J. *Advanced Materials* **2016**,

[42] Gao, W.; Kahn, A. *Applied Physics Letters* **2001**, *79*, 4040–4042.

[43] Choulis, S. A.; Kim, Y.; Nelson, J.; Bradley, D. D. C.; Giles, M.; Shkunov, M.; McCulloch, I. *Applied Physics Letters* **2004**, *85*, 3890–3892.

[44] Gao, J.; Roehling, J. D.; Li, Y.; Guo, H.; Moule, A. J.; Grey, J. K. *Journal of Materials Chemisry C* **2013**, *1*, 5638–5646.

[45] Zhu, L.; Kim, E.-G.; Yi, Y.; Brédas, J.-L. *Chemistry of Materials* **2011**, *23*, 5149–5159.

[46] Lubis, P.; Saito, M. *Japanese Journal of Applied Physics* **2014**, *53*, 071602.

[47] Chou, Y.-M.; Chen, W.-H.; Liang, C.-C. *Journal of Molecular Structure: THEOCHEM* **2009**, *894*, 117–120.

[48] Bhatta, R. S.; Tsige, M. *Polymer* **2014**, *55*, 2667–2672.

[49] Liu, T.; Troisi, A. *The Journal of Physical Chemistry C* **2011**, *115*, 2406–2415.

[50] Sweetnam, S.; Vandewal, K.; Cho, E.; Risko, C.; Coropceanu, V.; Salleo, A.; Brédas, J.-L.; McGehee, M. D. *Chemistry of Materials* **2016**, *28*, 1446–1452.

[51] Qiu, M.; Brandt, R. G.; Niu, Y.; Bao, X.; Yu, D.; Wang, N.; Han, L.; Yu, L.; Xia, S.; Yang, R. *The Journal of Physical Chemistry C* **2015**, *119*, 8501–8511.

[52] Do, K.; Huang, D. M.; Faller, R.; Moulé, A. J. *Physical Chemistry Chemical Physics* **2010**, *12*, 14735–14739.

[53] Newbloom, G. M.; Hoffmann, S. M.; West, A. F.; Gile, M. C.; Sista, P.; Cheung, H.-K. C.; Luscombe, C. K.; Pfaendtner, J.; Pozzo, L. D. *Langmuir* **2015**, *31*, 458–468.

[54] Pani, R. C.; Bond, B. D.; Krishnan, G.; Yingling, Y. G. *Soft Matter* **2013**, *9*, 10048–10055.

[55] Lee, C.-K.; Pao, C.-W.; Chu, C.-W. *Energy and Environmental Science* **2011**, *4*, 4124–4132.

[56] Gao, W.; Kahn, A. *Journal of Applied Physics* **2003**, *94*, 359–366.

[57] Duhm, S.; Salzmann, I.; Bröker, B.; Glowatzki, H.; Johnson, R. L.; Koch, N. *Applied Physics Letters* **2009**, *95*, 093305.

[58] Bruder, I.; Watanabe, S.; Qu, J.; Müller, I. B.; Kopecek, R.; Hwang, J.; Weis, J.; Langer, N. *Organic Electronics* **2010**, *11*, 589–593.

[59] Li, J.; Rochester, C. W.; Jacobs, I. E.; Friedrich, S.; Stroeve, P.; Riede, M.; Moulé, A. J. *ACS Applied Materials and Interfaces* **2015**, *7*, 28420–28428.

[60] Li, J.; Zhang, G.; Holm, D. M.; Jacobs, I. E.; Yin, B.; Stroeve, P.; Mascal, M.; Moulé, A. J. *Chemistry of Materials* **2015**, *27*, 5765–5774.

[61] Scholl, D. S.; Steckel, J. A. *Density Functional Theory: A Practical Introduction*; Wiley, 2009.

[62] Hohenberg, P.; Kohn, W. *Physical Review* **1964**, *136*, B864–B871.

[63] Becke, A. D. *The Journal of Chemical Physics* **1993**, *98*, 5648–5652.

[64] Becke, A. D. *Physical Review A* **1988**, *38*, 3098–3100.

[65] Lee, C.; Yang, W.; Parr, R. G. *Physical Review B* **1988**, *37*, 785–789.

[66] Kristyán, S.; Pulay, P. *Chemical Physics Letters* **1994**, *229*, 175–180.

[67] Grimme, S. *Journal of Computational Chemistry* **2006**, *27*, 1787–1799.

[68] Chai, J.-D.; Head-Gordon, M. *The Journal of Chemical Physics* **2008**, *128*, 084106.

[69] Tawada, Y.; Tsuneda, T.; Yanagisawa, S.; Yanai, T.; Hirao, K. *The Journal of Chemical Physics* **2004**, *120*, 8425–8433.

[70] Rohrdanz, M. A.; Martins, K. M.; Herbert, J. M. *The Journal of Chemical Physics* **2009**, *130*, 054112.

[71] Sun, H.; Hu, Z.; Zhong, C.; Zhang, S.; Sun, Z. *The Journal of Physical Chem-*

istry C **2016**, *120*, 8048–8055.

[72] de Queiroz, T. B.; Kümmel, S. *The Journal of Chemical Physics* **2014**, *141*, 084303.

[73] Boys, S. F. *Proceedings of the Royal Society of London A: Mathematical, Physical and Engineering Sciences* **1950**, *200*, 542–554.

[74] Cramer, C. J. *Essential of Computational Chemistry*, 2nd ed.; Wiley, 2004.

[75] Hehre, W. J.; Ditchfield, R.; Pople, J. A. *The Journal of Chemical Physics* **1972**, *56*, 2257–2261.

[76] Dunning, T. H. *The Journal of Chemical Physics* **1971**, *55*, 716–723.

[77] Schäfer, A.; Huber, C.; Ahlrichs, R. *The Journal of Chemical Physics* **1994**, *100*, 5829–5835.

[78] Wu, Q.; Van Voorhis, T. *Physical Review A* **2005**, *72*, 024502.

[79] Marques, M. A. L., Maitra, N. T., Nogueira, F. M. S., Gross, E. K. U., Rubio, A., Eds. *Fundamental of time-dependent density functional Theory*; Springer, 2012.

[80] Runge, E.; Gross, E. K. U. *Physical Review Letters* **1984**, *52*, 997–1000.

[81] Dreuw, A.; Head-Gordon, M. *Chemical Reviews* **2005**, *105*, 4009–4037.

[82] Grimme, S.; Parac, M. *ChemPhysChem* **2003**, *4*, 292–295.

[83] Peach, M. J. G.; Benfield, P.; Helgaker, T.; Tozer, D. J. *The Journal of Chemical Physics* **2008**, *128*, 044118.

[84] Dreuw, A.; Weisman, J. L.; Head-Gordon, M. *The Journal of Chemical Physics* **2003**, *119*, 2943–2946.

[85] Day, O. W.; Smith, D. W.; Garrod, C. *International Journal of Quantum Chemistry* **1974**, *8*, 501–509.

[86] Martin, R. L. *The Journal of Chemical Physics* **2003**, *118*, 4775–4777.

[87] Amos, A. T.; Hall, G. G. *Proceedings of the Royal Society of London A: Mathematical, Physical and Engineering Sciences* **1961**, *263*, 483–493.

[88] Jensen, F. *Introduction to Computational Chemistry*, 2nd ed.; Wiley, 2007.

[89] Truong, T. N.; Stefanovich, E. V. *Chemical Physics Letters* **1995**, *240*, 253–260.

[90] Cancès, E.; Mennucci, B.; Tomasi, J. *The Journal of Chemical Physics* **1997**, *107*, 3032–3041.

[91] Cancès, E.; Mennucci, B. *The Journal of Chemical Physics* **2001**, *114*, 4744–4745.

[92] Herbert, J. M.; Lange, W. In *Many-body effects and eelectrostatic in multi-*

scale ccomputation of biomolecules; Cui, Q., Ren, P., Meuwly, M., Eds.; Pan Stanford, 2015; Chapter 1, pp 1–54.

[93] Jacquemin, D.; Mennucci, B.; Adamo, C. *Physical Chemistry Chemical Physics* **2011**, *13*, 16987–16998.

[94] Laurent, A. D.; Jacquemin, D. *International Journal of Quantum Chemistry* **2013**, *113*, 2019–2039.

[95] Cossi, M.; Barone, V. *The Journal of Physical Chemistry A* **2000**, *104*, 10614–10622.

[96] Shao, Y. et al. *Molecular Physics* **2015**, *113*, 184–215.

[97] Tuckerman, M. E. *Statistical mechanics: theory and molecular simulation*; Oxford University Press, 2010.

[98] Jorgensen, W. L.; Maxwell, D. S.; Tirado-Rives, J. *Journal of the American Chemical Society* **1996**, *118*, 11225–11236.

[99] Moreno, M.; Mosè,; Meille, G. R. S. V.; Po, R. *Journal of Physical Chemistry B* **2010**, *114*, 1591–1602.

[100] Weiner, S. J.; Kollman, P. A.; Nguyen, D. T.; Case, D. A. *Journal of Computational Chemistry* **1986**, *7*, 230–252.

[101] Darling, S. B.; Sternberg, M. *Journal of Physical Chemistry B* **2009**, *113*, 6215–6218.

[102] Hockney, R. W.; Eastwood, J. W. *Computer simulation using particles*; IOP Publishing Ltd., 1988.

[103] Nosé, S. *The Journal of Chemical Physics* **1984**, *81*, 511–519.

[104] Hoover, W. G. *Phys. Rev. A* **1985**, *31*, 1695–1697.

[105] Grübmuller, H.; Heymann, B.; Tavan, P. *Science* **1996**, *271*, 997–999.

[106] Jarzynski, C. *Physical Review Letters* **1997**, *78*, 2690–2693.

[107] Park, S.; Khalili-Araghi, F.; Tajkhorshid, E.; Schulten, K. *The Journal of Chemical Physics* **2003**, *119*, 3559–3566.

[108] Park, S.; Schulten, K. *The Journal of Chemical Physics* **2004**, *120*, 5946–5961.

[109] Zwanzig, R. W. *The Journal of Chemical Physics* **1954**, *22*, 1420–1426.

[110] Blom, P. M.; Mihailetchi, V. D.; Koster, L. J. A.; Markov, D. E. *Advanced Materials* **2007**, *19*, 1551–1566.

[111] He, Z.; Xiao, B.; Liu, F.; Wu, H.; Yang, Y.; Xiao, S.; Wang, C.; Russell, T.; Cao, Y. *Nature Photonics* **2015**, *9*, 174–179.

[112] Huo, L.; Liu, T.; Sun, X.; Cai, Y.; Heeger, A. J.; Sun, Y. *Advanced Materials* **2015**, *27*, 2938–2944.

[113] Benfenati, V.; Toffanin, S.; Bonetti, S.; Turatti, G.; Pistone, A.; Chiappalone, M.; Sagnella, A.; Stefani, A.; Gianluca, G.; Ruani, G.; Saguatti, D.; Zamboni, R.; Muccini, M. *Nature Materials* **2013**, *12*, 672–680.

[114] Lüssem, B.; Riede, M.; Leo, K. *Physica Status Solidi A* **2013**, *210*, 9–43.

[115] Pingel, P.; Schwarzl, R.; Neher, D. *Applied Physics Letters* **2012**, *100*, 143303.

[116] Bartesaghi, D.; Turbiez, M.; Koster, L. J. A. *Organic Electronics* **2014**, *15*, 3191–3202.

[117] Han, X.; Wu, Z.; Sun, B. *Organic Electronics* **2013**, *14*, 1116–1121.

[118] Nuzzo, D. D.; Fontanesi, C.; Jones, R.; Allard, S.; Dumsch, I.; Scherf, U.; von Hauff, E.; Schumacher, S.; Como, E. D. *Nature Communications* **2015**, *6*, 6460.

[119] Tadaki, D.; Ma, T.; Zhang, J.; Iino, S.; Hirano-Iwata, A.; Kimura, Y.; Niwano, M. *Japanese Journal of Applied Physics* **2015**, *54*, 091602.

[120] Aziz, E.; Vollmer, A.; Eisebitt, S.; Eberhardt, W.; Pingel, P.; Neher, D.; Koch, N. *Advanced Materials* **2007**, *19*, 3257–3260.

[121] Dennington, R.; Keith, T.; Millam, J. GaussView Version 5. Semichem Inc. Shawnee Mission KS 2009.

[122] Hanwell, M. D.; Curtis, D. E.; Lonie, D. C.; Vandermeersch, T.; Zurek, E.; Hutchinson, G. R. *Journal of Cheminformatics* **2012**, *4*, 17.

[123] Allouche, A.-R. *Journal of Computational Chemistry* **2011**, *32*, 174–182.

[124] Breneman, C. M.; Wiberg, K. B. *Journal of Computational Chemistry* **1990**, *11*, 361–373.

[125] Zheng, Z.; Brédas, J.-L.; Coropceanu, V. *The Journal of Physical Chemistry Letters* **2016**, *7*, 2616–2621.

[126] Perdew, J. P. *Physical Review B* **1986**, *33*, 8822–8824.

[127] Perdew, J. P.; Burke, K.; Ernzerhof, M. *Physical Review Letters* **1996**, *77*, 3865–3868.

[128] Adamo, C.; Barone, V. *The Journal of Chemical Physics* **1999**, *110*, 6158–6170.

[129] Becke, A. D. *The Journal of Chemical Physics* **1993**, *98*, 1372–1377.

[130] Zhao, Y.; Truhlar, D. G. *The Journal of Physical Chemistry A* **2006**, *110*, 13126–13130.

[131] Chai, J.-D.; Head-Gordon, M. *Physical Chemistry Chemical Physics* **2008**, *10*, 6615–6620.

[132] Yanai, T.; Tew, D. P.; Handy, N. C. *Chemical Physics Letters* **2004**, *393*,

51–57.

[133] Falke, S. M.; Rozzi, C. A.; Brida, D.; Maiuri, M.; Amato, M.; Sommer, E.; De Sio, A.; Rubio, A.; Cerullo, G.; Molinari, E.; Lienau, C. *Science* **2014**, *344*, 1001–1005.

[134] Yi, Y.; Coropceanu, V.; Brédas, J.-L. *Journal of Materials Chemistry* **2011**, *21*, 1479–1486.

[135] Wells, N. P.; Boudouris, B. W.; Hillmyer, M. A.; Blank, D. A. *Journal of Physical Chemistry C* **2007**, *111*, 15404–15414.

[136] Liu, T.; Gao, J.-S.; Xia, B.-H.; Zhou, X.; Zhang, H.-X. *Polymer* **2007**, *48*, 502–511.

[137] Goeb, S.; De Nicola, A.; Ziessel, R. *The Journal of Organic Chemistry* **2005**, *70*, 1518–1529.

[138] Milián Medina, B.; Van Vooren, A.; Brocorens, P.; Gierschner, J.; Shkunov, M.; Heeney, M.; McCulloch, I.; Lazzaroni, R.; Cornil, J. *Chemistry of Materials* **2007**, *19*, 4949–4956.

[139] Samsonidze, G.; Ribeiro, F. J.; Cohen, M. L.; Louie, S. G. *Physical Review B* **2014**, *90*, 035123.

[140] Elandaloussi, E. H.; Frère, P.; Richomme, P.; Orduna, J.; Garin, J.; Roncali, J. *Journal of the American Chemical Society* **1997**, *119*, 10774–10784.

[141] Few, S.; Frost, J. M.; Kirkpatrick, J.; Nelson, J. *The Journal of Physical Chemistry C* **2014**, *118*, 8253–8261.

[142] Potai, R.; Kamphan, A.; Traiphol, R. *Journal of Polymer Science Part B: Polymer Physics* **2013**, *51*, 1288–1297.

[143] Jacobs, I. E.; Aasen, E. W.; Oliveira, J. L.; Fonseca, T. N.; Roehling, J. D.; Li, J.; Zhang, G.; Augustine, M. P.; Mascal, M.; Moulé, A. J. *Journal of Materials Chemisry C* **2016**, *4*, 3454–3466.

[144] Lemaur, V.; Steel, M.; Beljonne, D.; Brédas, J.-L.; Cornil, J. *Journal of the American Chemical Society* **2005**, *127*, 6077–6086.

[145] Mityashin, A.; Olivier, Y.; Van Regemorter, T.; Rolin, C.; Verlaak, S.; Martinelli, N. G.; Beljonne, D.; Cornil, J.; Genoe, J.; Heremans, P. *Advanced Materials* **2012**, *24*, 1535–1539.

[146] Gregg, B. A.; Hanna, M. C. *Journal of Applied Physics* **2003**, *93*, 3605–3614.

[147] Kuang, H.; Janik, M. J.; Gomez, E. D. *Journal of Polymer Science Part B: Polymer Physics* **2015**, *53*, 1224–1230.

[148] Madigan, C. F.; Bulovic, V. *Physical Review Letters* **2003**, *91*, 247403.

[149] Brown, P. J.; Thomas, D. S.; Köhler, A.; Wilson, J. S.; Kim, J.-S.; Rams-

dale, C. M.; Sirringhaus, H.; Friend, R. H. *Physical Review B* **2003**, *67*, 064203.

[150] Zang, D. Y.; So, F. F.; Forrest, S. R. *Applied Physics Letters* **1991**, *59*, 823–825.

[151] Check, C.; Faust, T.; Bailey, J.; Wright, B.; Gilbert, T.; Sunderlin, L. *The Journal of Physical Chemistry A* **2001**, *105*, 8111–8116.

[152] Chandrasekhar, J.; Andrade, J. G.; von Rague Schleyer, P. *Journal of the American Chemical Society* **1981**, *103*, 5609–5612.

[153] Cohen, A. J.; Mori-Sánchez, P.; Yang, W. *Science* **2008**, *321*, 792–794.

[154] Körzdörfer, T.; Brédas, J.-L. *Accounts of Chemical Research* **2014**, *47*, 3284–3291.

[155] Adamo, C.; Jacquemin, D. *Chemical Society Reviews* **2013**, *42*, 845–856.

[156] Magyar, R. J.; Tretiak, S. *Journal of Chemical Theory and Computation* **2007**, *3*, 976–987.

[157] Goerigk, L.; Grimme, S. *Physical Chemistry Chemical Physics* **2011**, *13*, 6670–6688.

[158] Jacquemin, D.; Perpète, E. A.; Ciofini, I.; Adamo, C.; Valero, R.; Zhao, Y.; Truhlar, D. G. *Journal of Chemical Theory and Computation* **2010**, *6*, 2071–2085.

[159] Sini, G.; Sears, J. S.; Brédas, J.-L. *Journal of Chemical Theory and Computation* **2011**, *7*, 602–609.

[160] Salzner, U.; Aydin, A. *Journal of Chemical Theory and Computation* **2011**, *7*, 2568–2583.

[161] Fornari, R. P.; Aragó, J.; Troisi, A. *The Journal of Physical Chemistry C* **2016**, *120*, 7987–7996.

[162] Miyamoto, Y. *MRS Proceedings* **2012**, *1455*.

[163] Sun, Q.; Park, K.; Dai, L. *The Journal of Physical Chemistry C* **2009**, *113*, 7892–7897.

[164] Jacquemin, D.; Wathelet, V.; Perpète, E. A.; Adamo, C. *Journal of Chemical Theory and Computation* **2009**, *5*, 2420–2435.

[165] Chan, C. K.; Zhao, W.; Kahn, A.; Hill, I. G. *Applied Physics Letters* **2009**, *94*, 203306.

[166] Yim, K.-H.; Whiting, G. L.; Murphy, C. E.; Halls, J. J. M.; Burroughes, J. H.; Friend, R. H.; Kim, J.-S. *Advanced Materials* **2008**, *20*, 3319–3324.

[167] Gao, J.; Niles, E. T.; Grey, J. K. *The Journal of Physical Chemistry Letters* **2013**, *4*, 2953–2957.

[168] Salzmann, I.; Heimel, G.; Oehzelt, M.; Winkler, S.; Koch, N. *Accounts of Chemical Research* **2016**, *49*, 370–378.

[169] Horke, D. A.; Roberts, G. M.; Verlet, J. R. R. *The Journal of Physical Chemistry A* **2011**, *115*, 8369–8374.

[170] Murata, T.; Saito, G.; Nakamura, K.; Maesato, M.; Hiramatsu, T.; Yoshida, Y. *Crystal Growth and Design* **2013**, *13*, 2778–2792.

[171] Nafady, A.; Le, T. H.; Vo, N.; Haworth, N. L.; Bond, A. M.; Martin, L. L. *Inorganic Chemistry* **2014**, *53*, 2268–2275.

[172] Torrance, J. B.; Mayerle, J. J.; Bechgaard, K.; Silverman, B. D.; Tomkiewicz, Y. *Physical Review B* **1980**, *22*, 4960–4965.

[173] Humphrey, W.; Dalke, A.; Schulten, K. *Molecular Graphics* **1996**, *14*, 33–38.

[174] Lange, A. W.; Herbert, J. M. *The Journal of Chemical Physics* **2010**, *133*, 244111.

[175] Lange, A. W.; Herbert, J. M. *Chemical Physics Letters* **2011**, *509*, 77–87.

[176] Schaftenaar, G.; Noordik, J. H. *Journal of Computer-Aided Molecular Design* **2000**, *14*, 123–134.

[177] Aziz, H.; Popovic, Z. D. *Chemistry of Materials* **2004**, *16*, 4522–4532.

[178] Jørgensen, M.; Norrman, K.; Krebs, F. C. *Solar Energy Materials and Solar Cells* **2008**, *92*, 686–714.

[179] Kumar, A.; Hong, Z.; Sista, S.; Yang, Y. *Advanced Energy Materials* **2011**, *1*, 124–131.

[180] Lin, W.-C.; Wang, W.-B.; Lin, Y.-C.; Yu, B.-Y.; Chen, Y.-Y.; Hsu, M.-F.; Jou, J.-H.; Shyue, J.-J. *Organic Electronics* **2009**, *10*, 581–586.

[181] Luo, Y.; Aziz, H.; Popovic, Z. D.; Xu, G. *Journal of Applied Physics* **2007**, *101*, 034510.

[182] Mi, B. X.; Gao, Z. Q.; Cheah, K. W.; Chen, C. H. *Applied Physics Letters* **2009**, *94*, 073507.

[183] Li, J.; Rochester, C. W.; Jacobs, I. E.; Aasen, E. W.; Friedrich, S.; Stroeve, P.; Moulé, A. J. *Organic Electronics* **2016**, *33*, 23–31.

[184] Irwin, M. D.; Buchholz, D. B.; Hains, A. W.; Chang, R. P. H.; Marks, T. J. *Proceedings of the National Academy of Sciences* **2008**, *105*, 2783–2787.

[185] Li, J.; Diallo, S. O.; Hong, K.; Zhang, G.; Stroeve, P.; Mascal, M.; Moulé, A. J. Unpublished.

[186] Yang, J.-H.; Park, J.-S.; Kang, J.; Wei, S.-H. *Physical Review B* **2015**, *91*, 075202.

[187] Jackson, N. E.; Kohlstedt, K. L.; Savoie, B. M.; de la Cruz, M. O.; Schatz, G. C.; Chen, L. X.; Ratner, M. A. *Journal of the American Chemical Society* **2015**, *137*, 6254–6262.

[188] Grimme, S. *Chemistry – A European Journal* **2012**, *18*, 9955–9964.

[189] Antony, J.; Sure, R.; Grimme, S. *Chemical Communications* **2015**, *51*, 1764–1774.

[190] Ho, J.; Ertem, M. Z. *Journal of Physical Chemistry B* **2016**, *120*, 1319–1329.

[191] Achazi, A. J.; von Krbek, L. K. S.; Schalley, C. A.; Paulus, B. *Journal of Computational Chemistry* **2016**, *37*, 18–24.

[192] Ye, R.; Nie, X.; Zhou, Y.; Wong, C. F.; Gong, X.; Jiang, W.; Tang, W.; Wang, Y. A.; Heine, T.; Zhou, B. *Chemical Physics Letters* **2016**, *648*, 170–177.

[193] Sai, N.; Leung, K.; Zádor, J.; Henkelman, G. *Physical Chemistry Chemical Physics* **2014**, *16*, 8092–8099.

[194] Tomasi, J.; Mennucci, B.; Cammi, R. *Chemical Reviews* **2005**, *105*, 2999–3094.

[195] Cramer, C. J.; Truhlar, D. G. *Chemical Reviews* **1999**, *99*, 2161–2200.

[196] Han, L.-L.; Li, S.-J.; Fang, D.-C. *Physical Chemistry Chemical Physics* **2016**, *18*, 6182–6190.

[197] Zhao, L.; Li, S.-J.; Fang, D.-C. *ChemPhysChem* **2015**, *16*, 3711–3718.

[198] Raos, G.; Famulari, A.; Marcon, V. *Chemical Physics Letters* **2003**, *379*, 364–372.

[199] Smyth, C. P.; Morgan, S. O. *Journal of the American Chemical Society* **1928**, *50*, 1547–1560.

[200] Boys, S.; Bernardi, F. *Molecular Physics* **1970**, *19*, 553–566.

[201] Rühle, V.; Kirkpatrick, J.; Andrienko, D. *The Journal of Chemical Physics* **2010**, *132*, 134103.

[202] Schwarz, K. N.; Kee, T. W.; Huang, D. M. *Nanoscale* **2013**, *5*, 2017–2027.

[203] Plimpton, S. *Journal of Computational Physics* **1995**, *117*, 1–19.

[204] Brown, W. M.; Wang, P.; Plimpton, S. J.; Tharrington, A. N. *Computer Physics Communications* **2011**, *182*, 898–911.

[205] Brown, W. M.; Kohlmeyer, A.; Plimpton, J. S.; Tharrington, A. N. *Computer Physics Communications* **2012**, *183*, 449–459.

[206] Brown, W. M.; Masako, Y. *Computer Physics Communications* **2013**, *184*, 2785–2793.

[207] Vassiliev, S.; Zaraiskaya, T.; Bruce, D. *Biochimica et Biophysica Acta (BBA)*

– *Bioenergetics* **2012**, *1817*, 1671–1678.

[208] Müller, L.; Nanova, D.; Glaser, T.; Beck, S.; Pucci, A.; Kast, A. K.; Schröder, R. R.; Mankel, E.; Pingel, P.; Neher, D.; Kowalsky, W.; Lovrincic, R. *Chemistry of Materials* **2016**, *28*, 4432–4439.

[209] Allen, M. P.; Tildesley, D. J. *Computer simulation of liquids*; Oxford Science Publications, Clarendon Press, 1987.

[210] Olsson, M. A.; Söderhjelm, P.; Ryde, U. *Journal of Computational Chemistry* **2016**, *37*, 1589–1600.